MEASUREMENTS OF IN-SITU PRODUCTION OF ^{14}C IN SiO_2: PRODUCTION RATES AND CROSS-SECTIONS

BY

© HERMINIA ROMAN, M.Sc.

A Thesis

Submitted to the School of Graduate Studies

in Partial Fulfillment of the Requirements

for the Degree

Doctor of Philosophy

McMaster University

June 1989

ISBN 0-315-52159-7

MEASUREMENTS OF IN-SITU PRODUCTION OF ^{14}C IN SiO_2

Doctor of Philosophy (1989)

McMaster University
Hamilton, Ontario

Title: Measurements of in-situ production of ^{14}C in SiO_2: production rates and cross sections.

Author: Herminia Román, M.Sc. (University of Manitoba)

Hons. B.Sc. (University of Seville).

Supervisor: Dr J.A. Kuehner/ Dr J.R. Southon

Number of Pages: xiii, 146.

ABSTRACT

The development of a technique for the extraction of ^{14}C from silicate materials is shown. This ^{14}C extraction technique and the ^{14}C Accelerator Mass Spectrometer detection technique were applied to the measurements reported in this work.

Samples of quartz chips were irradiated with neutrons produced by a 20 MeV tritium beam interacting with a deuterated Ti foil target. This irradiation permitted the first measurement of the $^{16}O(n,2pn)^{14}C$ cross section at 35 MeV for which a value of 16±3 mb was found.

Two stacks of quartz plates were irradiated with 63 MeV protons. The measurement of the $^{16}O(p,3p)^{14}C$ cross section at several energies below 63 MeV are presented.

The ^{14}C in-situ produced was measured in seven obsidian rock samples. In four cases the values obtained agree with the calculated production rate of 0.19±0.05 atoms Kg^{-1} min^{-1} at 46^{o} geomagnetic latitude and 640 g cm^{-2}.

ACKNOWLEDGEMENTS

It would be almost impossible to thank each person who has contributed in some way to make my stay at Mac a fruitful one. However there are some whom I would like to give special thanks.

First I would like to thank Dr. D.E. Nelson for accepting me as part of the RIDDL group, for his financial support and for his "long distance" helpful comments.

Thanks to Dr. J.A. Kuehner for his accessibility to helpful discussions and comments, and for his financial support throughout this thesis work.

Also thanks to Drs. J.C. Waddington and H.P. Schwarcz (members of my supervisor's committee) for their interest and constructive discussions.

Many thanks to Dr. J.S. Vogel for teaching me many skills and for his openness to valuable discussions.

Very special thanks to Dr. J.R. Southon for always being there ready for questions and discussions, for guiding me through those obscure corners of research, and for putting up with my long and sometimes slow learning process.

To both John Southon and John Vogel, I would like to express my gratitude for making, with their hard work, one of the best world wide AMS facilities without which this thesis never would have been possible. Thanks for showing me the meaning of NEVER GIVE UP.

My deepest thanks to my parents for their constant love and support from the other side of the Atlantic during all these years.

Todo mi agradecimiento a mis padres por el constante cariño y apoyo moral que me han dado desde el otro lado del Atlantico durante todos estos años. Gracias por mantener vuestra confianza en mi.

And last, I will never be able to thank Gary, my husband, enough. He has helped me throughout all my frustrations, depressions and exasperations during these years. Without his love, care and encouragement these years would have been infinitively more difficult.

TABLE OF CONTENTS

INTRODUCTION.....1

CHAPTER 1: BASIC CONSIDERATIONS

1.1 INTRODUCTION.....3

1.2 COSMIC RAYS

1.2.1 Introduction.....3

1.2.2 Galactic Cosmic Rays.....4

1.2.3 Solar Cosmic Rays.....5

1.2.4 Geomagnetic effects.....6

1.2.5 Cosmic Rays interaction with matter.....7

1.2.6 Production of isotopes by Cosmic Rays.....11

1.3 IN-SITU PRODUCTION

1.3.1 Introduction.....14

1.3.2 Production rates.....16

1.3.3 In-situ production applications.....20

1.4 IN-SITU PRODUCTION OF ^{14}C

1.4.1 Introduction.....21

1.4.2 Production rate.....25

1.5 PRODUCTION CROSS SECTIONS.....25

CHAPTER 2: SAMPLE PREPARATION

2.1 INTRODUCTION.....29

2.2 EARLY STUDIES ON EXTRACTION METHODS

2.2.1 Introduction.....30

2.2.2 Combustion tube method.....31

2.2.3 Induction furnace method.....37

2.2.4 Acid fluxes and combustion tube method.....38

2.3 CURRENT EXTRACTION METHOD

2.3.1 Introduction.....39

2.3.2 Description of the method.....40

2.3.3 Background.....41

2.3.4 Extraction efficiency.....48

2.4 SUMMARY.....56

CHAPTER 3: A MEASUREMENT OF THE $^{16}O(n,2pn)^{14}C$ CROSS SECTION

3.1 INTRODUCTION.....57

3.2 EXPERIMENTAL SET UP.....59

3.3 BACKGROUND

3.3.1 Introduction.....62

3.3.2 Anthracite, CuO and quartz tubing as background sources.....62

3.3.3 Adsorption of carbon by the samples.....63

3.3.4 Secondary reactions.....68

3.4 RESULTS.....85

3.5 SUMMARY.....87

CHAPTER 4: MEASUREMENT OF THE $^{16}O(p,3p)^{14}C$ CROSS SECTION

4.1 INTRODUCTION.....89

4.2 EXPERIMENTAL TECHNIQUE.....92

4.3 BACKGROUND.....96

4.4 RESULTS.....100

4.4.1 Comparison to previous results.....102

4.5 SUMMARY.....106

CHAPTER 5: MEASUREMENTS OF THE ^{14}C CONCENTRATIONS IN OBSIDIAN SAMPLES

5.1 INTRODUCTION.....107

5.2 DESCRIPTION OF THE SAMPLES

5.2.1 Introduction.....107

5.2.2 Samples used in this work.....108

5.2.3 Sample preparation.....111

5.3 BACKGROUND.....112

5.4 RESULTS.....114

5.5 IMPLICATIONS OF THE ^{14}C IN-SITU PRODUCTION RATE ON THE NEUTRON CROSS SECTION RESULTS.....119

5.6 SUMMARY.....122

CONCLUSIONS.....123

APPENDIX I: ACCELERATOR MASS SPECTROMETER.....126

APPENDIX II: MONTE CARLO CALCULATION OF THE NEUTRON DETECTOR TELESCOPE EFFICIENCY.....131

BIBLIOGRAPHY.....140

LIST OF TABLES

Table — Page

2.1 Comparison between the ^{14}C concentrations found in Anthracite and CuO samples with and without a 600°C prebake. 43

2.2 Comparison between the ^{14}C concentrations found in two proton irradiated quartz plates with and without a 600°C prebake. 45

2.3 Comparison between the ^{14}C concentrations obtained from neutron irradiated quartz chips with and without a 600°C prebake. .. 47

2.4 ^{14}C concentrations found in obsidian samples for different ratios of CuO weight to sample weight. 49

2.5 ^{14}C concentrations in three quartz plates crushed and sieved to three different powder size. ... 50

2.6 ^{14}C concentrations extracted from several quartz plates in two consecutive bakes. 53

2.7 ^{14}C concentrations found in a blank an irradiated quartz plates while they were crushed under vacuum and during the later 1000°C bake. ... 55

3.1 ^{14}C concentrations found in neutron irradiated quartz chips samples and blanks. 64

3.2 ^{14}C concentrations found in neutron irradiated SiO_2 powder samples and blanks. 65

3.3 ^{14}C concentrations in neutron irradiated water samples and blanks. 81

4.1 ^{14}C concentrations found in the back plates of each stack. 100

4.2 ^{14}C concentrations found in each plate and for each stack. The final cross sections at each energy are also given. 101

5.1 Expected and measured ^{14}C concentrations for each obsidian rock. 110

5.2 ^{14}C concentrations found in three zero exposure time quartz materials. 113

LIST OF FIGURES

Figure — Page

1.1 Neutron flux as function of their energy at several atmospheric depths obtained by Hess et al. (He61). 9

1.2 Neutron and proton fluxes as function of their energies at 640 g cm^{-2} atmospheric depth and 42° geomagnetic latitude (La67). 10

1.3 Neutron flux versus energy obtained by Merker et al. (Me77), Hess et al. (He61), and Armstrong et al. (Ar73). 12

1.4 Relative production rate factor versus altitude (Yo77). 17

1.5 Relative production rate factor versus geomagnetic latitude (Yo77). 18

1.6 Reedy and Arnold's cross section estimates 23

2.1 Diagram of the extraction line 32

3.1 Reedy and Arnold's $^{16}O(n,2pn)^{14}C$ cross section estimates and our measurement of this cross section at 35 MeV. 58

3.2 Relative position of the targets, the samples and the detector telescope during the neutron irradiation. 61

3.3 The energy loss in the second detector versus the energy loss in the first detector by the protons scattered in the convertor. The protons were scattered with neutrons from the deuterated target. 71

3.4 Monte Carlo simulation of the energy spectrum shown in figure 3.3. 71

3.5 Energy spectrum for the undeuterated target 72

3.6 Monte Carlo simulation of the energy spectrum shown in figure 3.5. 72

3.7 Energy distribution of the neutrons produced with the deuterated target. 74

3.8 Energy distribution of the neutrons produced with the undeuterated target. 74

3.9 Diagram of the extraction line used with the ^{17}O enriched water samples. 82

4.1 Proton flux at mountain altitudes and 45° geomagnetic latitude and the $^{16}O(p,3p)^{14}C$ cross section are plotted as function of the proton energy. 91

4.2 Profile of the proton beam at the Crocker Nuclear Laboratory. 94

4.3 Proton range in quartz materials versus the proton energy. 95

4.4 Our measurements together with Tamers and Delibrias' results of the $^{16}O(p,3p)^{14}C$ cross section. 105

5.1 ^{14}C concentrations measured in the obsidian samples versus the expected values. 120

5.2 ^{14}C concentrations measured by Jull et al (Ju88b) in high altitude volcanic rocks versus the expected values. 120

A.1.1 Simon Fraser AMS facility at McMaster University Tandem Accelerator Laboratory. 127

A.2.1 Diagram of the detector telescope geometry. 133

A.2.2 Mean free path of neutron in hydrogen and (n,p) cross section versus neutron energy. 135

INTRODUCTION

The idea of measuring the concentrations of isotopes produced by the interaction of cosmic ray particles with the Earth's surface (or in-situ production) is not new. For many years this production has been measured for some isotopes, but for many others only estimates were possible, as the detection sensitivities of the methods then available were too low. In recent years the development of Accelerator Mass Spectrometry, with a much higher detection sensitivity, has made possible the detection of the in-situ production of some of the longer-lived isotopes that could not be detected earlier.

The importance of the study of such production is related to the fact that it could be developed as a dating technique for exposed rock surfaces and therefore could become important in areas such as archeology (dating stone flake tools) or geology (studying glaciations, erosion rates, etc.).

This work has been dedicated to the study of the in-situ production of ^{14}C. We concentrated our efforts on two main points: 1) The development of an efficient extraction method for removing in-situ produced carbon from the silica

materials and 2) the estimation of the ^{14}C in-situ production rate by measurements of the cross sections of the nuclear reactions involved and also by the measurements of ^{14}C concentrations in rocks.

We have measured the $^{16}O(n,2pn)^{14}C$ cross section, which is the main channel generating ^{14}C at the Earth's surface, at an energy of 35 MeV. As we will discuss later, the experiment was not ideal since background contributions produced large uncertainties in our results. On the other hand, this measurement does represent the first experimental data on this cross section. Furthermore, it shows that it is possible to measure this type of neutron cross section using AMS and it helped us to design a future neutron irradiation experiment at higher energies. We have also measured the $^{16}O(p,3p)^{14}C$ cross section at energies below 63 MeV. This cross section has been used in the past to estimate the $^{16}O(n,2pn)^{14}C$ cross section. In addition we have also measured the ^{14}C concentrations in several volcanic rocks (obsidians). From those measurements we will derive some estimates of the ^{14}C in-situ production rate.

CHAPTER 1

BASIC CONSIDERATIONS

1.1 INTRODUCTION.

The following sections contain a discussion of Cosmic Rays (CRs) and the production of isotopes. An introduction to in-situ production is then given, including a review of work undertaken during the past few years.

1.2 COSMIC RAYS.

1.2.1 Introduction.

Before considering the production of isotopes either at the surface of the Earth, in the atmosphere, or outside the atmosphere, it is important to have some background knowledge about CRs and their behaviour.

First, a distinction should be made between Galactic Cosmic Rays (GCR), which are produced outside the solar system, and Solar Cosmic Rays (SCR), which are produced at the emission of solar flares. In general, either type of CR is formed mostly of protons, 10% of α particles and 1% of heavier nuclei (Z=3 to 92). Because of their different

origins, GCR have high energies but low fluxes while SCR have lower energies and higher fluxes.

1.2.2 Galactic Cosmic Rays.

There is evidence to believe that most of the GCR reaching the solar system are created in and propagated throughout our galaxy (Si83). The distribution of elements found in GCR is very similar to that in the sun , stars, nebulae and the spectrum of heavier elements similar to the non-volatile parts of meteorites. Hence the origin of GCR could be related to processes involving heavy bodies under low energy conditions compared to GCR energies. Supernova explosions are examples of such conditions (Re83).

It is not yet certain how GCR are transported to the solar system (Si83). Different mechanisms have been suggested such as random interactions with the interstellar magnetic fields and shocks propagating in the interstellar medium (Si83).

Variations in the GCR fluxes have been associated with changes in the solar activity. As a general rule, the GCR flux is higher when the activity of the sun is low. This solar cycle modulation occurs because of the GCR's interaction with the magnetic field carried by the solar wind which is directed outward from the sun in all directions. This interaction tends to direct the GCR out of the heliosphere, though particles of sufficient energy will

be able to reach the inner areas of the heliosphere. It is therefore expected that near the Earth the GCR flux would be lower than the flux in the interstellar medium. At distances of 1 AU (distance between the center of the Earth and the center of the Sun) very few GCR have energies below several hundred MeV (Si83).

Within 1 AU, GCR have an average of 3 particles cm^{-2} sec^{-1} and a mean energy of the order of 10^9 eV (Re80). The energy spectrum in space is approximately given by

$$dI/dE = \text{const.}(1 + E(GeV))^{-2.5}$$

for energies between several hundred MeV and several thousand GeV (Re80).

1.2.3 Solar Cosmic Rays.

The sun, near periods of solar maximum, emits energetic particles. In a single event the flux of particles could reach levels of up to 10^5 particles cm^{-2} sec^{-1} at 1 AU (Re80). The average flux over a solar cycle for particles with energies above 10MeV is approximately 100 particles cm^{-2} sec^{-1} (Re80). For energies between 10 and 100 MeV, the spectrum is approximately described by:

$$dI/dR = \text{const.}\ \exp(-R/R_o)$$

where R is the magnetic rigidity (cp to charge ratio, where p is particle momentum and c the velocity of light) of the particle.

R_o is a factor changing from 30-200 MV with the particle energy (Re83).

Below 50 MeV the energy spectrum is given by

$$dI/dE = \text{const. } E^{-\gamma}$$

where γ has values between 1 and 4 (Re80).

In general the SCR flux decreases rapidly as the energy increases.

1.2.4 Geomagnetic effects.

For the charged CR particles approaching the atmosphere vertically near the poles, the interaction with the geomagnetic field is small. On the other hand, the interaction is much greater near the equator where the magnetic field is perpendicular to the direction of the CR particles. Therefore, at a given latitude, only those charged particles with an energy above a critical value will be able to reach the surface of the Earth: CR particles with lower energies will be deflected back into space.

The minimum particle momentum, corresponding to the cut-off energy, is given by (Lt68)

$$Pmin = 14.85 \cos^4\lambda \quad (GeV/c)$$

where λ is the magnetic latitude.

As the geomagnetic field is directed from south to north, the positively charged CR particles will be deflected eastward. It has been observed that the intensity of the CR

particles incident from the west is 20% larger than those coming from the east (Lt68).

The geomagnetic field is believed to change with time and therefore any of such variation would influence the cosmic ray fluxes. The long term changes found in the ^{14}C concentrations measured in tree rings have been attributed to variations of the strength of the geomagnetic dipole moment (Da88)(Da86). The results indicate that the dipole moment relative to its present value was lower prior to the 5th century A.D. and higher during the later period (Da88).

1.2.5 Cosmic Rays interaction with matter.

There are two ways in which CR particles interact with matter: First, they produce ionization associated with energy losses, and second, they induce nuclear reactions which produce secondary cosmic ray particles. These secondary particles are mostly neutrons, protons, pions and muons with energies varying up to GeV.

As the primary SCR particles have energies below 100 MeV, most are stopped through ionization before they can produce nuclear reactions (Re83). In the few cases when they do induce nuclear reactions there is a very small production of secondary particles due to the low energy of the primary particles. This production would mostly occur in the first few g cm^{-2} of the interacted material (such as the top of the atmosphere and extraterrestrial materials).

On the other hand GCR primary particles produce large numbers of secondary particles due to their high energies: about 7 neutrons are produced per primary GCR particle (Re87).

As the primary particle flux decreases with depth travelled into the atmosphere due to ionization and nuclear reactions, the number of secondary particles produced also decreases. Figure 1.1 shows the flux of neutrons as a function of energy for several atmospheric depths. With increasing depth in the atmosphere, the proton flux decreases significantly due to ionization effects in comparison with other secondary particles such as neutrons. Figure 1.2 shows the neutron and proton fluxes at mountain altitudes and below 500 MeV. Once in the Earth's crust, the neutron production decreases sharply to the point that 2 meters below the surface their flux is negligible compared with that of muons (La67).

Unfortunately, the CR neutron fluxes in the atmosphere are not well known. We have found significant differences in reported values among the published articles. For example Merker et al. (Me77) derive a 1/E energy dependence while Hess et al. (He61) showed a $1/E^{1.44}$ dependence (see figure 1.1). The neutron flux at 700 g cm^{-2} atmospheric depth and 44^{o} geomagnetic latitude calculated by Hess et al. and Merker et al. were 6.0×10^{-5} and 2×10^{-4} neutron cm^{-2} sec^{-1} MeV^{-1} respectively for 100 MeV neutrons.

FIGURE 1.1. Neutron flux as a function of their energy at several atmospheric depths obtained by Hess et al. (He61).

NEUTRON FLUX

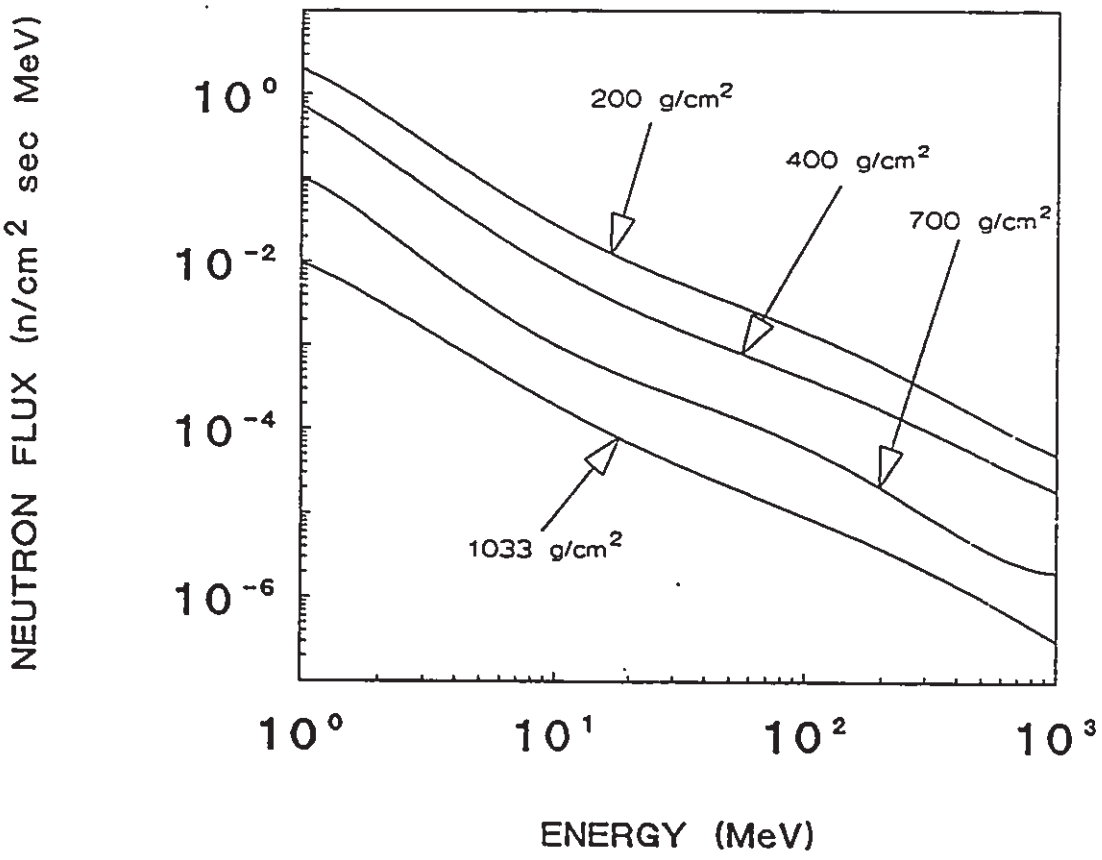

FIGURE 1.2. Neutron and proton fluxes as a function of their energies at 640 g cm^{-2} atmospheric depth and 42^{o} geomagnetic latitude (La67).

NEUTRON AND PROTON FLUXES

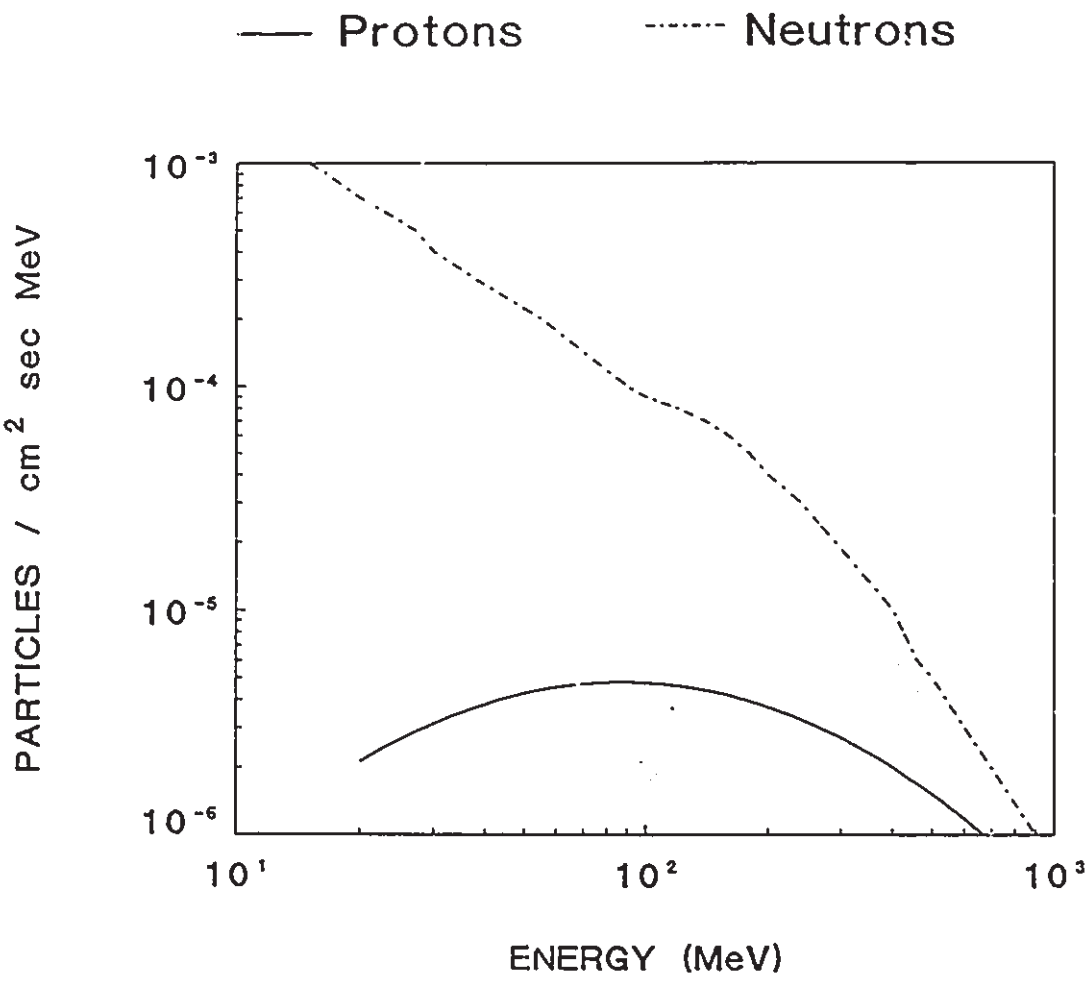

Hess et al. based their calculations on experimental data obtained at other atmospheric depths but at the same energy range, and Merker et al. based theirs on measurements done at low energies and other atmospheric depths. Armstrong et al. (Ar73) have carried out Monte Carlo calculations to find the neutron fluxes using the data obtained by Hess et al. at 1033 g cm^{-2} and 200 g cm^{-2} atmospheric depth. They calculated that at 800 g cm^{-2} of atmospheric depth and for 100 MeV neutrons the flux is $2x10^{-4}$ neutrons sec^{-1} MeV^{-1} (see figure 1.3).

On the other hand we have not found significant differences in the relative changes of the neutron flux with latitude within the published articles (Si51)(Yo77).

We believe the discrepancies found in the neutron flux values are due to the general difficulty of neutron detection. Additionally, neutron fluxes are subject to temporal changes which could be difficult to take into account.

1.2.6 Production of isotopes by Cosmic Rays.

Secondary GCR particles induce nuclear reactions which are responsible for most of the isotope production. However, most of the isotope production by SCR is due to primary particles themselves as a result of their low energies.

In general the isotope production would be directly

FIGURE 1.3. Neutron flux versus energy obtained by Merker et al. (Me77) and Hess et al. (He61) at 700 g cm^{-2} atmospheric depth. The neutron flux obtained by Armstrong et al. (Ar73) at 800 g cm^{-2} atmospheric depth is also shown.

NEUTRON FLUX

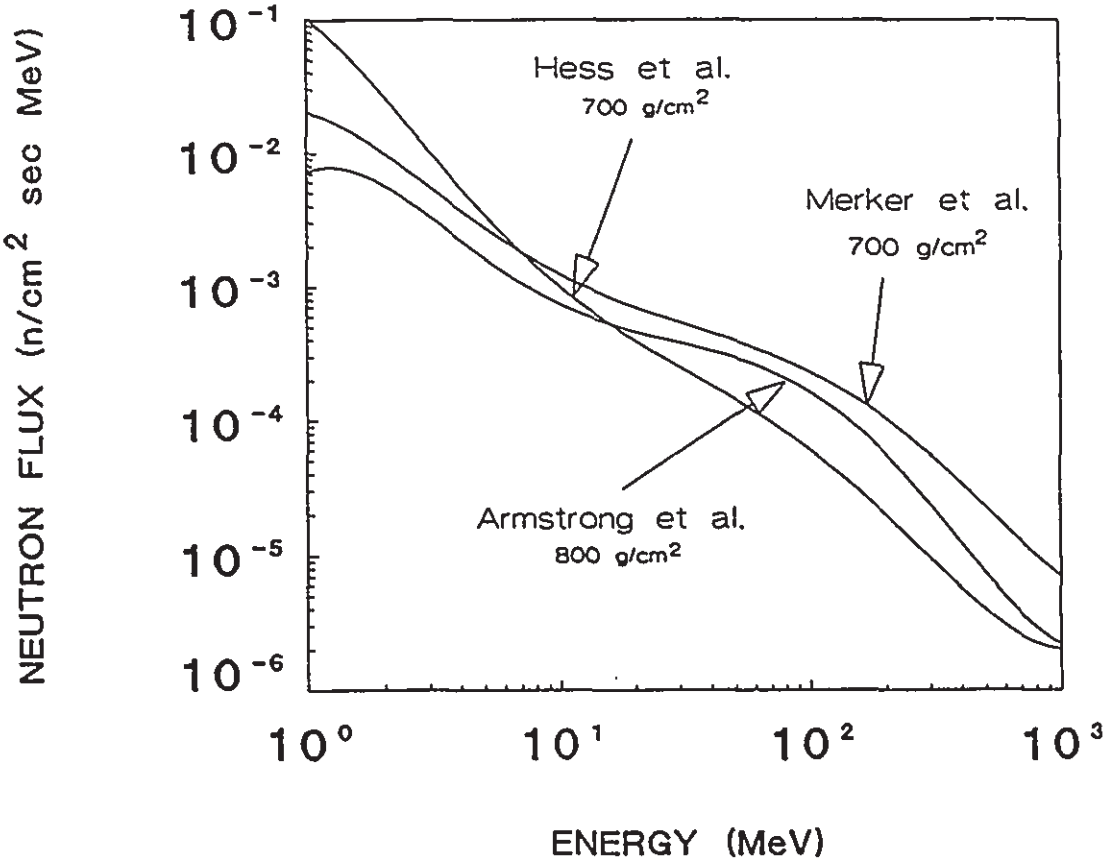

influenced by the spatial and temporal changes occurring in the CR fluxes (La87). In extraterrestrial materials (e.g. meteorites), secondary neutrons and protons are responsible for most of the isotope production. In the atmosphere, neutrons are mainly responsible for isotope production. They have a large mean free path compared to that of secondary protons which are stopped due to ionization before they can induce comparable amounts of nuclear reactions. In the Earth's crust, isotope production is due to neutrons through the first two meters below the surface, and further below muons (decay product of pions) dominate the production for several thousand meters (La67).

The possible applications from the study of isotope production by CR particles would depend on where the production takes place:

1. The study of isotope production in extraterrestrial materials could lead occasionally to information on changes of the CR fluxes due to changes in the sources of formation and changes in their transport to the solar system (Re87).

2. The study of isotope production in the atmosphere could give information on the variations of the CR fluxes due to the spatial and temporal changes of the geomagnetic field and solar cycles.

3. In the Earth's crust, the study of isotope production is based on the knowledge of CR fluxes and the geological history of interacted material. Therefore if we

know one of those, we could model the other (La87). In the next section more details about these applications will be provided.

1.3 IN-SITU PRODUCTION.

1.3.1 Introduction.

In-situ production refers to the production of any particular radioisotope by CRs interacting with materials at the surface of the Earth. The possibility of measuring ^{36}Cl produced in rocks was first mentioned by Davis and Shaeffer (Da55) and they measured the production of ^{36}Cl in surface rocks and saline waters by thermal neutrons. Rama and Honda (Ra61) detected the in-situ production of ^{39}Cl, ^{32}P, ^{7}Be, and $^{198}Au+^{199}Au$ in terrestrial materials at sea level and at mountain altitudes. Also, measurements of muon induced ^{26}Al in terrestrial rocks were carried out by Hampel et al. (Ha75). The importance of the existence of such production for many radioisotopes was stated by Lal and Peters (La67) when they published a very complete study about radioisotope production. They acknowledged the existence and potential applications of such production but they also recognized the impossibility of detecting the in-situ production of some radioisotopes with the methods then available.

Later, Yokoyama et al. (Yo77) calculated the

production rates of a number of radioisotopes at the surface of the Earth. These calculations were based on the measured production of ^{22}Na and ^{24}Na from aluminum by cosmic ray neutrons at two different altitudes. To be able to extrapolate to production rates for other isotopes, it was necessary to know the values of the neutron production cross sections as well as the attenuation of the CRs throughout the atmosphere. As many of the neutron cross sections have not been measured, these were estimated by using the cross sections for similar reactions induced by protons.

In 1977, the development of Accelerator Mass Spectrometry (AMS) raised new possibilities in the detection of in-situ production. This technique (described in Appendix I) involves the ionization, acceleration, and detection of the atoms of radioisotopes under study. This method is far more efficient than the conventional counting techniques since it measures a fraction of the total number of atoms instead of detecting decaying particles. The concentration of atoms needed is therefore much smaller than that required for the conventional counting method.

A few years ago, several groups decided to measure the in-situ production of different isotopes in some surface materials. Up to the present, in-situ production of ^{10}Be and ^{26}Al by cosmic ray neutrons have been detected by Yiou et al. (Yi84) and Nishiizumi et al. (Ni85) in quartz materials. In-situ production of ^{36}Cl was detected by

Kubik et al. (Ku84) and Phillips et al. (Ph86) in volcanic rocks. Jull et al. (Ju88b) recently detected in-situ production of ^{14}C, also in volcanic rocks. Middleton et al. (Mi88) have detected ^{41}Ca in terrestrial rocks.

1.3.2. Production rates.

The concentration of an isotope as a function of the depth from the surface of the material under study is given by the expression (La87):

$$C = \frac{ALP_r}{\lambda + \epsilon\rho\mu} (1-e^{-\lambda t}) e^{-\mu x}$$

where A is the altitude correction factor (see figure 1.4).

L is the latitude correction factor (see figure 1.5). Note that the latitude correction factor, L, is different at same geomagnetic latitude in Europe and North America. This is produced by the changes of the cut-off rigidity with the geomagnetic latitude.

P_r is the production rate given in atoms g^{-1} yr^{-1}

μ is the attenuation coefficient for neutrons.

x is the depth below the surface that the sample was taken from.

FIGURE 1.4. Relative production rate factor versus altitude (Yo77).

RELATIVE PRODUCTION RATE VS. ALTITUDE

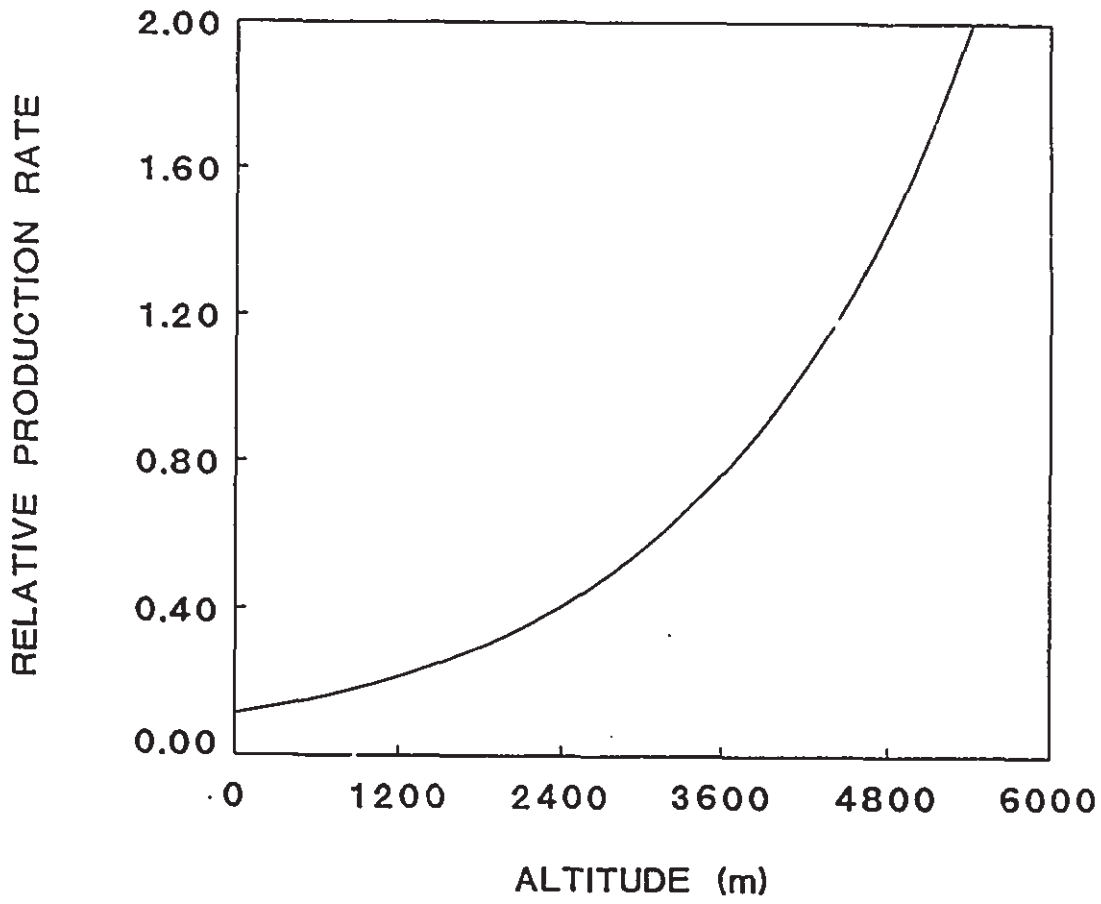

FIGURE 1.5. Relative production rate factor versus geomagnetic latitude (Yo77).

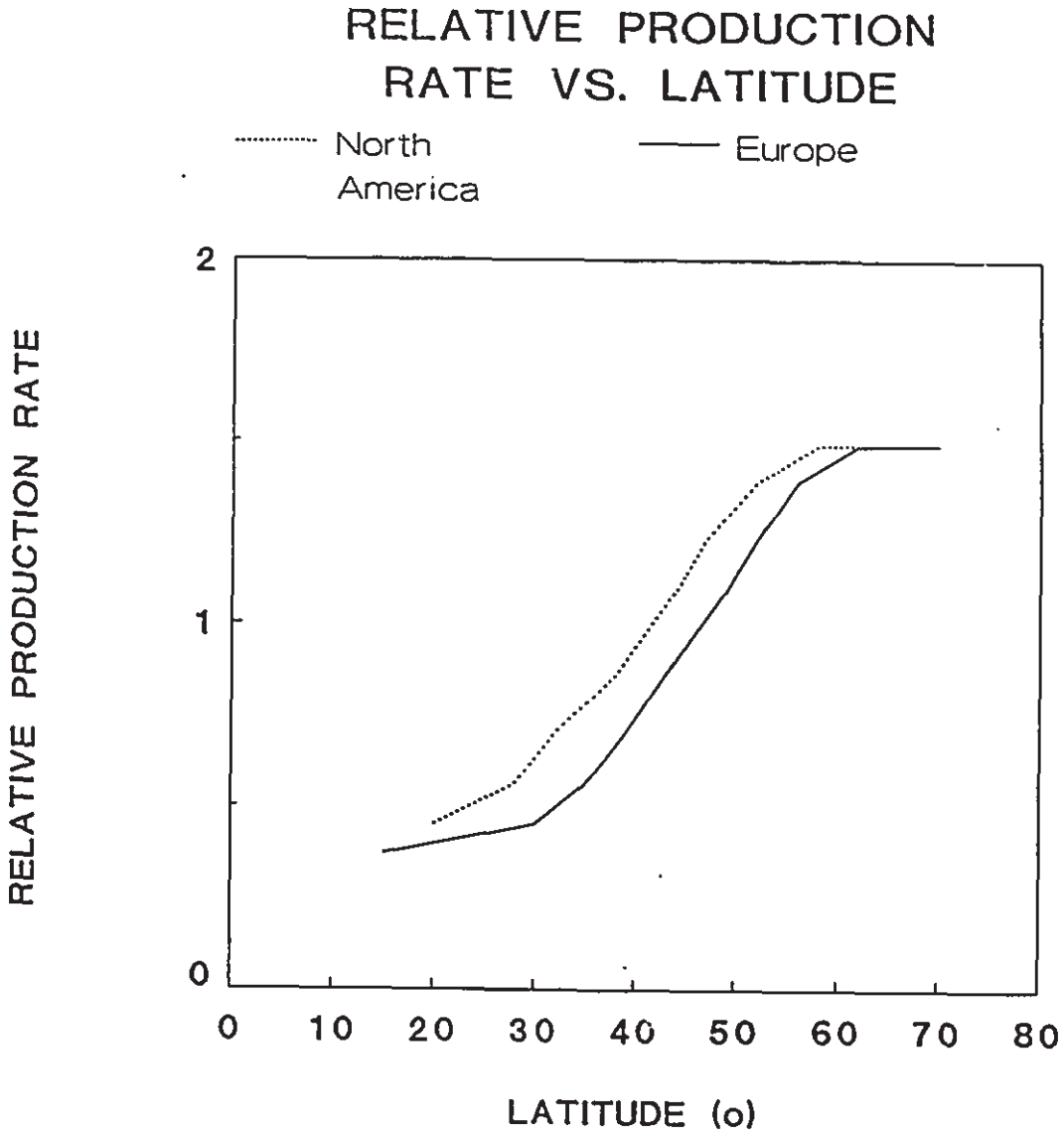
RELATIVE PRODUCTION
RATE VS. LATITUDE
North America
Europe
RELATIVE PRODUCTION RATE
2
1
0
0
10
20
30
40
50
60
70
80
LATITUDE (o)

λ is the decay constant for the radioisotope being produced.

ϵ is the erosion rate.

ρ is the mean density of the rock.

t is the time of exposure.

If $t >> 1/\lambda$ then the parenthesis term will have a value close to one and the isotope concentration will have reached saturation level.

To calculate the in-situ production rate of an isotope we need to know the production cross section and the CR flux at a given altitude.

The production P_r can be defined as:

$$P_r = \sum_i \sum_j No_i \int \psi_j(E)\sigma_{ij}(E)dE$$

where No is the number of atoms of the target element per gram of the sample.

$\psi(E)$ is the CR flux as a function of the energy.

$\sigma(E)$ is the cross section as a function of the energy for the production of the radioisotope under study.

In general, the neutron cross sections are not well known because of the difficulty of producing monoenergetic neutron beams strong enough to study those production reactions. As we will see later, some estimates based on

other similar proton reaction cross section data have been made.

1.3.3. In-situ production applications.

Lal (La87) divides samples for in-situ production studies into two classes: 1) well characterized and 2) non-characterized. In general the possible applications will depend on the type of sample available.

The first group includes samples with a well known geological history. These samples could be used to look for past changes in the CR fluxes, which could be due to changes in the Earth's magnetic field , altitude changes of the sample, or to changes of the primary CR fluxes due to solar modulation.

In the second group would be included samples for which the geological history is unknown but some qualitative assumptions can be made. Therefore the erosion rates of the rock's surface or the rates of accumulation of sediments could be studied. The study of the concentrations in a given sample of a pair of isotopes will give the mean erosion rate. Differences in erosion rates obtained from studies with more than one pair of isotopes can be used to find the changes of the erosion rate with time. The accessible time scale will depend on the half lives of the isotopes used.

Another important application possible with this

second group of samples is to find how long a surface has been exposed to CRs. One way to study this, if the production rate is unknown, is to use more than one isotope. At least one of these isotopes must have λ of the same order of magnitude as 1/t.

A calibration curve could be obtained by using the concentration of a specific isotope on a group of samples with well known past geological characteristics and times of exposure. To obtain a complete curve, the time of exposure for the samples should be different, and some of the samples should be well below saturation. This curve would be the result of plotting isotope concentration, normalized to altitude, latitude and erosion rate, versus the time of exposure. We could then use this calibration to study samples with poorly known past geological histories once we had measured the in-situ produced isotope concentrations.

1.4 IN-SITU PRODUCTION OF ^{14}C.

1.4.1 Introduction.

Until only a year ago, the detection of in-situ produced ^{14}C had not been achieved (Ju88b). Even though A.M.S. measurements of ^{14}C have been well under way for the last 5 years, the difficulty of extracting carbon from silica made hard to work with the ^{14}C in-situ produced.

The low ^{14}C concentrations produced in-situ made it impossible to apply traditional carbon extraction techniques used with other materials such as meteorites.

In order to determine the major reactions involved in the in-situ production of ^{14}C, the next four points should be taken into consideration:

1) The flux of neutrons is markedly higher than the proton flux below 300 MeV at the Earth's surface (see figure 1.2).

2) SiO_2 accounts for more than 50% of the composition of the Earth's crust, and much of the reminder consists of other oxides. Therefore the most abundant element in the Earth's crust is oxygen (approximately 45%) so it is expected to be the main target for the ^{14}C production. Some small contributions will come from Si which is the second most abundant element.

3) The $^{16}O(p,3p)^{14}C$ cross section was measured by Tamers and Delibrias (Ta61). Reedy and Arnold made estimates of the $^{16}O(n,2pn)^{14}C$ cross section based on these data (see figure 1.6).

4) The $^{28}Si(n,^{15}O)^{14}C$ cross section has not been measured. However we have estimated that it should be about two orders of magnitude smaller than the relevant cross section for oxygen. This is based on the number of competing channels and the number of possible excited states for each channel relative to the geometrical cross sections

FIGURE 1.6. Reedy and Arnold's cross section estimates.

REEDY AND ARNOLD'S CROSS SECTION ESTIMATES

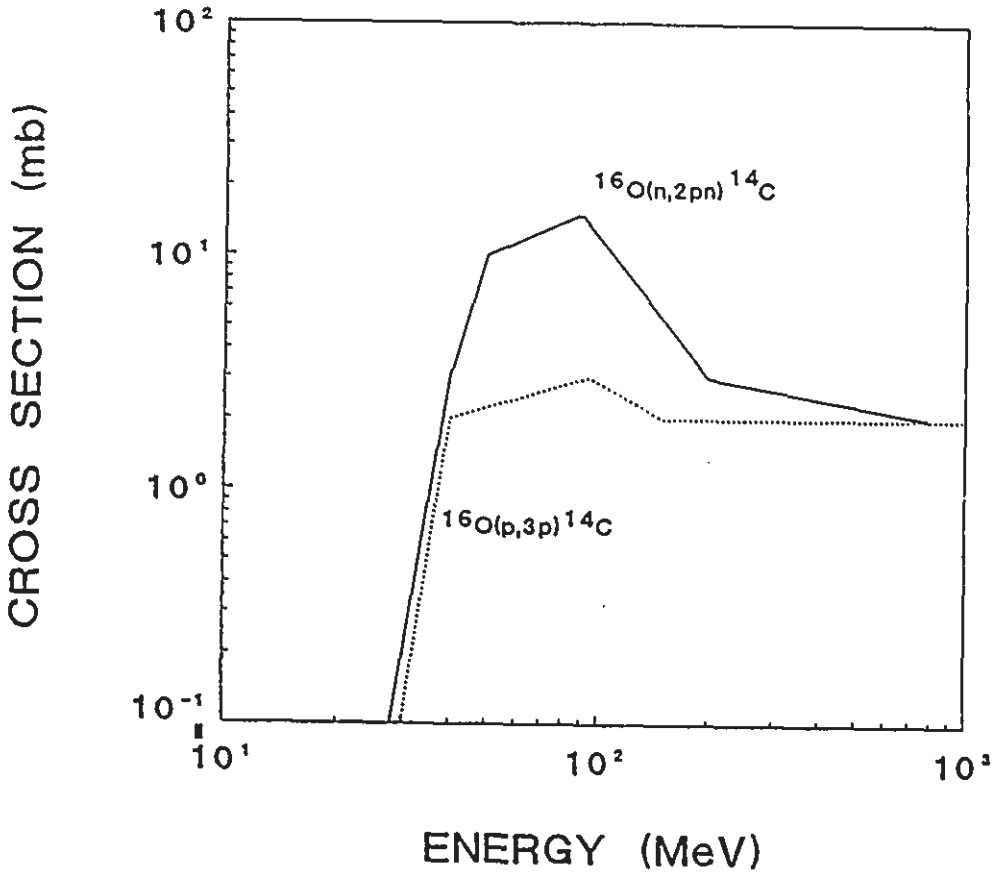

for both O and Si reactions.

The combination of those four factors indicates that the in-situ production of ^{14}C should be due to the $^{16}O(n,2pn)^{14}C$ (Q = -22.3 MeV) and $^{16}O(n,^{3}He)^{14}C$ (Q = -14.6 MeV) reactions with no more than 0.5% from the $^{28}Si(n,^{15}O)^{14}C$ (Q = -19.3 MeV) reaction. Negligible amounts would be produced by the equivalent proton reactions. In general throughout this thesis we will refer to $^{16}O(n,2pn)^{14}C$ as a short-hand way to referring to all $^{16}O + n \rightarrow {}^{14}C$ reactions. In fact, at energies lower than 23 MeV the ^{14}C production is due to the $^{16}O(n,^{3}He)^{14}C$ reaction because it has a Q = -14.6 MeV compared to a Q= -22.3 MeV for the $^{16}O(n,2pn)^{14}C$ reaction. When required, we will refer to both reactions separately.

Neutron production of ^{14}C would not be important 1-2 meters below the Earth's surface since the production of CR neutrons decreases with depth. As we have previously stated, muon production becomes more important at depths greater than two meters.

As the ^{14}C half-life is 5,730 years, the time frame at which the in-situ production of ^{14}C would be applicable is less than 15,000 years. Surfaces exposed longer than about 10,000 years would be close to the saturations levels. Therefore, in-situ produced ^{14}C would be especially useful to study surfaces exposed to cosmic rays after the last glaciation.

1.4.2. Production Rate.

Yokoyama et al. have made an estimate of the ^{14}C in-situ production rate. They found a value of 0.4±0.1 atoms kg^{-1} min^{-1} at 46^{o} geomagnetic latitude and 640 g cm^{-2} atmospheric depth. They considered that all the production came from the $^{16}O(n,2pn)^{14}C$ reaction. For their calculation, they used Reedy and Arnold's cross section estimate and a neutron flux similar to those obtained by Merker et al. (Me73).

To find out how the discrepancies we have found in the published neutron fluxes would influence the production rate calculations, we made a simple calculation of the ^{14}C production rate. We used the neutron fluxes given by Hess et al. (He61). Like Yokoyama et al., we considered all the production to be due to the $^{16}O(n,2pn)^{14}C$ reaction and we also used the same estimates for this cross section. We found a value of 0.19±0.05 atoms kg^{-1} min^{-1} at 46^{o} geomagnetic latitude and 640 g cm^{-2} atmospheric depth which is about half of Yokoyama's estimate.

1.5 PRODUCTION CROSS SECTIONS.

Part of the work carried out in this thesis has been the measurement of the $^{16}O(n,2pn)^{14}C$ and $^{16}O(p,3p)^{14}C$ cross sections. The proton cross section has previously been measured by Tamers and Delibrias (Ta61) at several energies

but with uncertainties of 25%. Beside its relation to in-situ production, it was important to measure it again to confirm the calculations made on the changes of SCR protons over the last 10,000 yrs using extraterrestrial material (Re87). The neutron cross section has not been measured until the present work but estimates were made by Reedy and Arnold using the data for the proton cross section (see figure 1.6).

At lower energies, the excitation function of both reactions can be explained by the compound nucleus theory. The neutron (or proton) interacts with the oxygen atoms which absorb them producing the compound nucleus. The energy of the incident particle is shared among a number of nucleons. Therefore no nucleon will have enough energy to escape the nucleus until by chance and by further collisions the energy is concentrated in one nucleon or a few nucleons (En66)(Se77). Each time the compound nucleus ejects out one more nucleon, it loses about 8 MeV because of the mass difference between the A system and the A-1 + (n or p) system. Hence, the last nucleon may be strongly affected by the Coulomb barrier when the reaction is taking place close to threshold (the Coulomb barrier between a ^{14}C nucleus and a proton is approximately 2.7 MeV). Additionally, the $^{16}O(n,^{3}He)^{14}C$ reaction is more affected by the Coulomb barrier as it has an additional factor of two from the Z = 2 of the He. On the other hand, its smaller Q value means

there is much more energy available than there is for the last nucleon in the $^{16}O(n,2pn)^{14}C$ and $^{16}O(p,3p)^{14}C$ reactions. The cross section of a particular channel depends also on how many energetically possible channels compete for the total reaction cross section. Because of the similarity in the particles involved in the above two reactions, the number of competing channels and their total number of energetically possible excited states for the neutron and proton reactions is very similar at all energies. However at low energies (near 35 MeV),the number of energetically possible excited states in which the neutron induced reactions to ^{14}C (both $^{16}O(n,2pn)^{14}C$ and $^{16}O(n,^{3}He)^{14}C$ reactions) can be found is three times larger than those for the $^{16}O(p,3p)^{14}C$ reaction. The main consequence is that at low energies the neutron cross section should be larger than the proton cross section. Because of the above arguments we believe that the differences between the neutron and proton cross sections should appear near threshold energies rather than at the energies shown in the Reedy and Arnold's neutron cross section estimates (see figure 1.6). Once the available energy for the last particle emitted is above the Coulomb barrier, both cross sections should be similar. Above 200 MeV, the direct interaction mechanism will dominate. In those cases, the incident particle interacts very rapidly with the nucleus, transferring enough energy to one or more

nucleons to allow them to leave the nucleus. The transfer is so rapid that the remaining nucleons are not involved. In addition, the incident particle keeps enough energy to stay unbound.

With our measurement of the neutron cross section at threshold energies we have been able to make a better estimate of the position and height of the peak. We have been able to more accurately measure the proton cross section.

CHAPTER 2

SAMPLE PREPARATION

2.1 INTRODUCTION.

One of the most challenging tasks in this study was the sample preparation. The samples used in this thesis were neutron irradiated quartz chips and powder, and proton irradiated quartz plates for the neutron and proton cross section measurements. The detection of ^{14}C in-situ produced was carried out in obsidian rocks. The ^{14}C concentrations present in the proton irradiated samples were two orders of magnitude higher than those produced in the neutron irradiated samples and in the obsidians.

The levels of ^{14}C that we study could not be measured without the use of AMS. New techniques for the extraction from the samples were developed since the conventional extraction methods used with meteorites were not designed to handle the small ^{14}C concentrations produced in-situ. In fact, the ^{14}C concentrations found in our samples are in the same order of magnitude as the background levels in those methods (Ko63)(Br84). Therefore, it was difficult, and in some cases impossible, to distinguish between the ^{14}C made in-situ and the ^{14}C produced by background sources using

these methods.

In this chapter we briefly review several extraction methods which we tested. The description and the reasons for the choice of our present method will be given.

2.2 EARLY STUDIES ON EXTRACTION METHODS.

2.2.1 Introduction.

In general, any method used for the extraction of carbon from the samples will require the crushing of the samples to a fine powder, to allow the extraction of the carbon from the inner layers of the material. It is also necessary to heat the sample to high temperatures where the carbon becomes mobile. The size of the sample will depend on the type and size of the combustion chamber used in each particular method. The use of an oxidizer will be required to convert C and CO into CO_2 which is easy to collect. As oxidizer we have used either oxygen gas (Canadian Liquid Air, 99.9% purity) or CuO powder (Fisher Scientific Co., 99.98% purity). And of course it is necessary to have a method to collect and measure that CO_2. It is essential that all of the above steps are carried out maintaining the contamination at a minimum value which allows one to differentiate between the in-situ produced ^{14}C and that from other sources.

2.2.2 Combustion tube method.

Our first extraction system had the following parts (numbers in brackets refer to part numbers in figure 2.1):

1. A combustion tube furnace (from Lindberg Co., Model 55035) with a maximum temperature of 1000°C (2).

2. A second oven containing CuO. This was maintained between 550 and 600°C, to ensure the conversion of any CO into CO_2 (4).

3. A -78° trap (isopropyl alcohol and dry ice) to condense and remove any water vapor present in the gas stream (5).

4. A liquid nitrogen trap to condense the CO_2 extracted from the sample (6).

5. A low temperature oven containing alternated layers of Ag-Cu-Ag to remove contaminants such as halogens and nitrogen from the CO_2 (8).

6. A calibrated volume where the amount of CO_2 collected is measured (7). The gas pressure was measured using a pressure transducer placed above the calibrated volume.

7. A bottle to store the CO_2 collected from the samples (9).

8. The oxygen gas used as oxidizer was bubbled through a saturated solution of $Ba(OH)_2$ (B.D.H. Chemical Ltd.) to eliminate contaminant CO_2 (1).

The system was originally made from glass with

FIGURE 2.1. Diagram of the extraction line.

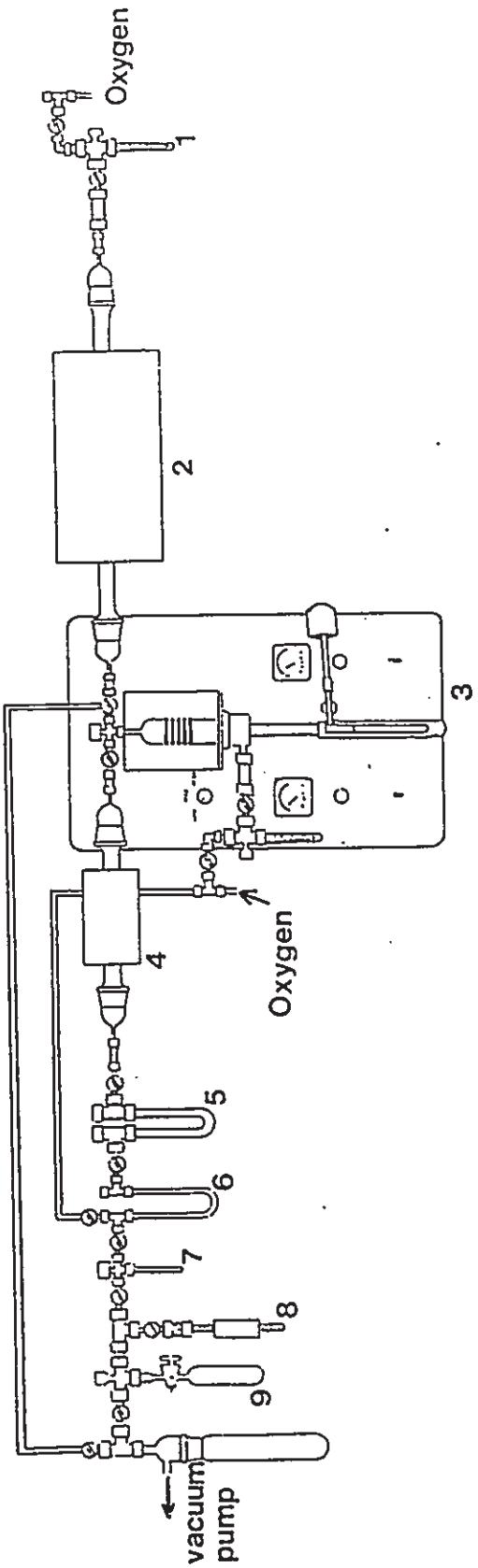
Oxygen
1
2
3
4
Oxygen
5
6
7
8
9
vacuum
pump

standard taper joints but later versions used metal Cajon Ultratorr fittings combined with simple glass tubes. This new system was easier to put together and therefore the required vacuum was faster achieved. The samples, with an approximate weight of 20g, were manually crushed in a steel mortar to a fine powder and placed in a boat which was then introduced into the combustion tube. The samples were prebaked for 1 hour at 500°C to eliminate any adsorbed CO_2 or CO. In this prebake, the sample was oxidized with flowing oxygen gas or by mixing it with CuO powder. The material was then oxidized at 1000°C with a weighed amount of anthracite was used to provide a dead CO_2 carrier gas for the sample. The ratio of CO_2 collected to that expected from the amount of carrier used gave us the combustion efficiency of the method.

The background levels were tested for two types of boats; nickel and ceramic (Fisher Scientific Co. brand Combax boat #07-651). The choice of nickel boats was based in the fact that they could be made by us using 0.125 mm thick Nickel foil (Alfa Products #00505) at any desired size while we were restricted to smaller sizes with the use of ceramic boats. The background in both cases was very similar.

Three methods to oxidize the samples were tested:

1. Closed tube combustion using oxygen. In this method pure oxygen (Canadian Liquid Air, 99.9% purity) was

introduced in the combustion tube and held for the combustion time at a pressure of 15 Torr. This closed system method gave the lowest background contribution, $(3\pm1)\times10^{6}$ atoms of ^{14}C, using either type of boat. However, it also gave the lowest yields for the extraction of the CO_2; typically (58±7)% of the carbon in the anthracite was extracted.

2. Closed tube combustion using CuO. In this case CuO powder (Fisher Scientific Co., 99.98% purity) was combined with the sample to provide the necessary oxidant. This method gave good yields, around (88±2)%, but the background levels were higher than method 1, $(1.4\pm0.5)\times10^{7}$ atoms of ^{14}C. The CuO contained up to 0.02% carbon. This amount should have been eliminated in the 1000°C air bake that the CuO was subjected to after it was crushed to powder and before it was used. Additionally, the mixed CuO and sample were vacuum prebaked at 500°C to eliminate any CO_2 adsorbed during storage or handling. However, after this latter prebake, the CuO and the sample were exposed to air briefly to add the anthracite before the high temperature bake. Therefore it is possible that some readsorption may have occurred. Although this step could have been avoided if dead CO_2 gas (^{14}C free gas obtained by combusting anthracite or graphite) had been added directly to the sample from a storage bottle, we believe that the use of the

anthracite was necessary as an indicator of the combustion efficiency.

3. In this last method a small flow of O_2 passed through the combustion tube keeping a similar pressure in the combustion tube as with the closed system method. In this case the background contributions were the worst of the three methods tested, $(1.9\pm0.9)\times10^7$ atoms of ^{14}C. Because the tube was open to the rest of the line, larger surface areas and more o-rings were involved in the system during the baking time than in the other methods. As a consequence, larger amounts of CO_2 adsorbed by the surfaces are more likely to have been released during the high temperature bake. The yields were (65±12)%.

As low background levels were essential, we decided to use the closed system method, and worked on raising the yields obtained with that method. We achieved this by testing different pressures inside the combustion tube. We found that pressures of 40 to 50 Torr were needed to obtain 80 to 90% yields from the combustion of anthracite using the nickel boats, and a pressure around 20 Torr when using ceramic boats. A higher pressure of oxygen was needed in the case of the nickel boats since part of the oxygen was used in oxidizing the boat.

Next, we investigated the ^{14}C backgrounds from the extraction line by passing samples of dead CO_2 through different sections of the line. Our main finding was that

the oven with CuO absorbed CO_2 while working at temperatures lower than 450°C. We therefore kept it between 550 and 600°C at all times to avoid poor yields and memory effects in the samples.

The background contributed by the CuO, anthracite and, the boat gave an approximate level of $(3\pm1)\times10^6$ atoms of ^{14}C. However, the levels found in the volcanic rock in which we measured in-situ production were $(7\pm2)\times10^6$ atoms of ^{14}C for a typical size of 20g. Unfortunately, the above levels are too similar to allow us to distinguish well between the in-situ ^{14}C concentrations and those produced by contamination.

Our other main concern in the use of this method was the fact that the temperature of the interior of the combustion tube was uneven due to heat conduction along the tube and convection in the gas which worsened with an increased gas pressure. Examination of the samples showed that only the powder in the middle of the boat was melted. The very center of the tube was the only place with the selected oven temperature leaving the rest of the oven at lower temperatures. Unfortunately, the maximum temperature achievable by the furnace was 1000°C. Therefore, in spite of the good yields from the anthracite, we felt that total extraction of carbon from the samples was unlikely to be reached. The option of decreasing sample size was not acceptable since it will also decrease the ^{14}C extracted

which would be impossible to distinguish from the background levels.

2.2.3 Induction furnace method.

We replaced the tube furnace with a high frequency induction furnace (from Leco Co., Model 521-000) (see figure 2.1, (3)). This is a common method used in the literature for the extraction of CO_2 from iron meteorites (Fi78) and stone meteorites (Ju88a) (Gu70), and is being used for in-situ production research in another laboratory (Ju88b). With the induction furnace, temperatures of up to 3000^{o}C could be reached, opening the possibility of using samples with higher melting points. The furnace requires the use of a metal powder mixed with the sample to bring it to the desired temperature. Powders of Ni (Fisher Scientific Co., reduced and purify), Cu (-100 mesh spherical, Alfa Products), Fe powder (-325 mesh spherical, Alfa Products) and Fe powder (B.D.H. Chemical Ltd., 95% purity) were tested for background levels. Oxygen gas was used as oxidizer maintained with a constant 20 Torr of pressure in the closed system manner. The background found using those metals were approximately $(3\pm2)\times10^{6}$ atoms of ^{14}C where the uncertainty calculation was based on the differences between separate blank measurements. Again, as in the case of the combustion tube, the background level is not very different from that expected in the samples. One possible source of

background for this method could have been the existence of impurities in the metal powders. Also it was observed that the discharge was not well confined to the boat because of the use of the oxygen gas and metal fittings. Therefore, the CO_2 adsorbed on the surfaces areas involved in the system (iron powder, boat, glass and metal fittings) could have been released during the bake. Furthermore, the oven was designed such that the boat used could not hold more than 1 g of sample in addition to the metal powder. This amount of sample was not sufficient to obtain ^{14}C concentration levels above the background levels produced by the carrier, boat, iron powder and oxidizer.

2.2.4 Acid fluxes and combustion tube method.

Since the induction furnace method did not appear to be promising, we returned to the combustion tube oven and investigated the use of acid fluxes to lower the melting point of the sample materials. This is another method for the extraction of carbon from stone and iron meteorites (Go62). Potassium pyrosulfate (Fisher Scientific Co., 37.5-38.6% purity), potassium dichromate (J.T. Baker Chemical Co., 99.9% purity), vanadium pentoxide (Fisher Scientific Co., 99.98% purity) and potassium chromate (Fisher Scientific Co., 99.98% purity) fluxes were tested. The main problem was that during baking, the flux-sample mixture contacted the combustion tube reducing its melting point

and occasionally causing fractures. Even when the combustion tube did not break, it was contaminated by those fumes carrying severe memory effects. To avoid these problems, we attempted to use a smaller disposable quartz tube around the boat. This solution was not successful as the addition of the disposable liner severely reduced the sample size which could be handled.

2.3 CURRENT EXTRACTION METHOD.

2.3.1 Introduction.

After trying the methods described above we started experimenting with a new method. The sample and CuO are introduced into a quartz tube which was evacuated while it was baked at 600^{o}C. Anthracite is then added and the tube sealed under vacuum. Then the tube was baked at 1000^{o}C for 3 hours in a muffle furnace.

With this method we have been able to reduce the background since we have minimized the surface areas involved and those are exposed to air for a shorter time than in the earlier methods. Another important improvement is the higher ^{14}C yields obtained with this method in comparison with the methods tested earlier. We believe that one important reason for this is that inside the muffle furnace the samples are heated uniformly to 1000^{o}C during the baking period. Another advantage of this method is the

possibility of processing several samples at the same time.

In the next few sections, we will describe this new method in detail. We will also discuss the steps taken to minimize the background. Additionally, the tests carried out to ensure the efficiency of the method will be described.

2.3.2 Description of the method.

The samples were weighed and they were crushed in a steel mortar inside of a glove bag with argon. Each sample was crushed to a powder size smaller than 180 microns. The sample and CuO, acting as oxidizer, were mixed and introduced into a 9 mm quartz tube. In some cases, which we will discuss later, the mixture was then prebaked under vacuum at 600^{o}C for half an hour. Anthracite or graphite, used as a carrier, was added to the mixture. The tube with the mixture was then sealed while being evacuated. In the case of the obsidian samples, the 9 mm quartz tube with mixture (sample, CuO and, anthracite) was placed inside a 12 mm quartz tube and then sealed under vacuum. This was done because the samples tended to react with the tubes during the bake, breaking them and allowing the CO_2 to escape. The outer tube ensured the collection of the CO_2. This method of double tubes was only used with the reacting samples because the outer tube increases the surface areas involved and, therefore, the background.

The tubes (or tube) were then baked for 3 hours at 1000^{o}C in a muffle furnace. After the bake, the tubes were introduced into a metal cylinder (or breaker). After evacuation, the quartz tubes were then broken allowing the CO_2 to be released into the vacuum line where it was collected in a liquid nitrogen trap. The device was designed in such way that the tubes could be broken maintaining the vacuum conditions in the interior of the cylinder or breaker.

The CO_2 was then graphitized using the method developed by Vogel et al. (Vo84) (Vo87). The ^{14}C concentrations were measured using the Simon Fraser University A.M.S. facility at McMaster University Tandem Accelerator Laboratory. The details about the A.M.S. technique and facility used are described in Appendix I.

2.3.3 Background.

In this section, we will discuss the different steps we decided to use in our sample preparation method to minimize the background contributions.

The major source of background in the sample preparation process comes from the adsorption of CO_2 from the air by the surface areas involved in the process. In general, we have detected a great affinity for silicate material to adsorb CO_2. Therefore it was necessary to

reduce the surface areas and to minimize the time that the samples were exposed to air.

We have distinguished between two sources of background:

1. The contribution due mostly to the adsorption of CO_2 from air by CuO powder or by any surfaces of the quartz tubes used.

2. A second contribution from the adsorption of C or CO_2 from air by the samples themselves during the sample preparation process.

In the first case, to reduce any possible contamination from the quartz tube, prior to their use the tubes were air baked for 3 hours at 1000^{o}C in a muffle furnace and stored under water vapour. It has been found (Vo87)(Zu82) that water vapour will exchange with any remaining CO_2 on the quartz surfaces, possibly due to stronger bonds existing between the surface and water rather than with CO_2 molecules.

To eliminate any type of contamination from the CuO, this was crushed to a fine powder and then baked for 1 hour at 1000^{o}C in air in a muffle furnace prior to being used. After the bake, CuO was stored in air tight bottles. We have tested the need for a later bake of the CuO just before it would be mixed with the sample and the carrier to eliminate the adsorbed CO_2. For this we prebaked samples of CuO at 600^{o}C for half an hour under vacuum. After cooling

it down, 0.5 g of anthracite are added and the tube was sealed. CuO and anthracite samples are baked at 1000°C for 3 hours in a muffle furnace. In table 2.1, we show the ^{14}C concentrations found from this process compared with the ^{14}C concentrations found in samples of CuO which did not receive the 600°C vacuum prebake. There is a substantial difference between both results which indicates the need for such a prebake of CuO. Note that some of the ^{14}C concentration found in the prebaked samples could be due to CO_2 being adsorbed by the surface of the quartz tubes and released during the high temperature bake.

TABLE 2.1. ^{14}C concentrations found in Anthracite and CuO samples when the CuO is prebaked at 600°C and with no prebake.

Sample type	Atoms of ^{14}C found with CuO prebake	Atoms of ^{14}C found without CuO prebake
CuO + anthracite	$(7\pm2)\times10^{5}$	$(1.3\pm0.2)\times10^{6}$

To minimize the background contribution from the quartz samples we proceeded as follows:

First, the quartz plates and chips used in the

irradiation experiments were baked in air for 3 hours at 1000°C in a muffle furnace to eliminate any contaminant present before the irradiations took place. After the irradiations the quartz plates and chips were stored under argon in sealed plastic bags. One of the most likely sources of contamination could come from the adsorption of CO_2 or other gases containing carbon present in air while crushing the sample. To reduce this problem, the samples were crushed inside a glove bag under argon. To further eliminate any CO_2 adsorbed by the quartz samples, we have tested the effects of prebaking the samples at 600°C before the high temperature bake.

For the first of these tests, we measured the ^{14}C concentration in proton-irradiated quartz plates. These were processed in two ways:

- Prebaked: after the sample is crushed, we mixed it with CuO and in a 9 mm quartz tube, the mixture was baked at 600°C for half an hour under vacuum conditions. Once the mixture was cooled down, it was brought to atmosphere pressure using oxygen gas. Then graphite carrier was quickly added to the mixture and the tube was sealed under vacuum. The tube containing the sample, CuO and, graphite was baked at 1000°C for 3 hours in a muffle furnace.

- Non-prebaked: after the CuO was prebaked at 600°C under vacuum in the 9 mm quartz tube, the sample, CuO and, graphite were simply mixed and the tube sealed under vacuum.

The tube was then baked for 3 hours at 1000°C in the muffle furnace.

The results are shown in table 2.2. The background contribution, $(7.1\pm0.5)\times10^{6}$ atoms of ^{14}C, from CuO, carrier and tubing have been subtracted. Notice that this background level is much higher than that shown in table 2.1. This is because the plate samples contained large amounts of ^{14}C and it was necessary to dilute this with large quantities of graphite carrier to avoid contaminating the sample line.

TABLE 2.2. ^{14}C concentrations from two proton irradiated quartz plates when they underwent a prebake at 600°C before the 1000°C bake and no prebake.

Type of sample	^{14}C Concentration with no prebake (atoms g^{-1})	^{14}C Concentration with prebake (atoms g^{-1})
QP#2	$(2.3\pm0.1)\times10^{8}$	$(2.1\pm0.1)\times10^{8}$
QP#3	$(2.8\pm0.1)\times10^{8}$	$(2.4\pm0.4)\times10^{8}$

Two samples from the same quartz plate, QP#3 (third plate from the front of the stack), were used for one of the prebake results. Therefore the uncertainty of the number was calculated using the difference between the results

obtained from the two samples. All other concentrations were based on one measurement and the uncertainties were mostly due to those of the background subtraction. For each plate, the results from the baked and unbaked samples agreed to within the uncertainties. Based on these results we decided not to prebake the proton irradiated quartz plates.

As the quartz chips irradiated with 35 MeV neutrons, contained much lower ^{14}C concentrations than those in the quartz plates, the effects of a 600^{o}C prebake could have been very different. Therefore we followed a similar study with the quartz chips as we have described above for the quartz plates. The results are shown in table 2.3. The background contribution, $(7\pm2)\times10^{5}$ atoms of ^{14}C, from CuO, anthracite and tubes has been subtracted. As we can see there are significant differences between the results obtained from the prebaked and non-prebaked samples. These differences indicate the need for the prebake of this type of samples to be able to eliminate the adsorbed CO_2 or C from the air.

The obsidian samples were prebaked based on the studies carried out by Des Marais (De83) and Swart et al. (Sw83) in meteorites. They showed that the carbon released below 600^{o}C from those samples was not of cosmogenic origin. The concentrations of ^{14}C released during the prebake were measured in several obsidian samples, giving a $^{14}C/^{12}C$ ratio of $(1.18\pm0.04)\times10^{-12}$. This indicates that the main source

was air adsorption, since the ratio is equal to the $^{14}C/^{12}C$ ratio present in the atmosphere today (1.18×10^{-12} (Sg83)) to within the experimental uncertainty.

TABLE 2.3. ^{14}C concentrations obtained from neutron irradiated quartz chips when they are prebaked at 600°C before the 1000°C bake and when they are not prebaked.

Type of sample	^{14}C Concentration with no prebake (atoms g^{-1})	^{14}C Concentration with prebake (atoms g^{-1})
Unirradiated	$(1.6 \pm 0.4) \times 10^6$	$< 1 \times 10^5$
Background Irradiation	$(2.0 \pm 0.1) \times 10^6$	$(3.9 \pm 0.6) \times 10^5$
Neutron Irradiation	$(3.3 \pm 0.1) \times 10^6$	$(1.3 \pm 0.1) \times 10^6$

The background contributed by the tube, CuO and carrier was subtracted as total atoms of ^{14}C since the amount of carrier used was very similar for a given type of sample. The background from adsorption of CO_2 and other gases containing carbon from air by the quartz and obsidian samples was subtracted as atoms of ^{14}C per gram of sample, since the sample weights varied. To reduce the handling of the samples during the crushing and weighting to a minimum,

we did not try to adjust the sample weights to get them the same.

As each of our experiments were carried out under different conditions we will dedicate a section in each of the corresponding chapters to explain what background was taken into consideration and how the correction was done for each case.

2.3.4 Extraction efficiency.

In this section we will discuss the tests carried out to ensure that the sealed tube combustion method was efficient in extracting the ^{14}C from the samples. Tests undertaken to show that the ^{14}C was not lost during the sample processing will also be discussed.

For those tests, samples of quartz plates irradiated with protons were used since the ^{14}C concentrations on them are high enough to display any variation easily. In some specific cases the quartz samples irradiated with neutrons as well as the obsidian samples were also tested.

A study of the optimum amount of CuO was done. If not enough CuO was used with the samples, not all the carbon released from the samples would get oxidized and consequently some would be lost. Relatively large amounts of CuO are needed because all our samples are crushed to a fine powder so we have to be sure that it is in good contact with CuO to obtain the maximum oxidation benefits. On the

other hand too much CuO would increase the background due to adsorption of CO_2 by the CuO used.

Obsidian samples were crushed under argon and mixed with different amounts of CuO (previously prebaked at 600°C) and same amounts of anthracite (approximately 0.5g). The mixture was introduced into the 9 mm quartz tube and sealed under vacuum. In these cases the tube with the mixture was introduced into a 12 mm quartz tube which was also sealed under vacuum. The sample mixture was baked at 1000°C for 3 hours. Table 2.4 shows levels of ^{14}C in obsidian samples after the background contributions from the CuO and the anthracite were subtracted from the total number of ^{14}C

TABLE 2.4. ^{14}C concentration found in obsidian samples for different ratios of CuO weight to sample weight.

$\frac{\text{CuO weight}}{\text{Sample weight}}$	^{14}C Concentration (atoms g^{-1})
2	$(2.5\pm0.1)\times10^6$
3	$(2.9\pm0.1)\times10^6$
4	$(2.9\pm0.2)\times10^6$
5	$(2.3\pm0.2)\times10^6$
6	$(1.8\pm0.2)\times10^6$
7	$(2.2\pm0.1)\times10^6$

atoms detected. The results show that the concentrations did not increase above a 3:1 ratio. We do not have an explanation for the lower value found using a ratio of 6, but it could have been due to the fact that the sample may not have been crushed uniformly enough. At the time of this test we had not carried out any test for the optimum powder size and we did not sieve the samples. We concluded that the best ratio was to mix two to three times as much weight of CuO as weight of the sample.

A study of the optimum powder size was carried out using the proton-irradiated quartz plates. Table 2.5 shows the concentrations found in quartz plate samples crushed and sieved at three different powder sizes. The ^{14}C concentrations found in the plate A samples crushed to sizes

TABLE 2.5. ^{14}C concentrations found in two quartz plates crushed and sieved to three different powder size.

Sample	Powder size	^{14}C Concentration (atoms g^{-1})
Plate A	<325 μm	$(3.5\pm0.1)\times10^{8}$
Plate A	<250 μm	$(3.6\pm0.1)\times10^{8}$
Plate B	unsieved	$(2.6\pm0.1)\times10^{8}$
Plate B	<180 μm	$(3.1\pm0.1)\times10^{8}$

smaller than 325 μm and 250 μm were similar. However the crushing of the powder to less than 180 μm increased the concentration found in the unsieved plate B samples by 19% for which similar concentrations to plate A were expected. We did not investigate smaller sizes because we believed that the use of finer powder would increase the exposed surface areas which could possibly increase the adsorbed CO_2 from the air and therefore increase the background of the sample processing. On the basis of these tests, we adopted a sieve size of 180 μm.

The ^{14}C produced in-situ in SiO_2 could be manifested in the material in four different forms: SiC, C, CO, and, CO_2. Even though it is difficult to say in which proportions they will be present, previous studies (Ro53), (Pa60) indicated that the most likely form of ^{14}C is CO which would be oxidized easily.

The extraction of C bonded to Si seemed problematic, as the bonds of the molecule of SiC are very strong. We therefore processed a sample of pure SiC powder (Alfa products, 98.8% purity) with the sealed quartz tube combustion method described earlier in this section. A weighed amount of SiC was processed and the pressure of CO_2 released was measured and compared with the expected amount. The result was 0.6% efficiency in the extraction of the carbon. Processing the SiC with a flux consisting of a 2:1 mixture of Lead Chromate (Fisher Scientific Co., 100%

purity) and Potassium Dichromate (J.T. Baker Chemical Co., 99.9% purity) and CuO raised the yield to 70%. The next step was to process some obsidian samples mixed with these fluxes to see if the levels obtained varied much from the ones found with CuO alone. This test would allow us to determine how much ^{14}C was present in the SiO_2 samples as SiC. The ^{14}C levels found in the samples, $(1.3\pm0.1)\times10^6$ atoms of $^{14}C\ g^{-1}$, were not significantly different from those found with the sample processing with CuO alone, indicating that the low extraction efficiency for SiC could be safely ignored. The fluxes were only used for these tests since during the baking they attacked the tubes, often breaking them.

To study if the sealed quartz tube combustion method was extracting most of the ^{14}C from the samples, we processed five samples with this combustion method twice. After the CO_2 from the first bake was collected, the metal cylinder or breaker containing the tube with the sample and CuO was filled up with oxygen gas and then taken to the glove bag. There, under argon, the sample and CuO were transferred to a new quartz tube. Graphite was added in similar amounts as it was used for the first bake, 0.39±0.01 mg. Then, it was sealed under vacuum and baked for 3 hours at 1000°C. The results are shown in table 2.6.

In creating table 2.6, we have subtracted the background contribution from CuO, graphite and the tubes,

$(7.1\pm0.5)\times10^{6}$ atoms of ^{14}C, from the ^{14}C found in each of the samples. The background contribution from the possible adsorption of CO_2 by the quartz sample during the sample preparation process has also been taken into account. For this we subtracted the ^{14}C concentrations found in the unirradiated quartz plate samples after each bake from the ^{14}C concentrations on the irradiated plates. The ^{14}C concentrations shown in table 2.6 for the irradiated plates are, therefore, those produced by the irradiations. The uncertainties on the values shown in table 2.6 were due

TABLE 2.6. ^{14}C concentrations extracted from several quartz plates in two consecutive bakes. The concentration found in the blank plate has been subtracted from the concentrations measured in the irradiated quartz samples.

Sample type	^{14}C Concentration 1st bake (atoms g^{-1})	^{14}C Concentration 2nd bake (atoms g^{-1})	%
Unirradiated plate	$(3\pm2)\times10^{6}$	$<1\times10^{6}$	--
QP#9	$(6.6\pm0.4)\times10^{7}$	$(2.0\pm1.0)\times10^{6}$	3
QP#4	$(3.1\pm0.2)\times10^{8}$	$(1.7\pm0.1)\times10^{7}$	5
QP#2	$(3.2\pm0.1)\times10^{8}$	$<1\times10^{7}$	3
QP#1	$(4.2\pm0.1)\times10^{8}$	$(1.0\pm0.1)\times10^{7}$	3

to the uncertainties carried out with the background subtraction.

We concluded that one bake was enough to extract most of the ^{14}C from the samples since the ^{14}C found in the second bake averaged only (3±1)% of that found in the first bake. This percentage is within the uncertainties of the results from the first bake. We also have to take into consideration that some extra background was possibly acquired by the sample during the processing after the first bake.

The possibility of losing ^{14}C during the crushing process was also investigated, since a certain amount of the ^{14}C made would be very close to the surface of the powder grains after crushing. To test this hypothesis we placed the irradiated quartz samples in the vacuum line. The crushing was done under oxygen and the evolved gases were passed through a CuO oven in case some carbon was released as C or CO. The results are shown in table 2.7.

The results for QP#4 and for the blank plate are average measurements of two and four samples, respectively; and the uncertainties are from the spread in the individual measurements. Dead CO_2 was taken through the vacuum line following the same steps as we have done with the CO_2 released during the crushing of the sample. The amount of $(3.6\pm0.2)\times10^5$ atoms of ^{14}C found in it was used as

background and therefore was subtracted from the total amount of ^{14}C found in the carbon released during the crushing process, to give the data shown in table 2.7.

TABLE 2.7. ^{14}C concentrations found in a blank and an irradiated quartz plate while they were crushed under vacuum and during the later 1000^{o}C bake.

Sample type	^{14}C released while crushing (atoms g^{-1})	^{14}C released during the bake (atoms g^{-1})
QP#4	$(1.1\pm0.2)\times10^{6}$	$(2.5\pm0.1)\times10^{8}$
Blank plate	$(1.2\pm0.4)\times10^{6}$	$(2\pm2)\times10^{4}$

The ^{14}C released during the crushing was a very small percentage of the total ^{14}C in the irradiated samples, and was comparable to the level in the blank as well as being within the uncertainties of the concentrations in the irradiated samples. Furthermore, the concentration of ^{14}C found in the CO_2 released was modern, i.e. a $^{14}C/^{12}C$ ratio of 1.18×10^{-12}. These data showed clearly that the only carbon lost during crushing was from CO_2 in air adsorbed at the surface of the powder.

2.4 SUMMARY.

We have developed a sample preparation technique capable of extracting ^{14}C concentrations as small as 10^6 atoms of ^{14}C per gram of sample. The method was tested successfully to ensure that most of the ^{14}C produced on the sample is collected. Our major source of background during the sample preparation was found to be the CO_2 adsorbed from the air by the surfaces involved in the process. Therefore any possible improvement of the present method will have to be directed into further reducing the surface areas as well as eliminating their exposure to air.

CHAPTER 3

A MEASUREMENT OF THE $^{16}O(n,2pn)^{14}C$ CROSS SECTION

3.1 INTRODUCTION

The $^{16}O(n,2pn)^{14}C$ reaction is the main contributor to the in-situ production of ^{14}C at the surface of the Earth. Its cross section has never been measured until the present. Reedy and Arnold (Re72) published some estimated values based on the experimental results for the $^{16}O(p,3p)^{14}C$ cross section measured by Tamers and Delibrias (Ta61). Reedy and Arnold assumed that, at high energies (over 300 MeV), the behavior of the protons and the neutrons are very similar and they extrapolated at low energies from the values for the proton cross section. They increased the value of the proton cross section at low energies by a factor of five to obtain the neutron cross section. The main reasons for the differences between the neutron and proton cross sections at low energies have already been discussed in chapter 1.

Reedy and Arnold's estimates show a peak between 30 and 200 MeV. The neutron flux reaching the surface of the Earth sharply decreases above 200 MeV (see figure 3.1). Those two effects taken together indicate that 80-90% of the total ^{14}C production from the neutrons in oxygen will be

FIGURE 3.1. Reedy and Arnold's estimates of the $^{16}O(n,2pn)^{14}C$ cross section are shown. The result for the cross section at 35 MeV from this work is also given. The neutron flux at mountain altitudes is included.

$^{16}O(n,2pn)^{14}C$ CROSS SECTION

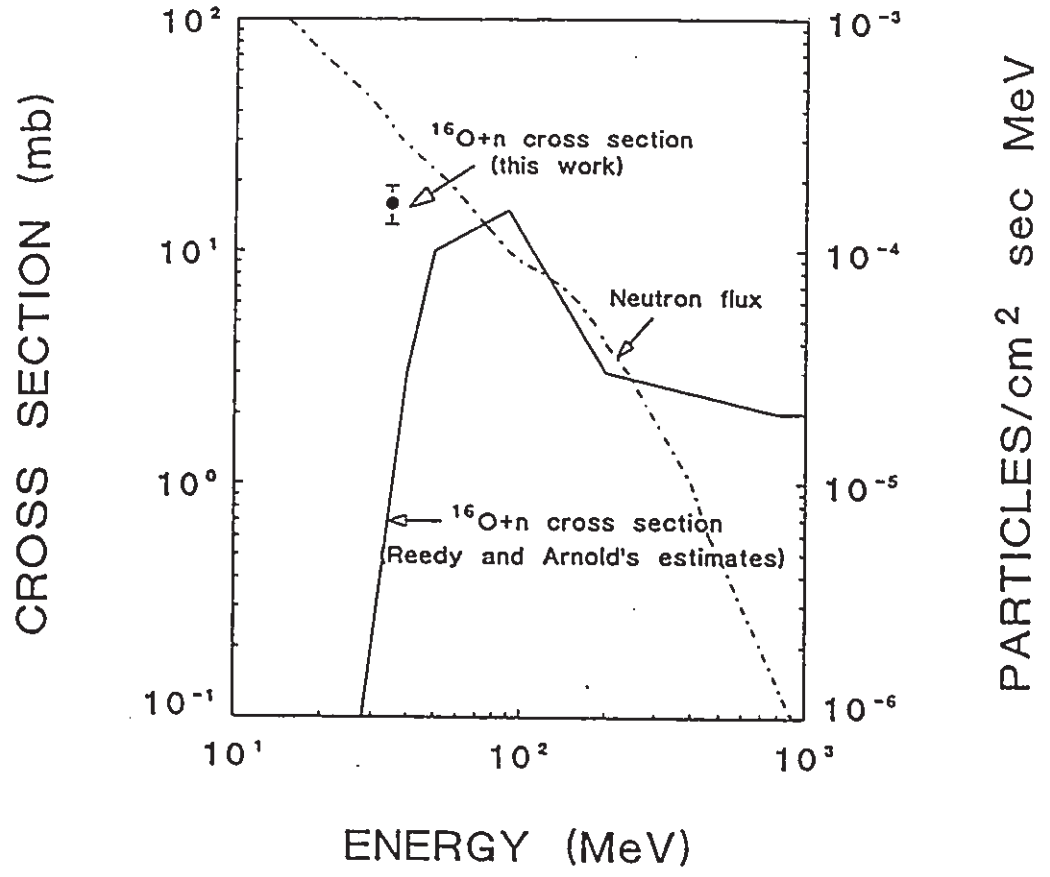

due to neutrons with energies below 200 MeV. The neutron cross section estimates (Re72) gave a threshold energy of about 24 MeV which is well above the Q value of -14.6 MeV for the $^{16}O(n,^{3}He)^{14}C$ reaction. A lower threshold energy could contribute to a larger ^{14}C production rate since the neutron fluxes have a $E^{-1.4}$ dependency with the neutron energy. Therefore we thought it would be interesting to measure the $^{16}O(n,2pn)^{14}C$ cross section at threshold energies since we had the possibility of producing 35 MeV neutrons using a beam of tritium on a deuterated target. In this chapter we will describe the techniques we followed to measure the $^{16}O(n,2pn)^{14}C$ cross section at 35 MeV.

3.2 EXPERIMENTAL SET UP

Samples of quartz chips (clear fused quartz from Quartz Scientific) and SiO_2 powder (Alfa Products -400 mesh and 99.5% purity) were irradiated with a total fluence of $(1.0\pm0.1)\times10^{11}$ neutrons cm^{-2}. From those, $(3.6\pm0.4)\times10^{9}$ neutrons cm^{-2} have energies of (35±2) MeV. The energy spread on the 35 MeV neutrons arose from the target thickness and the range of reaction angles subtended by the samples. These 35 MeV neutrons constituted just 3-4% of the total neutron production with most of the flux being lower energy neutrons from the tritium break up on the target. However, this neutron beam was easily available to us and in addition we thought it was a good test at threshold energies

which could help us to design later measurements of the same cross section at other energies. To produce the neutron beam, we used the D(t,α)n reaction. We used a 20 MeV tritium beam from the McMaster University FN Tandem Accelerator. The deuterium was absorbed in a .125mm Ti foil which was then coated with 300 angstroms of aluminum to reduce the loss of deuterium under bombardment. A similar Ti foil, this time without deuterium, was used to reproduce the neutron background spectrum. The experimental geometry is shown in figure 3.2.

The flux of neutrons was measured using a 2.3 mm polyethylene convertor and a telescope consisting of two solid state particle detectors (300 and 500 microns thick), which measured, in coincidence, the energy lost by the protons which were scattered from the convertor by the incident neutrons. A spectrum from this detector telescope is shown in figure 3.3. A Monte Carlo program was created to simulate the (n,p) scattering and neutron transport in the detector in order to calculate the efficiency of the detector system, which was found to be 2.3×10^{-2}% for the 35 MeV neutrons. More information about the computer program is given in appendix II.

As we have tested several sample processing methods, we had three groups of samples which were treated differently prior to the 1000^{o}C bake. The three groups

FIGURE 3.2. Relative positions of the targets, the samples and the detector telescope during the irradiations.

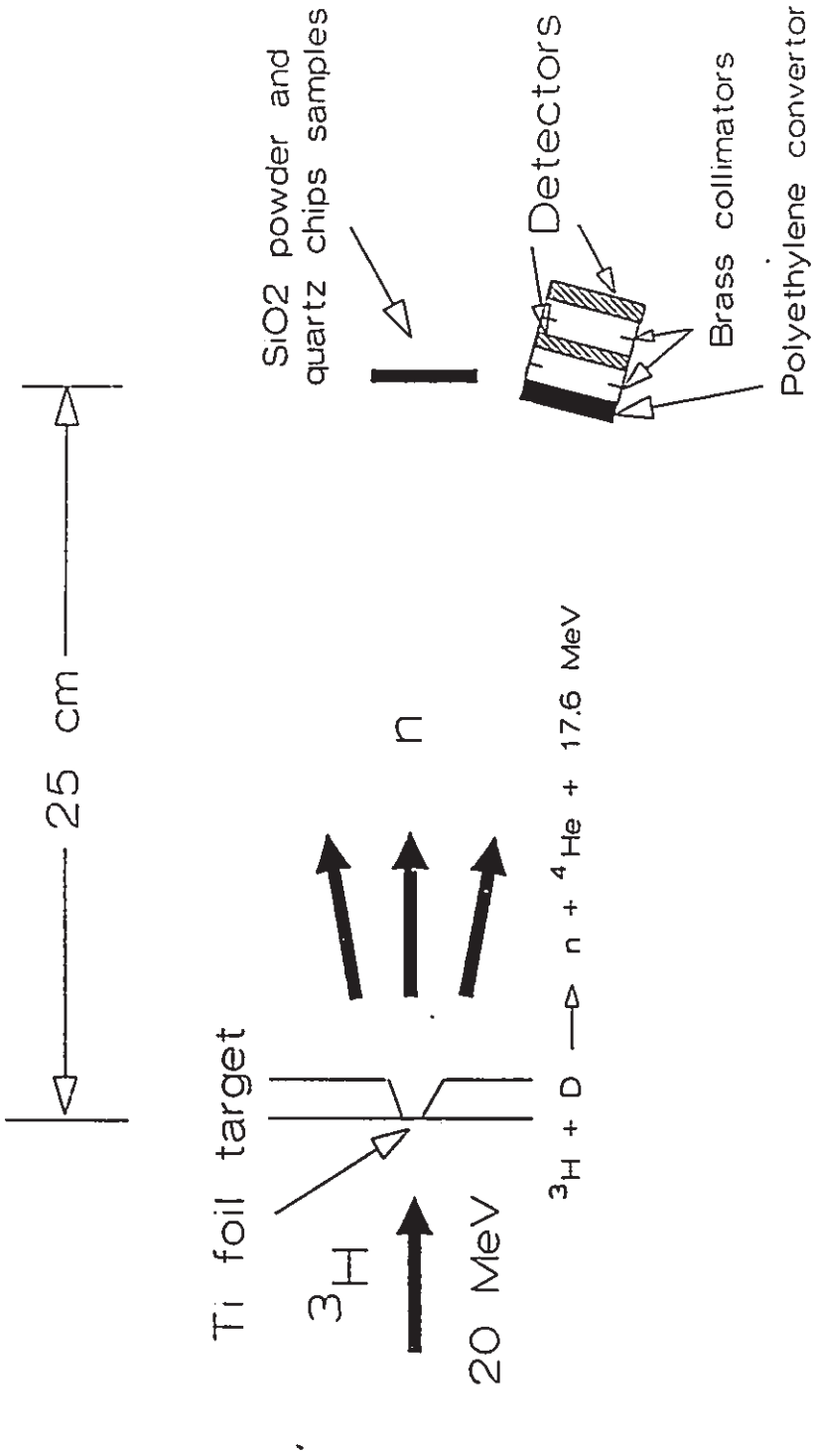
25 cm
Ti foil target
^3H
20 MeV
n
$^3H + D \longrightarrow n + {}^4He + 17.6$ MeV
SiO2 powder and quartz chips samples
Detectors
Brass collimators
Polyethylene convertor

were:

- The CuO and the sample with no prebake.
- The CuO only was prebaked at 600°C.
- Both the CuO and the sample were prebaked at 600°C.

The rest of the sample processing was identical in all three groups. Detailed descriptions of the extraction, graphitization, and ^{14}C measuring techniques are given in chapter 2. On average, the samples had a weight of 2.9±0.1 grams and 0.47±0.03 milligram of anthracite were used as dead carbon. The nominal weights for the samples and anthracite were 3 g and 0.5 g respectively and the uncertainties are due to losses in handling.

3.3 BACKGROUND

3.3.1 Introduction.

In this section we will study the three main sources of background for this experiment. An estimate of the ^{14}C levels contributed by each source also will be given.

3.3.2 Anthracite, CuO, and quartz tubing as background sources.

The ^{14}C released by the CuO, anthracite, and quartz tubing is mostly due to the adsorption of CO_2 from air. To evaluate this contribution, we processed samples of CuO and anthracite similar to those used with the quartz chips and

SiO_2 powder samples. As several quartz samples were prepared without the prebake of either CuO or the sample, we also evaluated the background contribution with no CuO prebake. The values obtained were $(1.3\pm0.2)\times10^6$ atoms of ^{14}C and $(7\pm2)\times10^5$ atoms of ^{14}C for no prebake and prebake of CuO respectively. The uncertainties in those numbers were calculated based on the differences between the results obtained from several samples.

3.3.3 Adsorption of carbon by the samples.

The second source of background to be considered is the adsorption of CO_2 and other gases by the quartz chips and SiO_2 powder during the sample preparation process. This is indeed a major source of background for our experiment. We tried to minimize this effect by storing the quartz chips and the SiO_2 powder under argon and by crushing the quartz chips samples inside a glove bag with argon. We have previously shown that a prebake of the samples at 500^oC removed any adsorbed CO_2 without losing a substantial amount of carbon made in the sample during the irradiation (see chapter 2). To examine the contribution from this background source, we measured the ^{14}C concentration in blank samples of quartz chips and SiO_2 powder processed both with and without a prebake. The results are shown in table 3.1 and table 3.2 for the quartz chips and SiO_2 powder samples respectively. The background contribution from the

TABLE 3.1. ^{14}C concentrations found in irradiated quartz chip samples and blanks. The different ways of sample preparation are indicated as well as the time when they were processed. The background level from the anthracite, CuO, and tubing has been subtracted.

Type of samples	^{14}C Concentration atoms per gram of sample			
	CuO + sample no prebake	CuO + sample no prebake 4 months later	CuO prebaked sample not prebaked	CuO + sample prebake
Unirradiated	$(9.5\pm0.9)\times10^{5}$*	$(2.5\pm0.5)\times10$	$(1.6\pm0.1)\times10^{6}$*	$<1\times10^{5}$*
Undeuterated target	$(2.0\pm0.1)\times10^{6}$*	$(1.4\pm0.3)\times10^{6}$	$(2.0\pm0.1)\times10^{6}$*	$(3.9\pm0.6)\times10^{5}$*
Undeuterated target (double nC)	$(1.6\pm0.1)\times10^{6}$	------	------	------
Deuterated target	$(2.9\pm0.1)\times10^{6}$*	$(2.7\pm0.1)\times10^{6}$*	$(3.3\pm0.1)\times10^{6}$*	$(1.3\pm0.1)\times10^{6}$*
Deuterated minus Undeuterated	$(9\pm1)\times10^{5}$	$(1.3\pm0.3)\times10^{6}$	$(1.3\pm0.1)\times10^{6}$	$(9\pm2)\times10^{5}$

* Value based on one measurement.

TABLE 3.2. ^{14}C concentrations found in the irradiated SiO_2 powder samples and blanks. The background from the CuO, anthracite and tubing has been subtracted.

Type of targets	^{14}C concentrations atoms per gram of sample: CuO + sample no prebake	CuO + sample no prebake 4 months later
Unirradiated	$(1.7\pm0.1)\times10^{6}$	$(4.8\pm0.8)\times10^{5}$
Undeuterated target	$(1.8\pm0.1)\times10^{6}$	$(1.0\pm0.2)\times10^{6}$
Deuterated target	$(3.7\pm0.1)\times10^{6}$	$(1.5\pm0.1)\times10^{6}$
Deuterated minus Undeuterated	$(1.9\pm0.1)\times10^{6}$	$(5\pm2)\times10^{5}$

first source of background mentioned above has been subtracted.

As part of the test carried out to check if we were losing any CO_2 while crushing the samples, we exposed SiO_2 powder (Alfa Prod. -400 mesh, 99.5% purity) to air in the laboratory for 24 hours. The intention was to find an accurate $^{14}C/^{12}C$ ratio in the air of the laboratory. Since dry ice was kept in the room more ^{12}C than normal was present and so we expected to obtain a ratio slightly lower than $1.18x10^{-12}$ which is the standard ratio for air in 1988 extrapolated from (Sg83). The result was four times the expected value of $1.18x10^{-12}$. In view of this result we decided to investigate the source of such high ^{14}C levels. The nearby nuclear reactor was an obvious possible source, and we also discovered that two solvent storage rooms in the basement below our sample processing laboratory contained waste compounds used as biomedical ^{14}C tracers. We placed saturated solutions of Barium Hydroxide (B.D.H. Chemicals) and samples of SiO_2 powder in four different places: 1. the nuclear reactor building, 2.the solvent storage rooms, 3. in the sample laboratory, and 4. in a place outside of campus. Additionally, samples of tree leaves were collected from around the nuclear reactor and outside the sample lab window.

The Barium Hydroxide reacts with the CO_2 in the air precipitating into carbonate, from which the carbon can be

easily extracted. The carbon from the SiO_2 powder was extracted following the sample preparation method used in this work. With the exception of one of the solvent storage rooms and the sample laboratory, all the other samples collected gave $^{14}C/^{12}C$ ratios similar to $1.18x10^{-12}$. The $^{14}C/^{12}C$ ratio obtained from the Barium Hydroxide solutions exposed in the solvent storage room and in the laboratory also had similar values to $1.18x10^{-12}$. Only the $^{14}C/^{12}C$ ratio found in the SiO_2 powder samples in both places were 3-4 times $1.18x10^{-12}$. We therefore concluded that the source for those high ^{14}C levels was in the solvent storage room and due to a poor design of the ventilation system, the air from those rooms was taken to a vent just outside of the laboratory window. Because the differences between the barium hydroxide and the silicate powder results, it is obvious that the ^{14}C does not come as CO_2. We believe that it was released as volatile fragments of the stored organic compounds, due to their breakdown by autoradiolysis.

To fully understand the characteristics of this fine silicate powder as adsorber of environmental carbon, further study will be required. In our particular case, this affinity for the adsorption of carbon is expected to produce great problems finding the real background of the powder samples since the ^{14}C levels from those compounds were variable with time as wastes were added and removed.

Another effect we observed in the SiO_2 powder was

that samples measured four months after the irradiations took place had lost significant amounts of the ^{14}C originally measured. The samples were stored under argon during that period of time, and we believe that significant quantities of ^{14}C were lost during that period as CO_2 diffused out of the fine (more than 50% is smaller than 25μm radius) powder. This same effect was not seen in the case of the quartz chips because they were stored as chips rather than as powder. The exposed surface area was a lot smaller, and only a thin surface layer was affected by diffusion losses.

The fused quartz contains micro-voids on a molecular scale which may allow easy transport of carbon and CO_2. These are absent from the more regular structure of crystalline quartz and are plugged by cations in glasses. Hence, the losses may only occur in fused quartz. Nevertheless, the measurement of in-situ production as a dating tool should be approached with caution until further studies have established the magnitude of this effect in other materials.

3.3.4 Secondary reactions.

The third source of background came from the ^{14}C production from reactions other than the one under study in this chapter. This is a contribution that should be carefully considered due to the large number of non-35 MeV

neutrons present in the irradiation. Those could contribute to the production of ^{14}C through reactions such as: $^{16}O(n,2pn)^{14}C$ (from non-35 MeV neutrons), $^{13}C(n,\gamma)^{14}C$, $^{14}N(n,p)^{14}C$, $^{17}O(n,\alpha)^{14}C$ and $^{28}Si(n,^{14}C)^{15}O$.

To evaluate the ^{14}C production from neutrons with energies other than 35±2 MeV, we irradiated the same types of samples with neutrons produced with the same tritium beam reacting with the undeuterated Ti target. Initially we did this type of irradiation for the same integrated beam current as we used with the deuterated target. However, the spectra from both types of irradiations showed that the production of low energy neutrons using the deuterated target was double that of the undeuterated target. These additional neutrons from the deuterated target were caused by deuteron break up and hence were not accounted for in the irradiation of the undeuterated Ti. Therefore we irradiated quartz chip samples with neutrons from the undeuterated target for double the integrated charge used originally to obtain a better background estimate. The ^{14}C concentration found in these samples did not show significant differences from those found in the earlier irradiation. The results are shown in tables (3.1) and (3.2) for the quartz chips and SiO_2 powder samples respectively.

In later calculations, we used the Monte Carlo program to simulate the energy spectra obtained from the irradiations carried out with the deuterated and

undeuterated targets. We placed four windows in the spectrum and found the number of counts in each. To build the simulated spectrum, we used the same windows and, added simulated spectra from different energies, starting with the highest. This process continued until the number of counts in each window and the intensity variations within the window were correct. Because of the thickness of the convertor and the thickness of the detectors, the lowest energy detectable was 7 MeV. Therefore to find the number of neutrons between 6 and 3 MeV, we used additional spectra obtained using a 0.01 mm thick convertor and a first detector just 25μm thick. The spectra obtained from the thicker detectors are shown in figure 3.3 and figure 3.5 for the deuterated and undeuterated target irradiations respectively. The spectrum simulations obtained with the Monte Carlo program for those irradiations are shown in figure 3.4 and figure 3.6. In the spectrum the high energy neutrons (36-34 MeV) are shown at the bottom of the left arm. When the high energy recoil protons go through the detectors they lose only a small fraction of their total energy. The energy losses in both detectors increase as the proton energy falls, and the protons lose more energy in the second detector than in the first detector since they have lower energy in the second one. This effect is what makes the left arm shape of the spectrum. Recoils from the neutrons with energies below 15 MeV are shown in the right

FIGURE 3.3. The energy loss in the second detector versus the energy loss in the first detector for recoil protons from the convertor, for the deuterated target. A total of 69,646 nC were considered in this spectrum. The energy scale is 128 keV per channel in both axes. The number of counts in each channel is between 2^N and 2^{N+1}, where N is the numbers shown in the spectrum. The box indicates the counts corresponding to 35±1 MeV.

FIGURE 3.4. Monte Carlo simulation of the energy spectrum shown in figure 3.3.

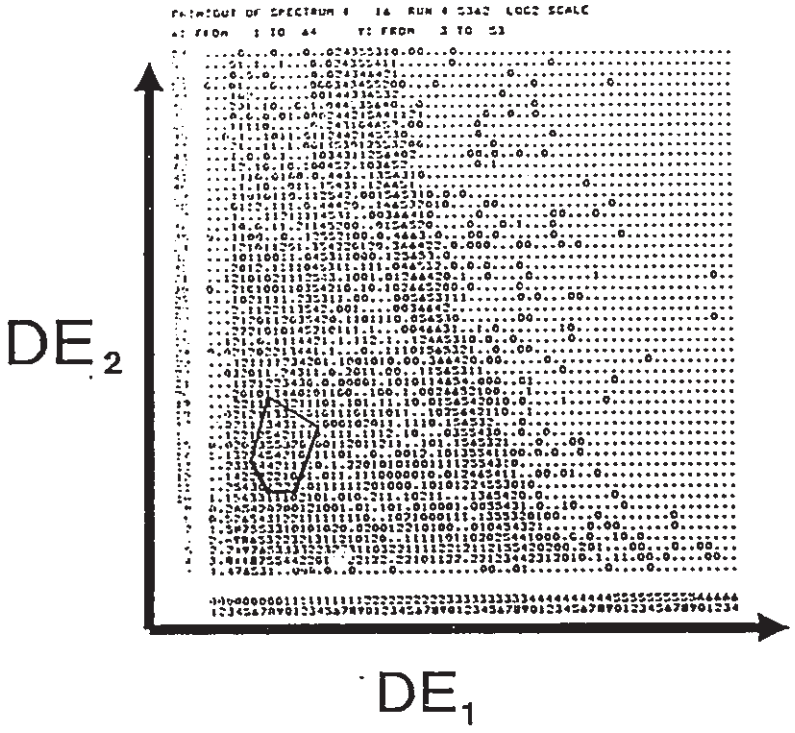
DE2
DE1

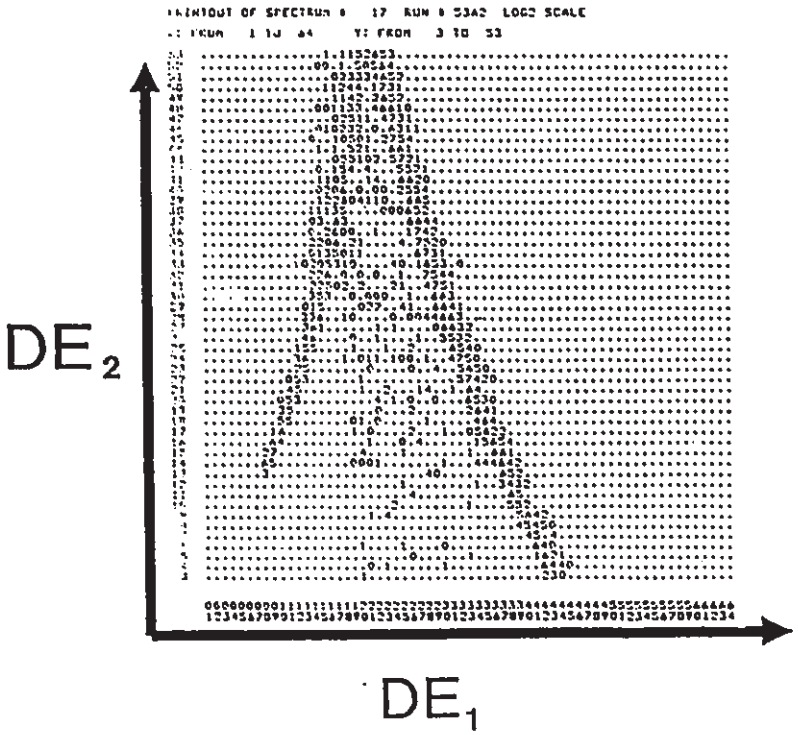
DE2
DE1

FIGURE 3.5. Energy spectrum for the undeuterated target. A total of 79,844 nC were considered for this spectrum. Note the smaller number of neutrons in the energy range of 34-36 MeV compared with figure 3.3.

FIGURE 3.6. Monte Carlo simulation of the energy spectrum shown in figure 3.5.

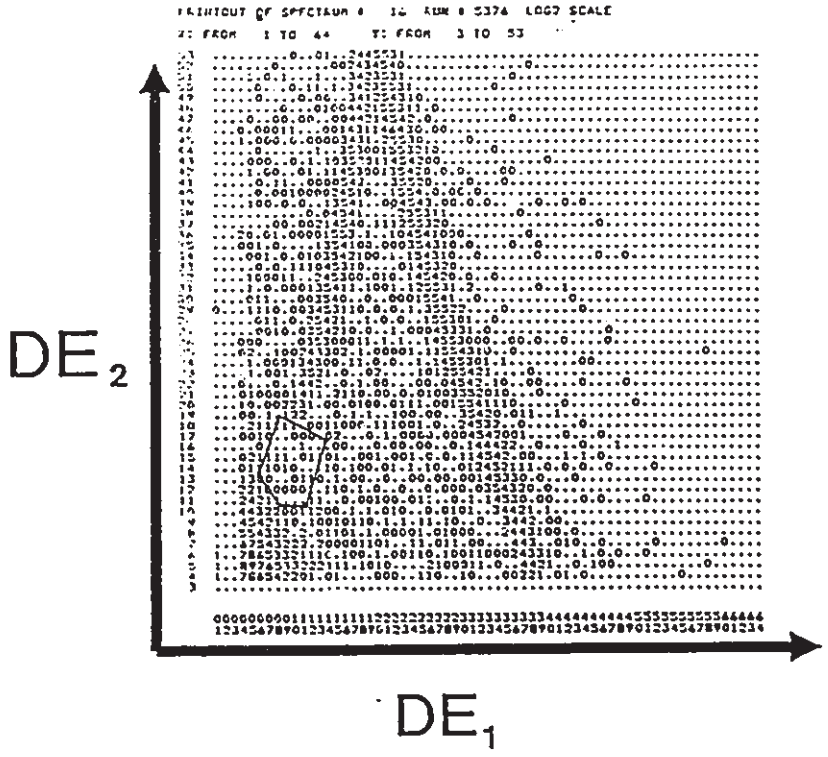
DE2
DE1

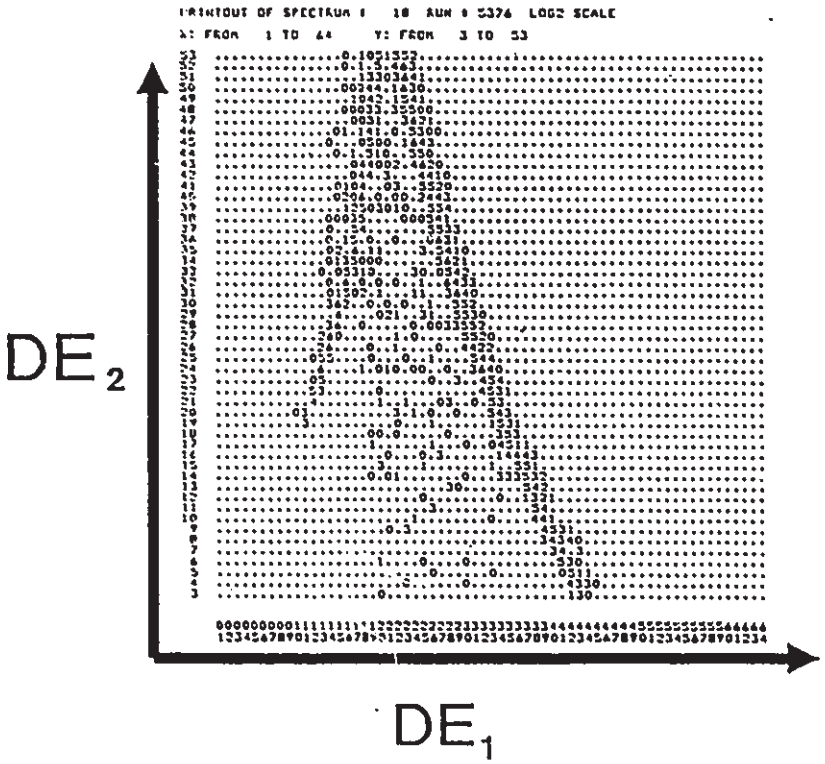
DE2
DE1

arm of the spectrum. Here the protons stop in the second detector, more and more of the total energy is lost in the first detector as the proton energy decreases. The additional low energy neutrons made with the deuterated target, which are not seen with the undeuterated target, have energies below 12 MeV and therefore appear in this right arm of the spectrum. Off-arm events in the simulated spectra correspond to recoil protons which lose a substantial amount of their energy going through a portion of the brass collimator. The wider arms observed in the spectra from the detectors relative to the simulation are caused by the finite detector resolution. Notice also the presence of low-energy detector noise which is not seen in the simulation.

The results were extrapolated to the total number of $1x10^5$ nC in both irradiations to estimate the neutron energy distributions, which are shown in figure 3.7 and figure 3.8. We estimate that the results for any one energy have at least a 20% uncertainty. However they give us an idea of the differences between the spectra for the irradiations carried out with either target. From 12 to 3 MeV, we see that the number of neutrons from the deuterated target is approximately double those from the undeuterated target, which confirms our earlier estimates. Therefore the run carried out with the undeuterated target, for double the integrated charge, gave a good reproduction of the number of

FIGURE 3.7. Energy distribution of the neutrons produced with the deuterated target. The results have been normalized to a total of $1x10^5$ nC.

FIGURE 3.8. Energy distribution of the neutrons produced with the undeuterated target. The results were normalized to a total of $1x10^5$ nC.

NEUTRON SPECTRUM FROM
DEUTERATED TARGET

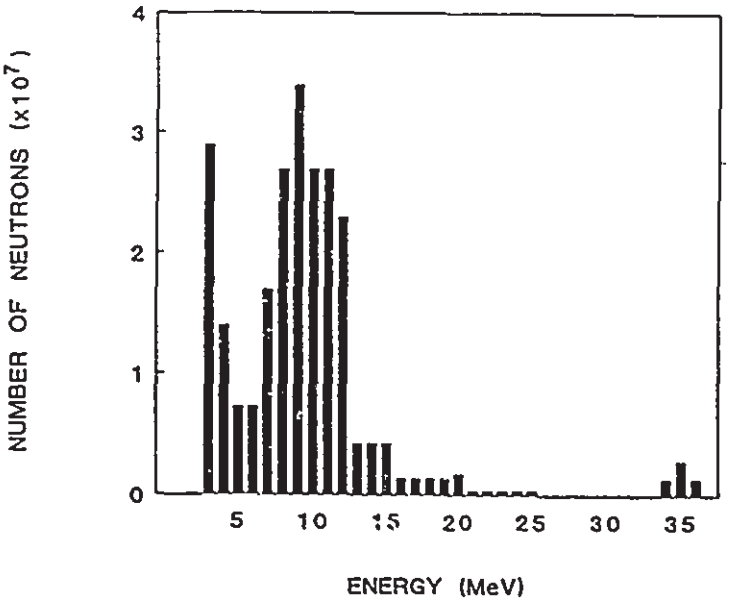

NEUTRON SPECTRUM FROM
UNDEUTERATED TARGET

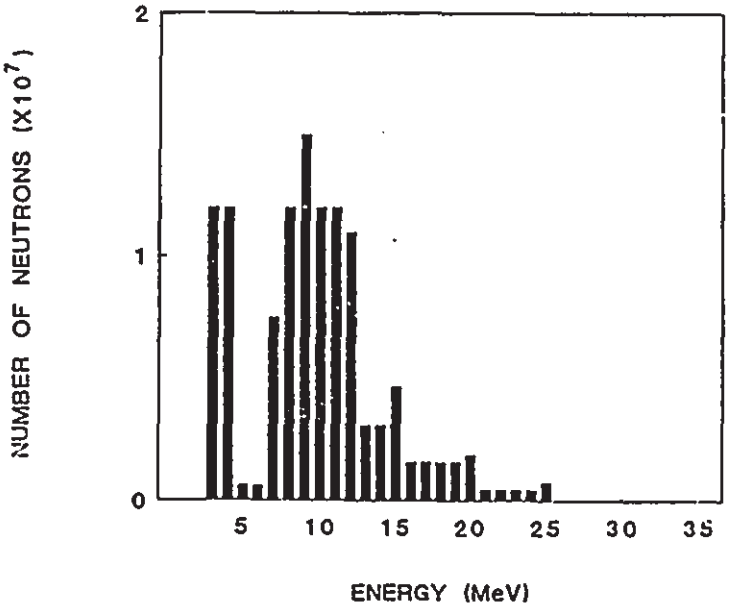

low energy neutrons produced by the deuterated target. The ^{14}C concentrations found in the quartz samples irradiated with the neutrons from the undeuterated target are good background estimates. This background should account for all those reactions produced in the samples by neutrons with energies other than 35 MeV.

In both figure 3.7 and figure 3.8, we can observe a decrease in the number of neutrons of 6 and 5 MeV and there is a sudden increase at 4 MeV and below. This effect is believed to be caused by the interaction of the tritium beam with the Ti foil used as target in both irradiations. The Ti adsorbs the tritium producing a compound state of V. During the cooling processes of heavy compound nucleus reactions, an emission of neutrons with energies of 1-3 MeV (Wa89) is observed. Neutrons boiling out with higher energies are unlikely since under the compound nucleus theory the tritium energy is distributed among a large number of nucleons of the compound nucleus. Because of the convertor and first detector thickness, the detector system could not detect particles below 3 MeV. Therefore the spectra in figure 3.7 and figure 3.8 cut off at this energy. The neutrons with energies between 25 and 12 MeV are due to reactions such as Ti(t,n). The neutrons with energies lower than 12 MeV are mostly due to (t,pn) and (t,2n) type reactions.

Some of the ^{14}C background concentrations could come

from the reactions induced by thermal neutrons. To find an approximate value for the number of thermal neutrons produced during the irradiations, we irradiated two pieces of Au foil with the neutrons from both deuterated and undeuterated targets. One foil was wrapped with a 0.5 mm Cd foil which absorbed the thermal neutrons preventing them from reaching the Au foil. The gamma activity was measured in the Au foil after each irradiation with a Ge(Li) detector. Extrapolating to the total charge with which we irradiated the quartz chips and SiO_2 powder samples, we had $(5.1\pm0.9)\times10^{9}$ neutrons cm^{-2} and $(1.0\pm0.06)\times10^{10}$ neutrons cm^{-2} for the irradiations carried out with the deuterated and undeuterated targets respectively. Notice that the value for the undeuterated target corresponds to the second irradiation in which integrated beam current was double that of the first one. From our results, we found that the number of thermal neutrons is independent of the type of target used for the irradiation but dependent on the total charge with which the samples are irradiated.

Next, we are going to study the ^{14}C contributions from several reactions which are most likely to occur during the irradiations:

<u>The $^{13}C(n,\gamma)^{14}C$ reaction</u>.

The thermal neutrons could contribute to the production of ^{14}C by the neutron capture reaction $^{13}C(n,\gamma)^{14}C$ (Q=8.18 MeV) which has a cross section of

0.91mb (Ga76). The ^{13}C could be found in the CO_2 (up to a monolayer) adsorbed on the surface of the quartz chips or the SiO_2 powder. Additionally, ^{13}C was present in the plastic bag containing the samples. Only an inner thickness of the bag equal to the range of 8 MeV ^{14}C ions in polyethylene (approximately 0.01mm) should be considered, as only the recoil ^{14}C atoms produced in that thickness would have a chance to reach and be adsorbed by the quartz samples. The ^{14}C production from the plastic bag was calculated to be 2.5±0.1 atoms of ^{14}C per gram of SiO_2 and 4.9±0.2 atoms of ^{14}C per gram of SiO_2 for the deuterated and undeuterated irradiations respectively. We have assumed that the ^{14}C produced would be distributed evenly throughout the chips or the powder. The ^{14}C production due to a monolayer of air on quartz chips was calculated to be $(2.3\pm0.4)\times10^{-7}$ and $(4.6\pm0.8)\times10^{-7}$ atoms of ^{14}C per gram of SiO_2 for the deuterated and undeuterated irradiations respectively. For the SiO_2 powder samples this contribution was found to be $(7\pm1)\times10^{-5}$ and $(1.4\pm0.1)\times10^{-4}$ atoms of ^{14}C per gram of SiO_2. The significant difference between the contribution from the quartz chips and the quartz powder is caused by the greater surface area in the powder than in the chips, 1.3×10^{3} cm^2 g^{-1} and 4.3 cm^2 g^{-1} respectively. The $^{13}C(n,\gamma)^{14}C$ cross section reaction has a resonance value of 20b at 150keV. If we consider that the number of neutrons with energies around this value was 1% of the thermal

neutrons produced in each irradiation, the ^{14}C production due to this resonance should be approximately the values given in the above cases but multiplied by 2.2×10^{2}. This is just the correction factor due to the different value of the cross section and the reduction in the number of neutrons. In both cases the contribution could be considered negligible compared to the levels obtained in the irradiated samples.

The $^{14}N(n,p)^{14}C$ reaction.

Considering a similar monolayer of N_2 on the SiO_2, the thermal neutrons could produce ^{14}C from the $^{14}N(n,p)^{14}C$ (Q=0.626 MeV) reaction which has a cross section of 1.823 b (Ga76). We have calculated that in the case of the irradiation performed with the deuterated target, the ^{14}C produced by this reaction was (130±23) atoms of $^{14}C\ g^{-1}$ of SiO_2 and $(3.0 \pm 0.5) \times 10^{4}$ atoms of $^{14}C\ g^{-1}$ of SiO_2 for the quartz chips and the SiO_2 powder samples respectively. When the undeuterated target was used for the irradiation, the ^{14}C concentration due to this source was calculated to have been (255±15) atoms of $^{14}C\ g^{-1}$ of SiO_2 and $(5.9 \pm 0.4) \times 10^{4}$ atoms of $^{14}C\ g^{-1}$ of SiO_2 for the quartz chips and SiO_2 powder samples respectively. Again these amounts are insignificant compared to the concentrations found in the samples.

The $^{17}O(n,\alpha)^{14}C$ reaction.

Another possible contribution to the production of

^{14}C could be due to the $^{17}O(n,\alpha)^{14}C$ reaction (Q=1.18 MeV),(Li87). The ^{17}O is present as 0.037% of the oxygen from the SiO_2. Even though this is a small amount of ^{17}O, the production reaction has a Q=1.18 MeV and also has a thermal cross section of 250mb (Hn61). We have estimated that the interactions of thermal neutrons with the ^{17}O in the quartz chips and SiO_2 powder would produce a total of $(1.0\pm0.2)\times10^4$ atoms of $^{14}C\ g^{-1}$ of SiO_2 and $(1.9\pm0.1)\times10^4$ atoms of $^{14}C\ g^{-1}$ of SiO_2 for the irradiations with deuterated and undeuterated targets respectively.

The $^{17}O(n,\alpha)^{14}C$ cross section should decrease with the increase in neutron energy up to the alpha particle Coulomb barrier value (about 6.3 MeV). As the neutron energy increases, the time it spends close to the nucleus decreases and so does the probability of interaction. At neutron energies of about 1 MeV the cross section is expected to have decreased to about 40 mb (assuming a probability of interaction inversely proportional to the neutron velocity). However, at neutron energies where the α energy is close to or above the Coulomb barrier there is no argument against the possibility that this reaction could have a cross section close to the thermal value (250 mb), as very few competing channels are available. In this case there would be significant contributions to the ^{14}C production from this reaction.

To find this possible contribution we irradiated 5%

^{17}O enriched water with a total charge of $(8.7\pm0.2)\times10^{6}$ nC and $(2.12\pm0.05)\times10^{7}$ nC on the deuterated and undeuterated targets respectively. The water samples were stored in 5 ml glass bottles. A few drops of 1N NaOH were added to the samples to ensure that any ^{14}C, which might have been oxidized to CO_2, would remain in solution.

The ^{14}C made in the water could be present not only as CO_2 but also as CO, and in fact CO is believed to be the most likely form for the ^{14}C produced in these reactions (La87). Because CO has a low solubility in water (Ro81), and because it cannot be frozen out at liquid Nitrogen temperatures, it is a difficult gas to handle. We had to take special care to find a method to oxidize CO into CO_2. A saturated solution of $PdCl_2$ was used for that purpose (Gr84); the reaction is:

$$CO + PdCl_2 + H_2O \text{ ----> } Pd + CO_2 + 2HCl$$

In a glove bag filled with argon gas, a mixture of 3ml of this solution and 20 drops of 0.5N HCl were introduced in a specially designed metal cylinder with the bottle containing the water samples. The strong acid solution was used to ensure that all of the CO_2 produced was evolved from the water. After evacuation, the bottle was then broken allowing the water sample to mix with the $PdCl_2$ solution. The metal cylinder was shaken thoroughly for 20 minutes to ensure good contact between the solution and any CO present. The water solution was then frozen with a dry

ice and isopropyl alcohol mixture and the CO_2 was collected using a liquid nitrogen trap. A diagram of the extraction line is shown in figure 3.9.

TABLE 3.3. ^{14}C concentrations in water samples. No background has been subtracted.

Type of sample	5% ^{17}O enriched water (atoms of ^{14}C per ml)	Regular ^{16}O water (atoms of ^{14}C per ml)
Irradiated with neutrons from deuterated target	$(7.1\pm0.9)\times10^5$	-----
Irradiated with neutrons from undeuterated target	$(1.6\pm0.2)\times10^6$	$(6.2\pm0.9)\times10^5$
Unirradiated	$(1.2\pm0.5)\times10^6$	$(4\pm3)\times10^5$

The efficiency of the method was tested using a measured volume of pure CO (Canada Liquid Air, 99.5% purity) and was found to be (100±10)%. Samples of distilled water were processed to obtain the sample processing background.

As we can see from the results in table 3.3, the ^{14}C contribution from the neutrons produced in the deuteron break up was not important. The levels measured in the ^{17}O enriched water samples, irradiated with neutrons from the deuterated and undeuterated targets, are the same as the

FIGURE 3.9. Diagram of the extraction line used with the ^{17}O enriched water samples. (1) is the metal cylinder specially designed to be able to break the bottle without losing any CO or CO_2 released by the water samples. (2) is a dry ice and alcohol trap to remove water. (3) is the Liquid Nitrogen trap to condense any CO_2 released by the water samples. (4) is the measured volume where the CO_2 is collected.

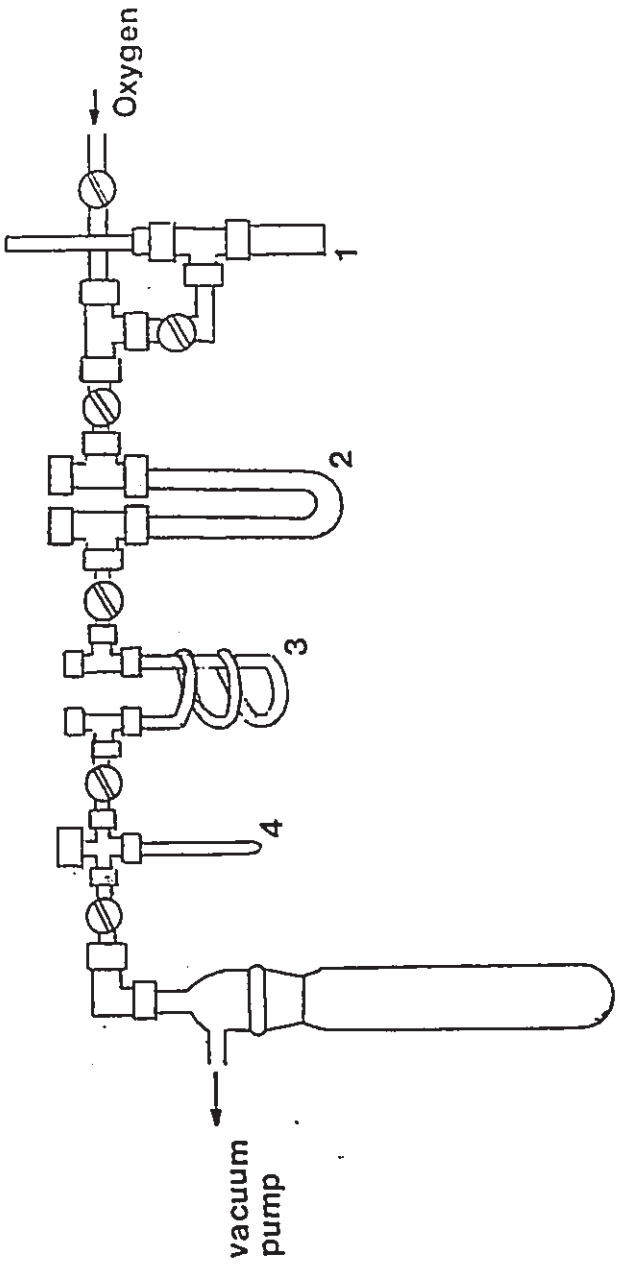
Oxygen
1
2
3
4
vacuum
pump

levels found in the background samples within the experimental uncertainties. Without background subtraction, we extrapolated to a ^{17}O concentration of 0.037% in the quartz chips and SiO_2 powder samples and to total charges of $(9.2\pm0.2)\times10^{7}$ nC and $(2.04\pm0.05)\times10^{8}$ nC. We estimated that concentrations of $(3.2\pm0.4)\times10^{4}$ atoms of $^{14}C\ g^{-1}$ of SiO_2 and $(6.2\pm0.8)\times10^{4}$ atoms of $^{14}C\ g^{-1}$ of SiO_2 were produced in the samples irradiated with neutrons from the deuterated and undeuterated targets respectively. The contribution from the $^{17}O(n,\alpha)^{14}C$ reaction is, therefore, unimportant.

The $^{28}Si(n,X)^{14}C$ reaction.

We also studied the possibility of ^{14}C production from the $^{28}Si(n,X)^{14}C$ (Q=-19.3 MeV) reaction. We estimated it to be small compared to that from the reaction studied here. This contribution could have been tested by irradiating some Si with neutrons from both deuterated and undeuterated targets and measuring the amount of ^{14}C made. Unfortunately we did not think about this possibility before the irradiations took place. However one can make a rough estimate of the contribution by taking into consideration the ^{28}Si + n total geometrical cross section and then applying the expression (Se77):

$$\sigma_i = \frac{\sigma_t}{\lambda_t}\ \lambda_i$$

where σ_i is the cross section of a particular reaction channel.

σ_t is the geometrical cross section for the reaction.

λ_t is the total number of excited states available to the reaction to breakup at a given temperature.

λ_i is the number of excited estates available to the reaction channel under study.

To find the number of available excited states we counted all the channels energetically possible. We then calculated the energy available in each channel and how many energetically possible excited states were available for the reaction products (Bw76). The higher the mass number of the target nuclei, the larger is the number of possible excited states where that nucleus could be found. At neutron energies around 35 MeV, the number of competing reactions and their possible excited states is three times larger for the $^{28}Si(n,X)^{14}C$ reaction than for the $^{16}O(n,2pn)^{14}C$ reaction. In addition, the number of energetically possible excited states of the $^{16}O(n,2pn)^{14}C$ reaction is 30 times larger than that of the $^{28}Si(n,X)^{14}C$ reaction. This calculation gives a cross section of 0.16 mb for the $^{28}Si(n,X)^{14}C$ reaction for 35 MeV neutron energy. Using this cross section estimate and taking into consideration that there are half as many atoms of Si than O in the quartz

samples, we estimate that 0.5% of the ^{14}C atoms per gram found in the quartz samples could be due to the above reaction.

4.4 RESULTS.

The ^{14}C concentrations found in the quartz chips and SiO_2 powder samples irradiated with the 35 MeV neutrons are shown in table 3.1 and table 3.2 respectively. To find the ^{14}C concentration produced by the 35 MeV neutrons, we subtracted the ^{14}C concentration found in the samples irradiated with the neutrons from the undeuterated target from the ^{14}C concentration found in similar samples irradiated with those neutrons produced with the deuterated target. All other possible background contributions discussed earlier have been considered negligible since they add less than 1% of the ^{14}C concentration found in the different samples. We have averaged the results from that subtraction for each type of sample preparation, obtaining a concentration of $(1.1\pm0.2)\times10^{6}$ atoms of $^{14}C\ g^{-1}$ of SiO_2. This value corresponds to a cross section of (16±3) mb, which is shown in figure 3.1. It was determined under the assumption that all the ^{14}C production comes from the $^{16}O(n,2pn)^{14}C$ reaction, but we estimate that the error introduced by this assumption is around 1%. The uncertainty in the cross section was calculated taking into consideration the uncertainty in the total number of 35 MeV

neutrons with which the samples were irradiated, and the uncertainty in the averaged ^{14}C measurements. To calculate this value of the cross section, we have taken into consideration only the results from the quartz chips. We did not have any SiO_2 powder sample left from the irradiations to be processed with our best sample preparation technique. We thought that the findings about the SiO_2 powder, discussed in the background section, could lead us to wrong results due to the great variability of the background values from adsorption and to the effects of diffusion losses.

Our result of (16±3) mb at 35 MeV is well above Reedy and Arnold's value of 1 mb. As Reedy and Arnold's estimates of the $^{16}O(n,2pn)^{14}C$ cross section were extrapolated from the experimental data for the $^{16}O(p,3p)^{14}C$ cross section, we do not find it surprising that our results do not agree with theirs. Our result at 35 MeV may indicate that the threshold energy, considered to be approximately at 24 MeV by Reedy and Arnold, has a lower value. Given that the Q value for the $^{16}O(n,^{3}He)^{14}C$ is -14.6 MeV, this is again not surprising. The implications of our result for the in-situ production of ^{14}C in rocks will be discussed later in chapter 5.

The main problems with this experiment were: 1) the small percentage of neutrons with the nominal energy and 2) the difficulty in lowering the background levels due to the

great affinity for the adsorption of CO_2 by the quartz materials once in the powder form. The ideal experiment would be to irradiate the samples with a much more monoenergetic beam such as those produced by the bombardment of ^{7}Li, ^{6}Li, or ^{9}B targets (Jg71). This would reduce the contributions from reactions at other neutron energies. To overcome the adsorption background problem, the ideal would be to irradiate the samples with a sufficient neutron fluence to produce ^{14}C concentrations well above the ^{14}C levels obtained from the blank samples. The major problem faced with this ideal irradiation is to find a facility which produces a monoenergetic beam ready to contribute with an irradiation which can last from a few days to more than a week depending on beam current, collimator, and target thickness used for the neutron production. However, given the difference between our result and the previous estimate, there is an obvious need for new measurements of this cross section at energies up to 150 MeV.

3.5 SUMMARY.

A value of (16±3) mb was found for the $^{16}O(n,2pn)^{14}C$ cross section at (35±2) MeV. The experiment was not the ideal one due to the great number of neutrons with other energies. However, our estimates of contributions from reactions with lower energy neutrons suggest that the

contributions are small. Our result is larger than previous estimates, and additional measurements at higher energies are clearly needed.

CHAPTER 4

MEASUREMENT OF THE $^{16}O(p,3p)^{14}C$ CROSS SECTION

4.1 INTRODUCTION.

The in-situ production of ^{14}C at the surface of the Earth is mostly due to the $^{16}O(n,2pn)^{14}C$ reaction. The contribution due to the $^{16}O(p,3p)^{14}C$ reaction is negligible, since the neutron flux at the surface of the Earth is much greater than the proton flux due to the neutron's longer range (for more details see chapter 1). However the $^{16}O(p,3p)^{14}C$ cross section has been used in the past by Reedy and Arnold (Re72) to estimate the $^{16}O(n,2pn)^{14}C$ cross section which was later used by Yokoyama et al. (Yo77) to estimate the ^{14}C in-situ production rate. The $^{16}O(p,3p)^{14}C$ reaction is therefore of interest in studies of in-situ production.

In addition, the $^{16}O(p,3p)^{14}C$ reaction is an important channel in the study of the ^{14}C production in extraterrestrial materials. In particular this cross section has been used to estimate changes in the fluxes of the Solar Cosmic Rays (Re87). In the first few centimeters below the Moon's surface, the ^{14}C production is due to GCR and SCR. Further in the SCR are stopped due to their low energies and

thus only GCR are responsible for such production. It is therefore possible to estimate the GCR contribution to the total ^{14}C production in the first few centimeters which can be subtracted from it giving the production due to SCR. The SCR proton fluxes therefore could be determined by comparing the ^{14}C activity to the SCR depth profile (Re87). This can be obtained by using the relations between ionization and energy loss.

The $^{16}O(p,3p)^{14}C$ cross section has been measured for the energy range 35 MeV to 3 GeV by Tamers and Delibrias (Ta61). However, the results had uncertainties of 25% which was due to the counting decay statistics and the uncertainty in the cross section used to find the total charge given to the samples. This is why Reedy (Re87) has pointed out the need for better measurements of this cross section.

For the above mentioned reasons, we became interested in measuring the $^{16}O(p,3p)^{14}C$ cross section since the use of A.M.S. made possible its measurement with higher accuracy. With A.M.S. we count a fraction of the ^{14}C atoms while Tamers and Delibrias observed the ^{14}C beta decay.

The range of energies relevant to the in-situ production of ^{14}C from oxygen by cosmic ray protons is determined by the shape of the cross section and of the proton spectrum at different altitudes. In figure 4.1, we show the CR proton flux at mountain altitudes and the proton cross section measured by Tamers and Delibrias (Ta61). The

FIGURE 4.1. The proton flux at mountain altitudes and 45^{o} geomagnetic latitude is plotted versus the proton energy (La67). The $^{16}O(p,3p)^{14}C$ cross section as a function of the proton energy is also given.

160(p,3p)14C CROSS SECTION
AND PROTON FLUX

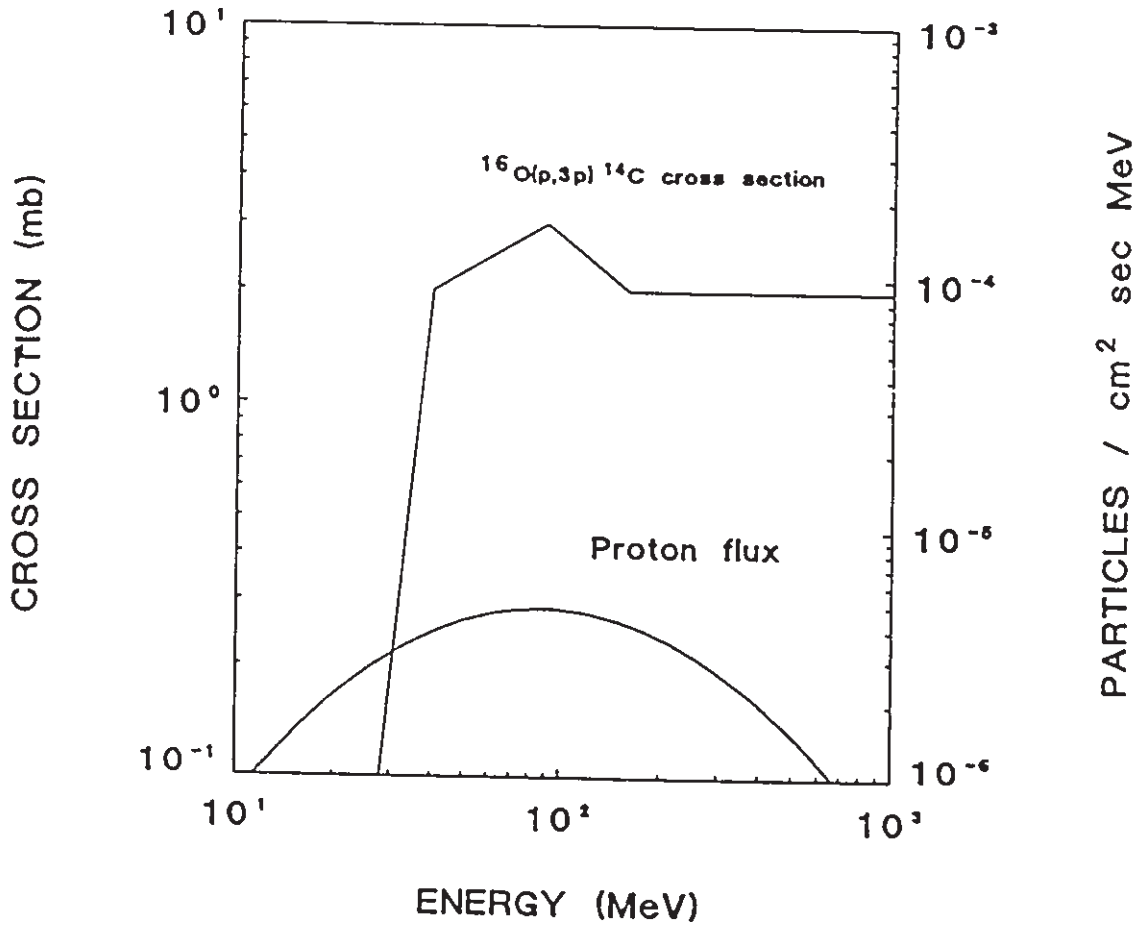

cross section data obtained by Tamers and Delibrias showed a peak between 40 and 150 MeV of 3 mb. As a result of the presence of this peak in the cross section and the fall off in intensity of the proton flux above 300 MeV, most of the production from $^{16}O(p,3p)^{14}C$ occurs at energies below 200 MeV. This is also the range at which the neutron production of ^{14}C from oxygen has been estimated to be important (see chapter 3). Also, SCR protons predominantly have energies below 100 MeV (Re83). Therefore, the relevant energies at which to measure the $^{16}O(p,3p)^{14}C$ cross section are also below 200 MeV.

In this chapter we will show the results from measurements of the $^{16}O(p,3p)^{14}C$ cross section below 63 MeV. To measure the cross section at different energies, we placed a sufficiently thick stack of quartz plates in the proton beam to stop the incident protons. We have recently irradiated a stack of quartz plates with 200 MeV protons at TRIUMF, so in the near future we will be able to extend the cross section data up to 200 MeV.

4.2 EXPERIMENTAL TECHNIQUE.

Two stacks of 17 plates (clear fused quartz, from Quartz Scientific) each of dimensions 1/4x1x1 inches, were irradiated with (63.0±0.2) MeV protons at the Crocker Nuclear Cyclotron at the University of California at Davis.

The 17 plates were tightly packed and held together with thick aluminum foil with the front and back faces left open. Each stack was placed in the experimental line where irradiations were routinely done. The proton beam had a radius of 2.5 cm and was centered on the plates to within 3 mm. The intensity profile of the beam had been measured by means of the thermoluminiscence technique with an uncertainty of 15% (Ca87). The profile is shown in figure 4.2. Using these data, the total fluences of protons irradiating the stacks were calculated as (10.7±1.6) and (10.3±1.5) microcoulombs for stack 1 and 2 respectively.

The transverse and longitudinal straggling of the proton beam were estimated for our beam in the quartz material using data from Littmark and Ziegler (Li80) for protons in oxygen and silicon. We calculated a longitudinal straggling of 0.02 cm and a transverse straggling of 0.06 cm. These results are not significant since the beam of 2.5cm in radius was centered on the square plates which were 2.54 cm on each side, so proton losses out of the side of the stack were small.

In figure 4.3, the proton range versus the proton energy is plotted (Al64). As the plates were thin, a good estimate of the mean energy for each plate was simply the mean of the initial and final energies.

Each plate was cut into four pieces, each of which typically corresponded to a sample of 0.5 g of SiO_2. The

FIGURE 4.2. Profile of the proton beam at the Crocker Nuclear Laboratory.

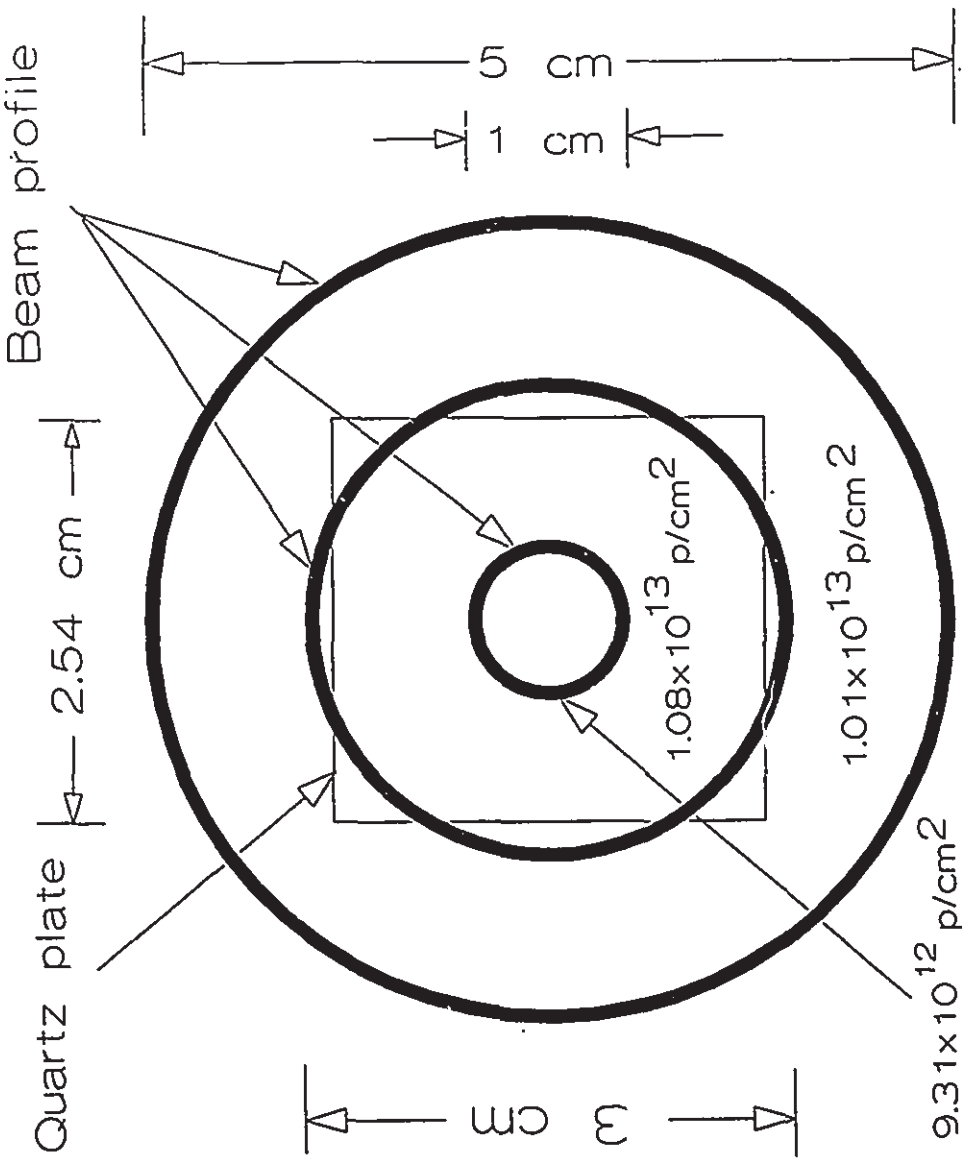
Beam profile
5 cm
1 cm
Quartz plate
2.54 cm
3 cm
1.08x10^13 p/cm^2
1.01x10^13 p/cm^2
9.31x10^12 p/cm^2

FIGURE 4.3. The proton range in quartz materials is plotted versus the proton energy (Al64).

PROTON RANGE IN QUARTZ MATERIALS

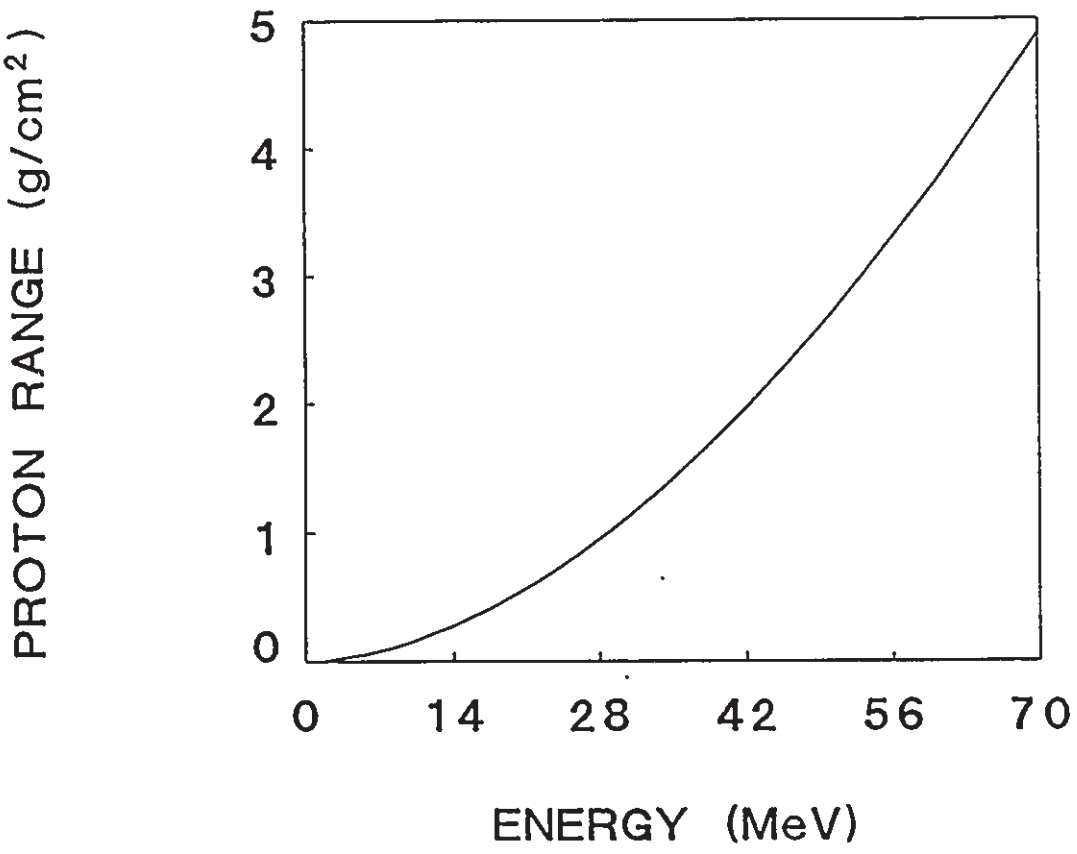

samples were handled with aluminum foil during the cutting and subsequent weighing to avoid accidental contamination by fingerprints, etc. We followed the sample preparation procedure described in chapter 2. However, in these measurements, an average of 4 mg of graphite was used in each sample as carrier. This large amount was necessary to dilute the $^{14}C/^{12}C$ concentration to a ratio of 1 to 1.5 times modern, since higher $^{14}C/^{12}C$ concentrations could contaminate the extraction and the graphitization lines.

4.3 BACKGROUND.

In this experiment we considered three sources of background:

1. First, background produced by any possible source of contamination in the CuO, graphite and quartz tubing was considered. To estimate the ^{14}C levels produced by these sources, we processed samples which contained similar amounts of CuO and graphite to those used with the plates. The level found was $(7.0\pm0.5)\times10^{6}$ atoms of ^{14}C and it was subtracted from the total number of atoms of ^{14}C found in each measurement carried out using the plates. The uncertainty in this background value was found from the variations in the results obtained from different measurements of such samples.

2. Second, background produced during the processing of the SiO_2 samples was considered. In this case, most of

the ^{14}C contributed to the samples was due to the adsorption of CO_2 and other gases containing carbon present in air by the quartz powder. Even though we took care to avoid and eliminate such adsorption during the sample preparation process (see chapter 2), small amounts of ^{14}C where found in the processed blank samples. To determine the amount of contribution, we processed unirradiated plate samples which would give us an estimate of the possible contaminants picked up during the sample preparation and ^{14}C measurement. The ^{14}C concentration found was $(3\pm2)x10^{6}$ atoms of ^{14}C g^{-1}, after the background #1 was subtracted from the total amount of ^{14}C found in those blank samples. The uncertainty in this result was found from the variability of the result obtained from the several blank samples processed.

3. Third, background introduced by the production of ^{14}C from nuclear reactions other than the one under study in this chapter was considered. The main source for this background would be those reactions such as $^{16}O(n,2pn)^{14}C$, produced by the secondary neutrons which were produced by the interaction of the protons throughout the plates. To induce the $^{16}O(n,2pn)^{14}C$ reaction, neutrons with energies above 14 MeV must be produced. Protons with energies of 65 MeV or less are unlikely to interact and transfer all their energy to a small number of nucleons since at 65 MeV the compound reaction mechanism is more prevalent than the direct reaction mechanism. Even in the most optimum case,

in which 10% of the protons are producing high energy neutrons, the contribution would be negligible. Other possible reactions could be those induced by thermal neutrons in the ^{14}N and ^{13}C from a monolayer of air absorbed by the surface plates. However it is believed that this contribution would be insignificant. Considering a similar monolayer of air as in chapter 3, we have estimated that to make a substantial amount of ^{14}C from this source, about $8x10^{14}$ thermal neutrons cm^{-2}, should have been produced. This amount is unlikely to be present since it is 13 times the total number of protons produced. To evaluate this source of background, we measured the ^{14}C concentration on the back plates of the stacks, QP#16 (16th quartz plate from the front of the stack) and QP#17, beyond the range of the protons. Table 4.1 shows the ^{14}C concentrations found in QP#16 and QP#17 for each stack after the two background sources discussed earlier were subtracted. The uncertainties in those concentrations were calculated based on the differences found in the measurements carried out on different portions of the same plate. In general the concentrations in QP#16 are higher than those found in QP#17. The stack thickness was such that the beam was stopped in the fifteenth plate (QP#15). Therefore the concentrations found in QP#16 and QP#17 should be just from secondary reactions and adsorption from air. We took the QP#16 concentration to obtain an upper limit on the

measurement of such background. It is possible that by taking the concentrations from the back plates we over estimated the background levels from this source. Many of the neutrons made at the front of the stacks would reach the back, in addition to those made there; and the actual neutron backgrounds near the front of the stack might be somewhat less. This background contribution corresponds to about 10% of the ^{14}C concentrations found in the plates. In addition to the oxygen target reactions, there will be some production from neutrons and protons reacting with the Si in the quartz. We have not measured this contribution but we have estimated it to be negligible. The fraction between the number of the possible excited states for $p+^{16}O \rightarrow {}^{14}C$ and the total number of possible excited states for $p+^{16}O$ is four times larger than the equivalent fraction for $p+^{28}Si$ at 63 MeV. Similar value was found for the equivalent neutron reactions. A way to evaluate this contribution would have been to irradiate a block of Si material with 63 MeV protons and measure how much ^{14}C would have been produced.

If the contributions from the unirradiated samples are not subtracted from the results for QP#16, the values for the QP#16 plates are $(4.6\pm0.5)\times10^{7}$ and $(2\pm1)\times10^{7}$ ^{14}C atoms g^{-1} for stack 1 and 2 respectively. These values give us both background contributions: from adsorption and from secondary reactions. We subtracted both of these values for QP#16 from the results obtained from the measurements

carried out with the irradiated plates.

TABLE 4.1. ^{14}C concentrations found in the back plates of each stack. Backgrounds of $(7.0\pm0.5)X10^{6}$ atoms of ^{14}C for adsorption on the quartz tube, CuO and graphite, and $(3\pm2)x10^{6}$ ^{14}C atoms g^{-1} for adsorption during processing, have been subtracted.

Type of sample	^{14}C Concentration Stack 1 (atoms g^{-1})	^{14}C Concentration Stack 2 (atoms g^{-1})
QP#16	$(4.3\pm0.6)x10^{7}$*	$(1\pm1)x10^{7}$
QP#17	$3x10^{6}$*	$(4\pm2)x10^{6}$*

* *Values based on one measurement.*

4.4 RESULTS.

The average ^{14}C concentrations for each plate in each stack are shown in table 4.2. The final results for the cross section at several energies are also shown in table 4.2 These were calculated by averaging the cross sections obtained for each stack.

The uncertainty in the cross sections were calculated by adding in quadrature the fractional uncertainties in the total number of protons, and the fractional uncertainties in the ^{14}C concentration in each plate.

In most cases, the major uncertainties in the ^{14}C

TABLE 4.2. The ^{14}C concentrations found in each plate and for each stack. The energy corresponding to each plate as well as the final cross section are also given.

Sample plate	Energy (MeV)	^{14}C Concentrations (atoms g^{-1}) Stack 1	Stack2	Cross Section (mb)
QP#1	(61±2)	(3.76±0.08)x10^{8*}	(3.7±0.4)x10^{8}	(1.8±0.2)
QP#2	(58±2)	(2.80±0.06)x10^{8*}	(2.0±0.1)x10^{8}	(1.2±0.2)
QP#3	(54±2)	(2.81±0.06)x10^{8*}	(2.7±0.1)x10^{8*}	(1.4±0.1)
QP#4	(50±2)	(2.2±0.2)x10^{8}	(3.4±0.1)x10^{8}	(1.4±0.3)
QP#5	(46±2)	(2.52±0.07)x10^{8*}	(2.4±0.1)x10^{8*}	(1.2±0.1)
QP#7	(36±2)	(2.06±0.06)x10^{8*}	(1.8±0.1)x10^{8*}	(1.0±0.1)
QP#9	(25±3)	(3.2±0.5)x10^{7*}	(4.5±0.5)x10^{7}	(0.19±0.04)

* *Values based on one measurement. The uncertainties are those of the ^{14}C measurements and the background subtractions. The other values are the means of the separate measurements of portions of the same plate.*

concentrations found in the plates came from the background subtractions and their uncertainties carried through the calculations. In two cases, stack 1 QP#4 and stack 2 QP#1, the uncertainties due to the differences between the results from several portions of those plates were larger and were used instead.

Excluding QP#4 and QP#2, the ^{14}C concentration for each plate agreed within uncertainties between the two stacks. We do not know, with certainty, the reasons for the large disagreements between stacks in the QP#4 and QP#2 samples. The spread in the results from the separate measurements carried out on portions of these plates were only 3% and 8% for QP#4 and QP#2 respectively, which means that there was consistency in the extraction efficiency within the same plate. It could be that one of those plates was externally contaminated with, say, finger prints in spite of the precautions taken to avoid this. The uncertainties in the cross sections at 50 and 58 MeV, corresponding to these plates, were found from the disparity between the results from the 2 stacks. Those at other energies were due to the uncertainties carried through the calculations.

4.4.1. Comparison to previous results.

As we mentioned, Tamers and Delibrias measured the $^{16}O(p,3p)^{14}C$ cross section. They irradiated water samples

with 55 MeV to 3 GeV protons, and the ^{14}C was detected by β decay counting. The $^{27}Al(p,3pn)^{24}Na$ reaction was used to monitor the proton beam. The $^{27}Al(p,3pn)^{24}Na$ cross section was later reviewed by Cumming (Cu63) and Tamers and Delibrias' data were renormalized to the new results by Audouze et al. (Au67). With this renormalization, the cross section increased between 60% and 27% at energies lower than 70 MeV and was unchanged or lowered slightly (4%) at higher energies.

More recent experimental results for the $^{27}Al(p,3pn)^{24}Na$ cross section reaction, published by Hogan and Gadioli (Hg78), indicate a significant departure from the results of Cumming (Cu63) below 50 MeV. Hogan and Gadioli (Hg78) irradiated stacks of 3 (.779 mil each) aluminum foils with a proton beam whose intensity was measured in a Faraday cup. A known thickness of beryllium degrader was used to obtain the desired beam energy. The middle foils of each stack were analyzed by both beta proportional counters and NaI(Tl) gamma-ray detectors. The differences between Hogan and Cumming's results are due to the uncertainties in the proton energies rather than in the measurements of the cross section because Cumming used a target which was thicker than the range of the lowest energy of the incident protons. Hogan and Gadioli's (Hg78) data showed a much steeper increase in the $^{27}Al(p,3pn)^{24}Na$ cross section than the data obtained by Cumming (Cu63). Therefore

the cross section values given by Hogan and Gadioli are lower than the Cumming's results by factors of 17 and 2 at proton energies of 40 and 50 MeV respectively. They are also lower than those originally used by Tamers and Delibrias to obtain the $^{16}O(p,3p)^{14}C$ cross section. More recent data on the $^{27}Al(p,3pn)^{24}Na$ cross section by Winsberg et al. (Wn80), Michel et al. (Mc85) and Schneider et al. (Sc87) fall also between those values obtained by Cumming and those obtained by Hogan and Gadioli.

In figure 4.4 we compare our results with Tamers and Delibrias values renormalized to the $^{27}Al(p,3pn)^{24}Na$ data of Cumming and of Hogan and Gadioli. All our results had uncertainties lower than 17%, except at 50 and 25 MeV where the uncertainties were 21%. At 25 MeV, the cross section is very small so the uncertainties carried out through the calculations from the background levels were comparably large. In the case of 50 MeV, the high uncertainty came from the disagreement between the results obtained for each stack. The uncertainties on the proton energy in our experiment was about 3% compared to about 14% in the case of Tamers and Delibrias' experiment. In figure 4.4 we have not included horizontal error bars in our data since the uncertainties in the energies are too small to be plotted.

Excluding the range of energies below 50 MeV, our results agree with those of Tamers and Delibrias. The differences below 50 MeV are the result of the very steep

FIGURE 4.4. Our results of the $^{16}O(p,3p)^{14}C$ cross section are shown together with those from Tamers and Delibrias (Ta61) renormalized with the data of Hogan and Gadioli (Ho78) (closed triangles) and of Cumming (Cu63) (open triangles) on the $^{27}Al(p,3pn)^{24}Na$ cross section.

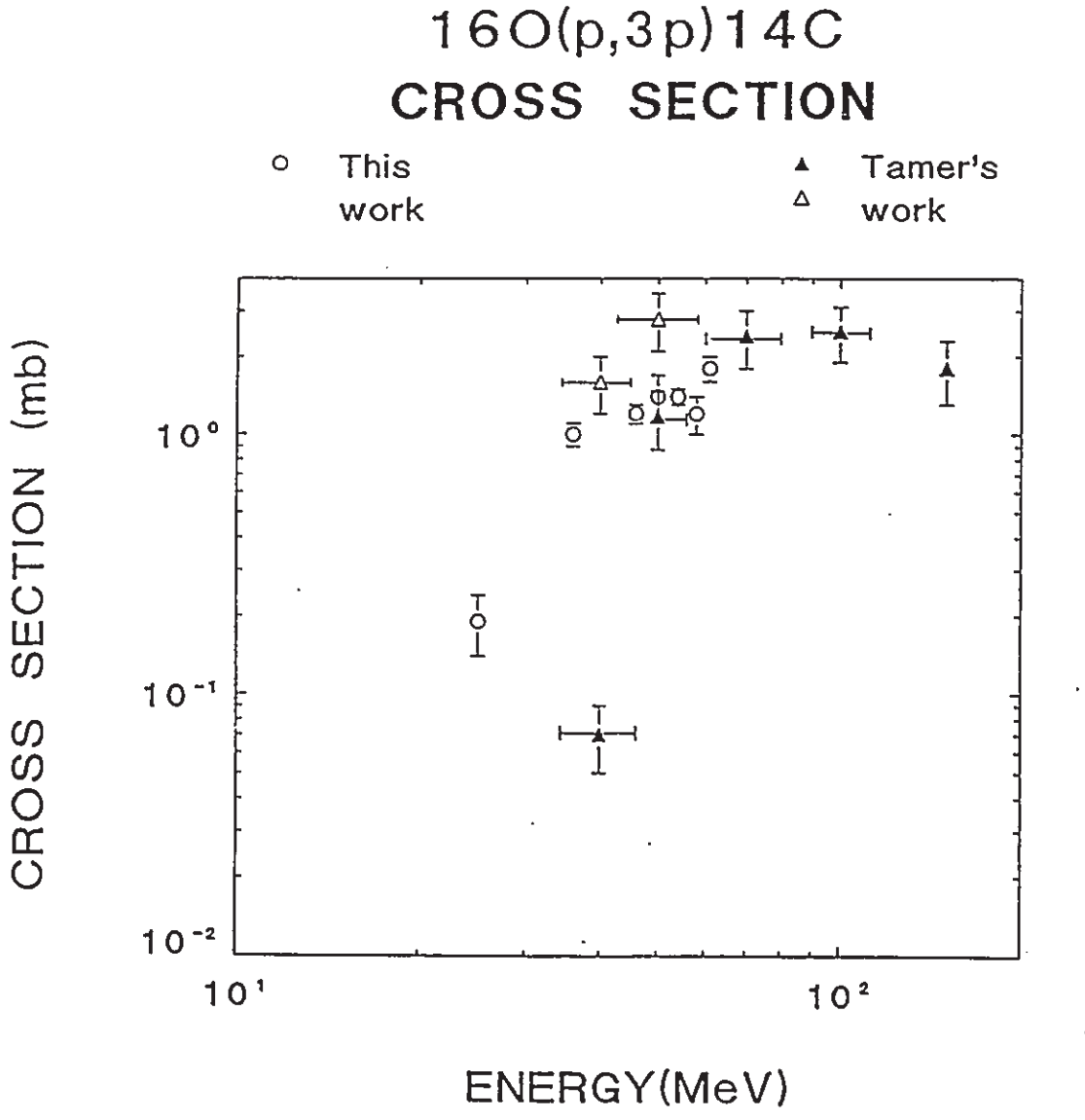
16O(p,3p)14C
CROSS SECTION
This work
Tamer's work
CROSS SECTION (mb)
10⁰
10⁻¹
10⁻²
10¹
10²
ENERGY(MeV)

fall-off of the Hogan and Gadioli $^{27}Al(p,3pn)^{24}Na$ cross section data at those energies. Given that the Q value of the $^{16}O(p,3p)^{14}C$ reaction is -22.34 MeV, we would expect the ^{16}O+p cross section to be significant at 30-35 MeV (i.e. 10 MeV above threshold). This is contrary to what Tamers and Delibrias' data show when they are normalized with Hogan and Gadioli's results.

4.5 SUMMARY.

We have measured the $^{16}O(p,3p)^{14}C$ cross section for energies below 63 MeV. Two cases of discrepancies between the results for the two stacks were found. Those differences could have been produced by variations in the ^{14}C extraction method efficiency or some accidental contamination such as finger prints. Our results show agreement with Tamers and Delibrias data renormalized with the $^{27}Al(p,3pn)^{24}Na$ cross section data from Hogan and Gadioli at energies above 50 MeV. Below this energy our values are higher than the earlier measurement.

CHAPTER 5

MEASUREMENTS OF THE ^{14}C CONCENTRATIONS IN OBSIDIAN SAMPLES

5.1 INTRODUCTION.

In this chapter, we describe the measurements of the ^{14}C concentrations taken from several obsidian samples. The main purpose of these measurements was to study the possible detection of the ^{14}C produced in-situ in the rocks. A discussion of the implications of our results for the ^{14}C in-situ production rate and of the results from our cross section measurements will follow.

5.2 DESCRIPTION OF THE SAMPLES.

5.2.1 Introduction.

The selection of the right kind of sample for the study of in-situ production is very important. The contributions from other sources of the isotope under study should be able to be eliminated, measured, or at least estimated. Altitude and latitude positions are other important factors to consider. Because the CR fluxes increase with both altitude and latitude the choice of high altitudes and latitudes would facilitate the detection of

the isotope under study. The possible applications of the measurement of in-situ produced isotope will depend on the degree of knowledge about the geological history of the samples under study. A more complete discussion of the applications of in-situ production measurements is given in chapter 1.

5.2.2 Samples used in this work.

The samples used in this project were obsidians. Obsidian is a glassy form of rhyolite containing tiny crystals of opaque iron oxide which give it a characteristic black color (Bu76). When magma cools rapidly, within seconds or minutes, the compounds do not have time to segregate themselves into large crystals, (i.e. the viscosity is too high to permit crystallization (Dd81)) and the result is a glass (Bu76). Obsidian flows can be found in most volcanic areas. Typical obsidians are composed of 68-79% SiO_2, 8-12% Al_2O_3, 1-10% Fe_2O_3, 4-6% Na_2O and 4-5% K_2O (Gs85). Notice the lack of carbon in the composition.

Obsidian is a good material for the purposes of our study because the date of the eruption in some cases coincides with when the obsidian is first exposed to cosmic rays. The date of the eruption can be determined by using dating methods such as ^{14}C (by dating associated plant material or paleosols) and K-Ar (An62)(An64). Thus the total exposure time of the obsidian to CRs can be known. In

addition, obsidian is an extremely hard, non-porous material which prevents external contaminants from entering it via weathering processes (e.g. the absorption of CO_2 from the air). An indication of this is the hydration rate found in obsidians: 220 years per micron (Mg83)(Mg88). The high SiO_2 content in obsidian makes it a desirable material to work with since it gives a high concentration of oxygen atoms which are the main target for the in-situ production of ^{14}C.

The location, altitude and the time of exposure to cosmic rays of the samples used here are given in table 5.1 (Ne85). The samples were small flakes from larger blocks and fragments which (with one exception) were exposed at collection time. GB (Hf79)(Bo74) and 3S are from ancient eruptions. FH, OC, and ED were ice-covered until the end of the last glaciation. BF and LM (Wl87) are from dated eruptions. We had to estimate the exposure time of the Lipari sample. The obsidian blocks were excavated from a quarry and were found together with breccias from the Roche Rosse and Furgia Vecchia eruptions (Gi86). Paleosol associated with those breccias were ^{14}C dated as 1400 yrs. old (Gi86), but K/Ar dating and fission track dating of the obsidian blocks themselves showed they were approximately 6000 yrs old (Gi86) (Vi86). It is believed that they were originally formed in the throat of the volcano and were swept down the sides of the mountain during the later

TABLE 5.1. The location, altitude and exposure time for each of the obsidian samples are given. The expected concentrations for each obsidian, based on both the Yokoyama et al. and our estimates of the ^{14}C in-situ production rate, are also given. The ^{14}C concentrations measured in the obsidians are shown.

Samples	Location	Altitude (meters)	Exposure time (years)	^{14}C concentration Yokoyama's estimate (atoms/g)	^{14}C concentration our estimate (atoms/g)	^{14}C concentration measured** (atoms/g)
Glass Buttes (GB)	High Desert Oregon (43°N)	1,830	10^6	$(4\pm2)\times10^5$	$(2.6\pm0.6)\times10^5$	$(2.6\pm0.5)\times10^5$
Three Sisters (3S)	North Mt. Pitt Oregon (44°N)	2,000	10^6	$(4\pm2)\times10^5$	$(2.6\pm0.6)\times10^5$	$(2\pm1)\times10^5$
Feather Hill (FH)	McKenzie Mt. (N.W.T.) (62°N)	2,000	10,000	$(6\pm2)\times10^5$	$(3.2\pm0.8)\times10^5$	$(1.4\pm0.4)\times10^5$
Obsidian Creek (OC)	Anahim Peak (B.C.) (52°N)	1,200	10,000	$(3\pm1)\times10^5$	$(2.0\pm0.5)\times10^5$	$<4\times10^4$
Edziza (ED)	Goat Mt. (B.C.) (58°N)	2,030	10,000	$(6\pm2)\times10^5$	$(3.2\pm0.8)\times10^5$	$(1.6\pm0.5)\times10^5$
Big Flow (BF)	Paulina Peak Oregon (43°N)	2,000	1,200	$(8\pm3)\times10^4$	$(4\pm1)\times10^4$	$(5\pm2)\times10^4$
Lipari Mediterranean (LM)	Aqua Calda Lipari, Italy (38°N)	800*	4,600	$(3\pm1)\times10^4$	$(2.2\pm0.6)\times10^4$	$<3\times10^4$

The samples were taken up from a quarry 70 meters above sea level but we have assumed the samples were exposed to cosmic rays for 4,600yrs at 800m of altitude.

** *After background subtraction*

eruptions (Gi86). It is therefore certain that these samples were not exposed to cosmic rays for the past 1400 years but it is difficult to know their condition with respect to CR exposure during the first 4600 years after their formation. They could have been at any altitude, from deep in the crater to near the top of the mountain (800 meters high). Additionally, they could have been at the surface or deeply buried.

5.2.3 Sample preparation.

The obsidian flakes used in the samples were chosen from among those from the interior of the obsidian block or fragment, to avoid the flakes from the exterior surfaces. The carbon in the obsidian samples was extracted following the method described in chapter 2. Each sample weighed approximately 2.9±0.1 grams and 0.47±0.03 milligrams of anthracite were used as dead carbon carrier (the nominal weights were 3 grams and 0.5 milligrams and the uncertainties are due to losses in handling). In general, the process followed with these samples was very similar to the one used with the quartz chips samples from the neutron irradiation, the only major difference being the use of a double combustion tube with the obsidians to prevent sample losses due to tube breakage. Obsidian is made of 65-80% SiO_2 with the remainder being composed of Na_2O, K_2O, Al_2O_3 and Fe_2O_3. In some cases, some of those oxides must react

with the quartz tubing to form glass. This has the effect of lowering the melting point of the tubing and eventually causing it to break during baking.

5.3 BACKGROUND.

We have taken into consideration two types of background: First the ^{14}C contribution from anthracite, CuO, and the quartz tubing used with the obsidian samples, and second, the contribution due to the adsorption of ^{14}C in the air by the obsidian during the sample preparation process.

To evaluate the first type of background contribution we processed samples of anthracite and CuO in double quartz tubing as we did with the obsidian samples. As all the samples had approximately the same amount of CuO and anthracite, this measurement should give a good approximation to the contribution from any contamination left in the CuO after the prebake, and from any adsorbed CO_2 on the surface of the quartz tubing. The ^{14}C level measured was $(9\pm2)\times10^5$ atoms. This is slightly higher than the background found from the same type of samples with a single tube, [$(7\pm2)\times10^5$ atoms of ^{14}C]. This difference is due to the use of the double tubing which increases the surface area prone to air adsorption. The uncertainty in the background level was calculated based on the differences between several measurements.

TABLE 5.2. ^{14}C concentrations found in three zero exposure time quartz materials used as blanks for the obsidian samples.

Type of sample	Concentration (atoms of $^{14}C\ g^{-1}$)
Natural quartz	$(2.6\pm0.1)x10^{5}$*
Quartz rod	$(1.1\pm0.1)x10^{5}$*
Quartz chips	$(2.5\pm0.1)x10^{5}$*

* *Values based on one measurement.*

To evaluate the second background source, samples of natural quartz, quartz chips, and quartz rod were processed as blank samples with zero exposure time. The ^{14}C concentrations found in those samples give us an indication of the contamination due to the adsorption of CO_2 and other gasses containing carbon from the air by the samples during the sample preparation process. The results are shown in table 5.2. No subtraction of the first type of background was made on these results. The average value was $(6.3\pm1.5)x10^{5}$ atoms of ^{14}C from a 3 gram sample (i.e. $(2.1\pm0.5)x10^{5}$ atoms of $^{14}C\ g^{-1}$). From the results obtained on both backgrounds, we deduce that most of the background contribution comes from the first source: the prebake of

the quartz samples eliminates most of the ^{14}C adsorbed by the sample during the processing. Therefore, either type of measurement could be used for the ^{14}C background subtraction for the obsidian samples. We chose to use the ^{14}C levels found in the blank quartz samples

5.4 RESULTS.

The ^{14}C concentrations found in each obsidian sample are shown in table 5.1. The ED sample result was based on only one measurement, since it was difficult not to lose this sample during baking even though double tubing was used. The element responsible for lowering the melting point of the tubing (possibly Na or K) is probably present in ED samples in greater concentration than in the others.

The final ^{14}C concentrations in the other obsidians came from the average between the measurements of the samples prepared at different times. The uncertainties for most of the samples were due largely to the uncertainties in the background subtraction. In two cases, 3S and BF, the uncertainties were mostly due to the differences between the several measurements carried out on them. The expected value of the ^{14}C concentrations for each obsidian are also shown in table 5.1. To calculate the expected ^{14}C concentrations in the samples, we used the following expression:

$$C = P_r A L e^{-\mu x} \lambda^{-1} (1-e^{-\lambda t}) e^{-\lambda t'}$$

where P_r is the production rate estimate in atoms g^{-1} yr^{-1}.

A is the relative altitude factor.

L is the relative latitude factor.

μ is the neutron attenuation coefficient, 1/192 cm^2 g^{-1}.

x is the number of cm below the surface at which the sample was picked up.

t is the exposure time of the sample to cosmic rays.

λ is the decay constant, 1.21×10^{-4} y^{-1}.

t' is the time the sample has been shielded from cosmic rays subsequent to being exposed to them for the time t.

We have calculated two expected ^{14}C concentration values for each obsidian: first by using the production rate that we estimated in chapter 1 using the neutron spectrum of Hess et al. (He61), and Reedy and Arnold's cross section estimates (Re77). We have assigned an uncertainty of 25% to our estimates since it is the quoted uncertainty for the neutron flux spectrum. The second set of expected values were calculated using the production rate estimates of Yokoyama et al. (Yo77) which have a 35% uncertainty.

In the calculation of those production rate

estimates, we assumed that all of the production is due to the $^{16}O(n,2pn)^{14}C$ reaction. We also assumed a 100% SiO_2 material. With this approximation we obtained an oxygen concentration that is 10% greater than the average oxygen concentration in ED obsidian samples (Gs85). The production due to the $^{28}Si(n,X)^{15}C$ reaction was considered negligible compared to the production in oxygen for the reasons given in chapter 3. Production of ^{14}C from protons was also neglected, since the proton flux at the Earth's surface is much lower than the neutron flux. In addition, the proton cross sections producing ^{14}C from different targets are likely to be smaller than the equivalent neutron cross sections due to Coulomb barrier effects, (see chapter 1). Notice that the assumption of 100% SiO_2 tends to counteract the neglect of the $^{28}Si+n$ and $^{16}O+p$ reactions.

The altitude and latitude factors considered here were those given by Yokoyama et al. (Yo77). The LM sample was assumed to have been at the surface and at the top of the mountain (800 meters) for the first 4600 years and buried a few meters below surface during the past 1400 yrs. It was assumed that all the other samples were continuously exposed. Some small CR flux attenuation was considered in the case of the GB samples since they were taken from the interior of a split block approximately 18 cm in diameter. The corresponding attenuation was calculated to be .884.

All other samples were taken from no more than 2 to 5 cm below the obsidian surface.

GB, 3S, BF and LM samples agree within uncertainties with our expected values. The other obsidian samples, FH, OC and ED, have ^{14}C concentrations lower than our estimates, by a factor of two or more. The reason for these differences is not known. One possibility is that we are not extracting all the ^{14}C produced in the obsidian. We have shown in chapter 2 that in quartz samples only 3% of the ^{14}C extracted in the first bake was extracted in the second bake. This could be different for obsidian. Since it is a glass with fewer voids than fused quartz, it could be more difficult to extract carbon. However, in chapter 2 we have also described how we processed an obsidian sample with acid fluxes to lower the melting point of the obsidian. From that measurement we got ^{14}C concentrations of $(1.6\pm0.1)\times10^{6}$ ^{14}C atoms g^{-1}, similar to the levels of $(2.0\pm0.2)\times10^{6}$ ^{14}C atoms g^{-1} obtained when the sample was processed without fluxes under similar conditions. Therefore it seems likely that we did extract all of the ^{14}C from the samples. As the differences between the expected and measured values are not consistent for all the obsidian samples, we also find it unlikely that the cause is an overestimate of the cross section. On the other hand, there is a high probability that those obsidians could have been shielded from cosmic rays for long periods (Ne89). The

three came from high latitudes and in two cases, FH and ED, also from high altitudes. Assuming that FH and ED were covered with snow an average of 9 months a year for the last 10,000 years, a layer of 175 g cm^{-2} (5 meters) of snow over those obsidians during that period would have decreased the ^{14}C production by half assuming an average density of 0.35 g cm^{-3} (Kt66). The concentration found in the OC sample was at the background level. However, it could be explained if the sample had until recently been buried under 1 meter of earth. This possibility does not seem too unlikely because of the little knowledge we have about the geological history of those samples (Ne89).

Recently, data have been published by Jull et al. (Ju88b) on the detection of the ^{14}C in-situ production in high-altitude volcanic rocks. To extract the CO_2 from the samples they used an induction furnace with oxygen gas as an oxidizer. The background levels produced by their system without the sample was $(8\pm1)x10^5$ atoms of ^{14}C, which is very similar to our equivalent background of $(9\pm2)x10^5$ atoms of ^{14}C from CuO, anthracite and double quartz tubing. They found $<2x10^5$ atoms g^{-1} in samples with zero exposure time. This value is equivalent to what we found for similar samples with our extraction method. It was possible for Jull et al. to detect the ^{14}C produced in-situ even in non-saturated samples because all the samples were collected at very high altitudes; between 3300 to 5400 meters. This

compares with the approximate maximum of 2000 meters for our samples. Altitude makes a significant difference since the relative production rate factor increases exponentially with altitude. We have therefore found a limit in the altitude at which ^{14}C produced in-situ can be studied with either of the extraction methods available at present. Figure 5.1 shows the ^{14}C concentrations measured in our obsidian samples versus our expected concentration estimates. Figure 5.2 shows the same type of graph with the data from Jull et al. The solid line shown in both figures corresponds to agreement between the measured and expected values and the dotted lines represent the uncertainties in the estimates. The percentage uncertainties in Jull's data are smaller than ours because in both cases the uncertainties arose from the background subtractions. With a few obvious exceptions, both sets of measurements show fair agreement with the expected values calculated with our production rate estimates.

5.5 IMPLICATIONS OF THE ^{14}C IN-SITU PRODUCTION RATE ON THE NEUTRON CROSS SECTION RESULTS.

Our 35 MeV neutron irradiation result indicates a cross section of (16±3) mb compared with 1 mb estimated by Reedy and Arnold (Re72). The $^{16}O(n,2pn)^{14}C$ cross section estimates (Re72) showed a peak from the compound nuclear component between 40 and 150 MeV with a maximum of 17 mb at

FIGURE 5.1. The ^{14}C concentrations measured in the obsidian samples are plotted versus the expected values calculated with our production rate estimate.

FIGURE 5.2. The ^{14}C concentrations measured by Juli et al. in high-altitude volcanic rocks versus the expected values calculated with our production rate estimates.

14C CONCENTRATIONS
IN OBSIDIAN SAMPLES

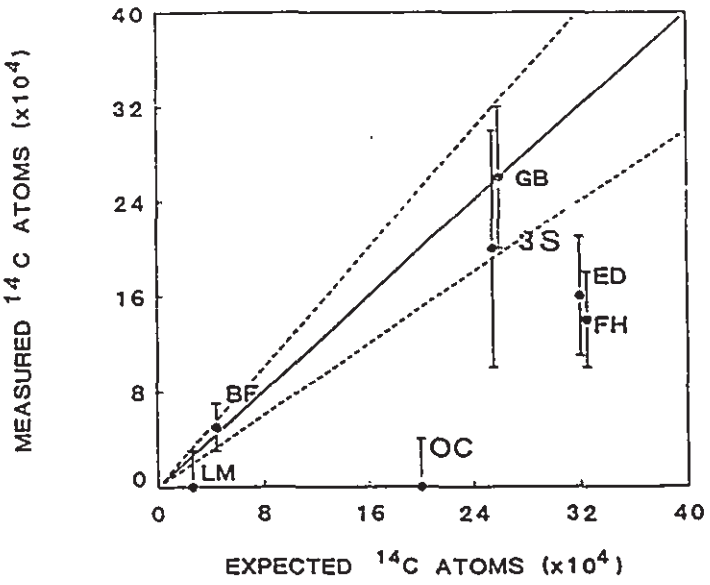

14C CONCENTRATIONS
IN HIGH-ALTITUDE ROCKS

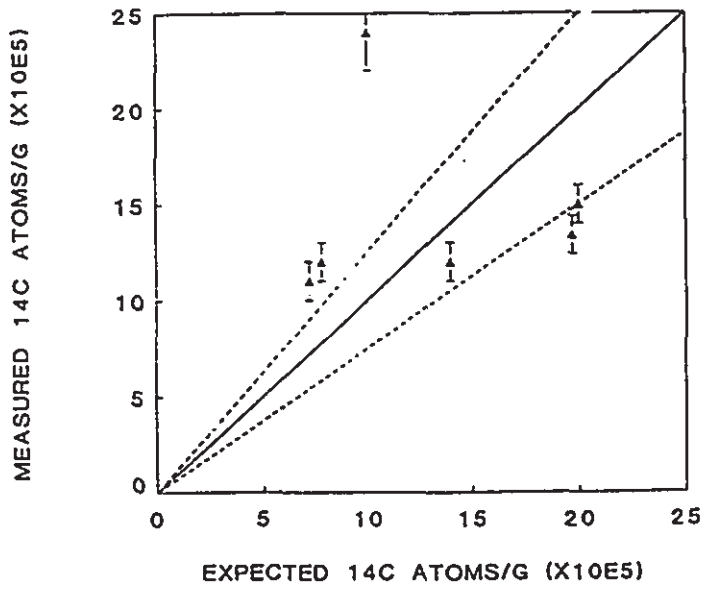

100 MeV. Our result suggests that this peak actually occurs at lower energies. Since there are more cosmic ray neutrons at lower energies, the peak would have to be narrower than Reedy and Arnold's estimates if our experimental estimates of the production rate are correct. We have made an approximate calculation of how wide it would have to be, assuming a cross section value of 16 mb between 35 MeV and *X* MeV, 3 mb between *X* MeV and 500 MeV, and 2 mb above 500 MeV. We found that the value of *X* should be about 100 MeV to be consistent with the production rate. This narrower peak could be feasible since similar peaks have been observed in other cross section reactions such as the ^{10}Be production from ^{12}C (La67). As mentioned in chapter 3, Reedy and Arnold's $^{16}O(n,2pn)^{14}C$ cross section estimate was based on the experimentally measured $^{16}O(p,3p)^{14}C$ cross section. The $^{16}O(p,3p)^{14}C$ cross section presents a peak approximately from 36 MeV to 120 Mev, with a maximum value of 3 mb at 100 MeV. There is no theoretical argument supporting the need for the $^{16}O(n,2pn)^{14}C$ cross section to have its maximum value also at 100 MeV. Furthermore, it is more likely that the difference between the neutron and the proton cross sections is greatest at lower energies when the Coulomb barrier for the out-going protons has a greater effect. At higher energies the number of possible reaction channels is approximately the same for both $n+^{16}O$ and $p+^{16}O$, and the

Coulomb barrier has little effect so the two cross sections should be similar.

5.6 SUMMARY.

We have detected ^{14}C in-situ production in obsidian samples with exposure times above 3 half lives and below 2 half lives. We have also found that the detection of in-situ produced ^{14}C in samples much below the saturation level is not possible with existing methods unless the samples come from altitudes higher than 2,000 meters.

The expected ^{14}C concentrations produced in-situ in those obsidian samples were calculated using our own estimates of the production rate and those of Yokoyama et al.. Except in three obsidians from which the exposure history was not well known, the measured ^{14}C concentrations agree well with our expected values.

A value of the neutron induced spallation cross section at 35 MeV of (16±3) mb was found instead of 1 mb as predicted by Reedy and Arnold. This result, taken together with the production estimates from the obsidian data, suggest that the predicted peak in the excitation function is between 35 and 100 MeV.

CONCLUSIONS

The method developed for the extraction of ^{14}C from silicate materials combined with the use of A.M.S. has enabled us to study the in-situ production of ^{14}C by estimating its production rate and by measuring the related cross sections.

The ^{14}C in-situ produced was measured in seven obsidian samples (two at saturation). The values obtained in four of those agree with our estimates of the ^{14}C production rate. The discrepancies were found in three cases for which the past geological histories were not well known. Further studies should be carried out with samples with well known geological histories to confirm the production rate estimate. Our results have shown that the measurements of ^{14}C in-situ produced are restricted to samples with saturated or close to saturated levels of ^{14}C. Samples well below saturation should be collected from sites at altitudes higher than 2000 meters. Otherwise, the concentrations of ^{14}C in-situ produced would not be high enough to be identified over the background levels characteristic of the ^{14}C extraction methods available at the present.

We have reported the first measurement of the $^{16}O(n,2pn)^{14}C$ cross section. The value of (16±3) mb at 35 MeV indicates a different behaviour of the excitation function from that provided by Reedy and Arnold's estimates. Taking into account the given ^{14}C in-situ production rate estimate and assuming 100% in-situ production from the $^{16}O(n,2pn)^{14}C$ reaction, we have estimated that the $^{16}O(n,2pn)^{14}C$ cross section should have a peak between 35 and 100 MeV with a value of about 16 mb. Measurements of the $^{16}O(n,2pn)^{14}C$ cross section to energies of up to 150 MeV should be carried out to confirm our predictions.

Our measurements of the $^{16}O(p,3p)^{14}C$ cross section at energies up to 65 MeV have confirmed the earlier measurements carried out by Tamers and Delibrias except possibly below 50 MeV. Their results depend on the value assumed for the $^{27}Al(p,3pn)^{24}Na$ cross section and a recent measurement of this cross section decreases Tamers and Delibrias' 40 MeV data by a factor of 17. However, this latest renormalization implies that the $^{16}O(p,3p)^{14}C$ reaction only becomes significant at energies greater than 20 MeV above threshold, which seems unlikely. With our new irradiation at 200 MeV, we will be able to verify the completed range of energies measured by Tamers and Delibrias (excluding 3 GeV). Studies of SCR protons and their interaction with matter, based on the production of

^{14}C in extraterrestrial materials, are of special interest to the space program. A check on the earlier cross section measurements is very important for these studies.

In general, with the measurement of the $^{16}O(n,2pn)^{14}C$ and $^{16}O(p,3p)^{14}C$ cross sections, we have shown a way of using AMS to find low production cross sections for which conventional methods are not effective.

APPENDIX I

ACCELERATOR MASS SPECTROMETER

The Accelerator Mass Spectrometer (A.M.S.) used for this work is shown in figure A.1.1. In this section we will describe the A.M.S. method and the details of our specific system.

Carbon samples in graphite form (Vo84) (Vo87) are pressed into a 1.2 mm diameter hole in the center of a round aluminum holder (1.3 cm diameter). 20 holders are placed in the ion source at once. This is a UNIS type sputter source (Mi76). In this type of source a beam of Cs^+ is produced and reflected into the sample producing C^- ions by sputtering. These C^- ions are accelerated into the injector section due to a 30KV potential difference between these two sections. In the injector, a dipole magnet separates the $^{12}C^-$, $^{13}C^-$ and $^{14}C^-$beams. An electrostatic quadrupole then bends the off axis beams ($^{12}C^-$ and $^{14}C^-$) so that the central rays of the $^{12}C^-$, $^{13}C^-$ and $^{14}C^-$ beams are parallel to each other. At the mid point of the injector a set of apertures allows the $^{13}C^-$ and $^{14}C^-$ beams to go through and the $^{12}C^-$ beam is stopped. A mirror image of the first dipole-quadrupole pair recombines the $^{13}C^-$ and $^{14}C^-$ beams.

FIGURE A.1.1. The figure shows the Simon Fraser A.M.S. facility at McMaster University used for this work.

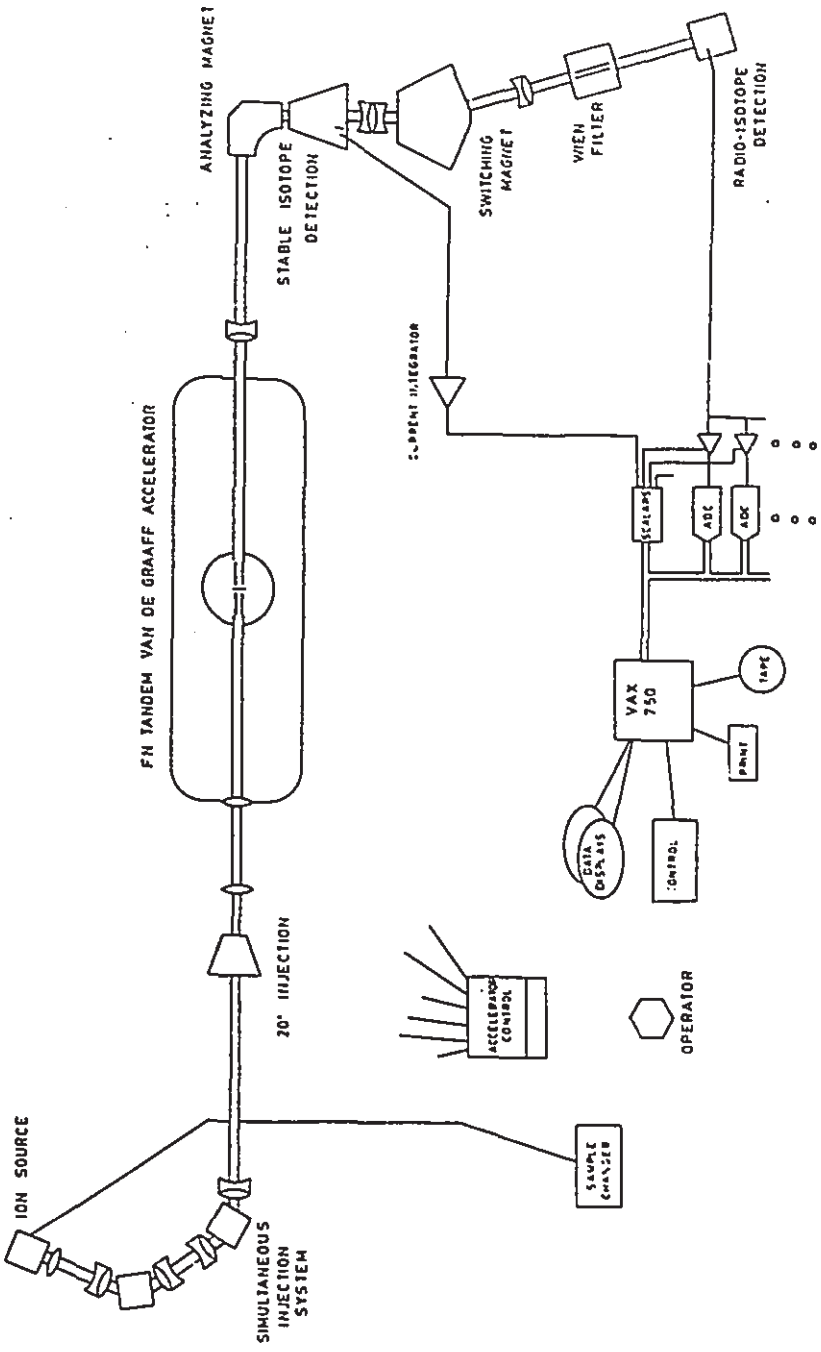
ION SOURCE
SIMULTANEOUS INJECTION SYSTEM
20° INJECTION
FN TANDEM VAN DE GRAAFF ACCELERATOR
ANALYZING MAGNET
STABLE ISOTOPE DETECTION
SWITCHING MAGNET
WIEN FILTER
RADIO-ISOTOPE DETECTION
VAX 750
OPERATOR

Acceleration is accomplished by a High Voltage Engineering Corporation Model FN Tandem Van der Graaff accelerator. The C^- beam is accelerated to the high voltage terminal which is set at 7 MV. Here the C^- ions are stripped of some electrons by collision with a carbon foil stripper. Beams of C^{3+}, C^{4+} and C^{5+} are produced. At 7 MV, about half of the original C^- beam goes into C^{4+} charge state. The positive beam undergoes a second acceleration from the high voltage terminal to the end of the tank.

After acceleration, the 35 MeV C^{4+} beam is taken through a 90^o analyzing magnet. This magnet's field was set up to send the $^{14}C^{4+}$ ions down the beam line. The $^{13}C^{4+}$ ions were stopped in a faraday cup containing stabilizing slits. These slits are used to sense the $^{13}C^{4+}$ beam position and detect any drifts and this information is used to stabilize the accelerator high voltage terminal. The total $^{13}C^{4+}$ beam current was measured by adding the currents in both slits and the cup.

The ^{14}C beam is then directed to a 22^o switching magnet which takes the beam into the radioisotope direct detection line. A potential background contribution comes from ^{13}C which can emerge from the FN stripper with 5+ and charge exchange in the second acceleration to 4+. Some of these ions have the appropriate momentum to pass through the two magnets so they have to be eliminated by some other means. A Wien filter (or velocity filter) in the beam line

is used to remove this contaminant. This is done by applying perpendicular electric and magnetic fields to the beam. The velocity resolution $\Delta v/v$ is 2% for the $^{14}C^{4+}$ ions with 35 MeV.

$^{14}C^{4+}$ ions are then counted in a ΔE-E detector system. In the first detector the ions lose energy through ionization and the detector measures this energy ions (ΔE). The ions are stopped in the second detector and the residual energy (E) is measured. The knowledge of $E+\Delta E$ gives the total ion energy (E_t). Since the energy lost in a given detector is characterized by the initial ion energy and the ion mass and atomic number, this information allows the ^{14}C ions to be distinguished from other ions reaching the detector system. For data acquisition a CAMAC-based system interfaced to a VAX 11/750 computer was used. The background in our measurements was limited by the background in the sample preparation process.

The A.M.S. system is designed to eliminate as many major contaminants as possible. $^{14}N^-$ have a very short half-life so they are not expected to reach the acceleration stage. Other ions such as $^{13}CH^-$ break apart during the stripping of electrons. Other ions reaching the detectors would be identified by the energy lost in the particle detectors. A.M.S. technique is based on counting a percentage of the atoms present rather than detecting the beta decay of ^{14}C. It is therefore possible to detect ^{14}C

levels that can not be detected with conventional counting method. These are important reasons why A.M.S. is a more powerful tool than conventional counting for the detection of ^{14}C.

Because of the difficulty in determining the absolute efficiency of the spectrometer, we normalize the results. For every two unknown samples a known standard sample was measured. The standards used were National Bureau of Standards oxalic acid samples. The accuracy of the ^{14}C measurements was typically 2-3%. The $^{14}C/^{13}C$ ratio was converted into the $^{14}C/^{12}C$ ratio using the appropriate isotope fractionation $\delta^{13}C$ correction. The uncertainty of each final result was based on the differences between the several measurements carried on the same sample.

APPENDIX II

MONTE CARLO CALCULATION

OF THE NEUTRON DETECTOR TELESCOPE EFFICIENCY

Because of the difficulties of directly measuring the efficiency of the neutron detector telescope used in our experiment, we calculated it by applying the Monte Carlo Method. The purpose of this method is to find the probability P(x)dx for an event to happen between x and x+dx using a large number of randomly generated numbers (Na76). This approach is taken in those cases that are too complicated to be solved analytically. Let P(x) be a normalized probability distribution, i.e.,

$$\int_{x_{min}}^{x_{max}} P(x')dx' = 1$$

If R is a random number between 0 and 1, then the probability of choosing r between R and R+dR is P(R)dr = dR, making P(R)dr = P(x)dx then

$$\int_{x_{min}}^{x} P(x')dx' = R$$

Therefore it would be possible to solve this equation for each value of R with x values following the probability distribution P(x) (Na76). For example, if we have a probability distribution given by

$$P(x) = -\frac{1}{a} e^{-x/a} \text{ then}$$

$$\int_0^x \frac{1}{a} e^{-x/a} dx = R$$

Solving the integral, we have

$$-e^{-x/a} + 1 = R$$

so $x = -a\ln(1-R)$ which is the same as $x = -a \ln R'$, where R' is another random number between 0 and 1.

The efficiency of the detector system can be determined by this method since the input data needed for the calculations (the geometry and the n-p cross section) are well known. The geometry of detector telescope shown in figure A.2.1.

First we calculate the angles with which the neutrons leave the target using spherical coordinates with the origin on the neutron source and the positive z axis is the

FIGURE A.2.1. A diagram of the detector telescope geometry is shown.

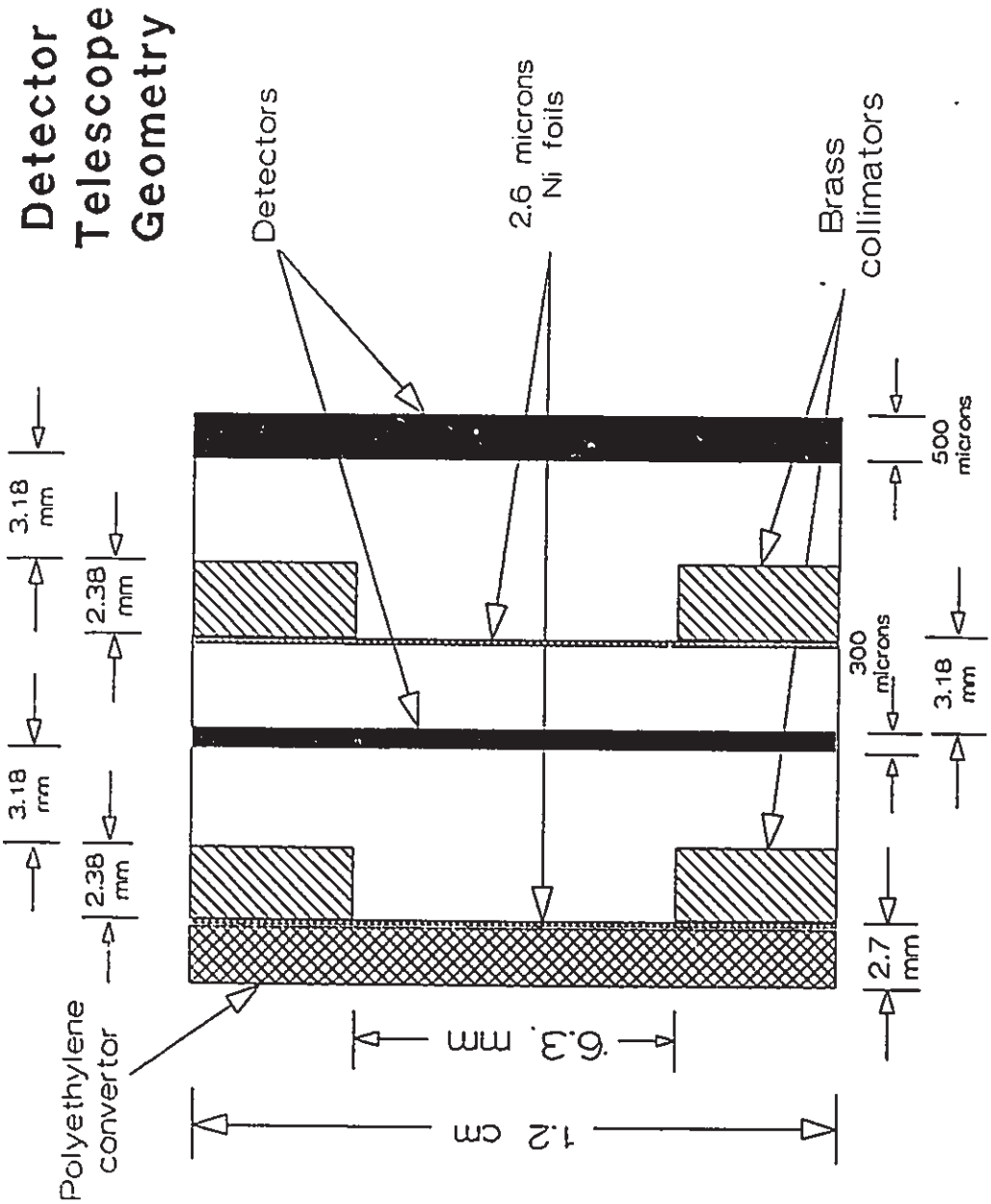
Detector
Telescope
Geometry
Detectors
2.6 microns
Ni foils
Brass
collimators
3.18
mm
2.38
mm
3.18
mm
2.38
mm
500
microns
300
microns
3.18
mm
2.7
mm
6.3 mm
1.2 cm
Polyethylene
convertor

detector axis. The expressions used for this are (Gr75):

$$\phi = 2\pi R_1$$

$$\theta = \arccos[1 + R_1(\cos\theta_m - 1)]$$

where R_1 is a random number

θ_m is the maximum angle possible for the neutron to have and still remain inside the polyethylene plate. It was calculated as the ratio between the polyethylene radius and the distance neutron source-polyethylene.

With those angles we can calculate the direction cosines of the neutrons in a Cartesian coordinate system centered at the neutron production target, with the z axis on the detector axis:

$$W_{nx} = \cos\phi \sin\theta$$

$$W_{ny} = \sin\phi \sin\theta$$

$$W_{nz} = \cos\theta$$

Next we calculate the distance z that the neutron travels in the polyethylene convertor before scattering. The cumulative probability is given by (Na76)

$$P(z) = (1 - e^{-z/\lambda})$$

where

σ is the total n-p cross section (see figure A.2.2).

ρ is the polyethylene density equal to 0.92 g cm^{-3}.

A is the atomic weight of hydrogen.

N_o is the Avogadros number.

FIGURE A.2.2. The mean free path of the neutrons in hydrogen versus the neutron energy is plotted. The (n,p) cross section as a function of the neutron energy is also given.

TOTAL (n,p) CROSS SECTION
IN POLYETHYLENE

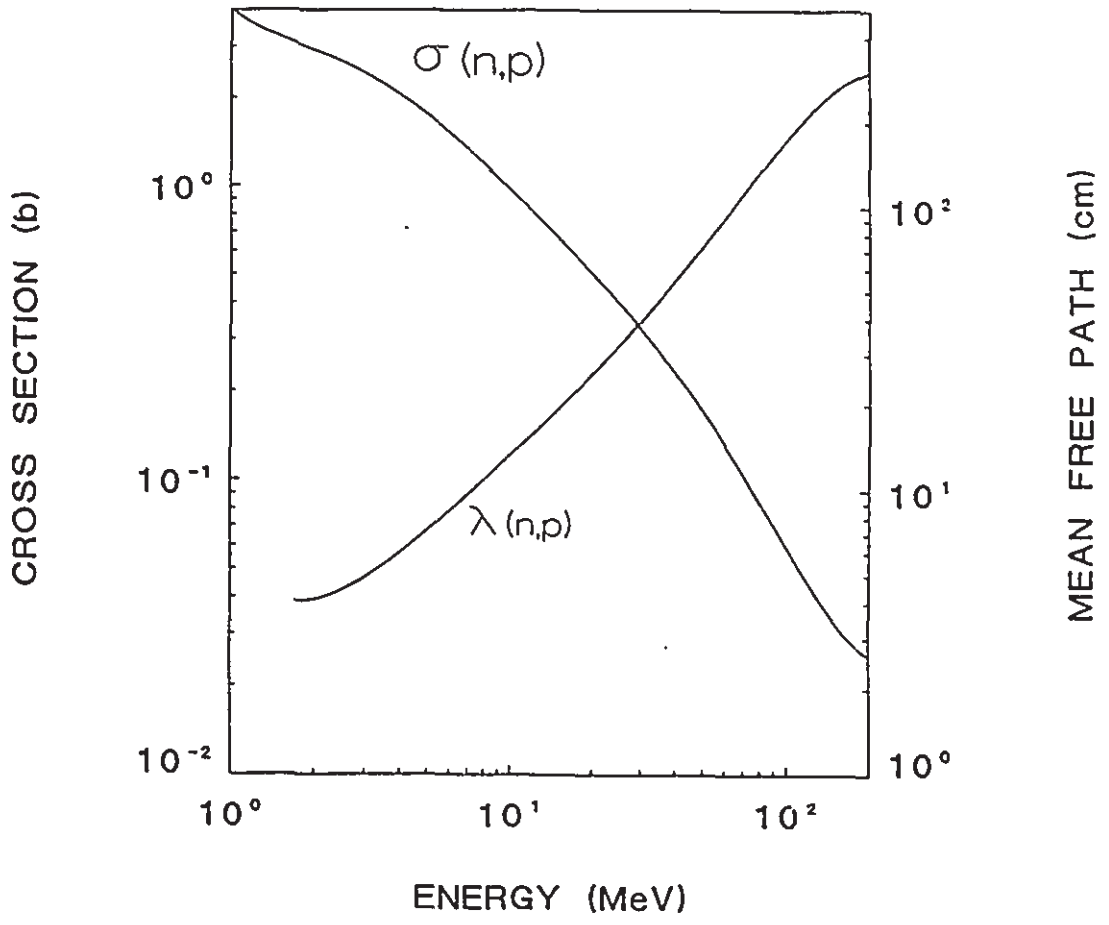

λ is the neutron mean free path in hydrogen equal to $(\sigma\rho AN_o)^{-1}$ (see figure A.2.2).

We have assumed interaction only with the hydrogen in the polyethylene. The correction factor at energies between 20 and 100 MeV is close to one (Na76) and this assumption should also be valid at lower energies due to the small thickness of the polyethylene. The information to whether the neutron will scatter or not will be given by solving the equation

$$\int_0^z e^{-z/\lambda}\, dz = R$$

As this equation is of the same type as our earlier example, the solution to it is $z = -\lambda \ln R_2$ where R_2 is a second random number.

Once the neutron has interacted with the convertor we next calculate the neutron scattering angles. Evidence of isotropic distribution for the differential cross section at energies around 30 MeV (Pr88) and below 20 MeV (Na76) have been given. Therefore we will assume it isotropic for our case so it will have a $\sin(2\Psi_n)$ distribution in the lab frame. To calculate the angles we followed the next argument (Na76): We found the zenith angle Ψ_n as

$$\Psi_n = R_3\pi/2$$

This angle should follow the probability distribution $P(\Psi_n) = \sin(2\Psi_n)$, therefore for a given Ψ_n, $P(\Psi_n) > R_4$ where R_4 is a random number. If this condition is not fulfilled, a new value of Ψ_n should be obtained. Once we had obtained the right value of Ψ_n, we could then calculate the azimuth angle which is given by

$$\chi_n = 2\pi R_5$$

Now we can calculate the recoil proton angle and direction of scattering as well as the neutron energy. For this we use a relativistic kinematic expression:

$$\tan(\Psi_n + \Psi_p) = \left(\frac{2mc^2}{E_n} + 1\right) \tan(\Psi_n) + \frac{2mc^2}{E_n} \cot(\Psi_n)$$

As the incident neutron, the scattered neutron, and the recoil proton are coplanar, we can say that

$$\chi_p = \chi_n + \pi$$

The scattered neutron direction is given by (Sp69)

$$W_{n'z} = W_{nz} \cos(\Psi_n) + \sin(\Psi_n) \cos(\Psi_n) \sqrt{1 - (W_{nz})^2}$$

$$W_{n'y} = \frac{1}{1 - (W_{nz})^2} \{ W_{ny} (\cos(\Psi_n) - W_{nz} W_{n'z}) + \sin(\Psi_n) \sin(\chi_n) W_{nx} \sqrt{1 - (W_{nz})^2} \}$$

$$W_{n'x} = \frac{1}{1 - (W_{nz})^2} \{ W_{nx} (\cos(\Psi_n) - W_{nz} W_{n'z}) - \sin(\Psi_n) \sin(\chi_n) W_{ny} \sqrt{1 - (W_{nz})^2} \}$$

Similar equations can be derived for the recoil proton using the angles Ψ_p and χ_p. Assuming identical

neutron and proton masses, the energies of the scattered neutron and proton are

$$E_{n'} = E_n \cos^2(\Psi_{n'}/2)$$
$$E_p = E_n \sin^2(\Psi_{n'}/2)$$

To reduce the computing time, the recoil proton scattering angles were checked to be smaller than a critical value given by $\Psi_p < 33.8^o$. Above this value the proton would never reach the second detector because it would lose most of its energy going through a section of one of the brass collimators.

As with any charged particle, the recoil proton will lose energy by ionization when passing through material. The range will depend on the kinetic energy of the particle and on the type of material traversed. The range is given in general by the expression

$$R = \alpha E^{\beta}$$

We have calculated α and β for the different materials present in our telescope using the tables from (Al64). Once we know the range we can calculate the energy loss $E - E_f$ by the proton in any part of the telescope (polyethylene, collimators, air or detectors). E and E_f are the energy of the proton before and after a given section of the telescope.

$$E_f = (R_f/\alpha)^{1/\beta}$$

We can therefore find if the proton has enough energy

to go through the next section of the telescope. With this expression we assume that there is no range of straggling since small thicknesses of material are always present (Na76). We can therefore check if the recoil proton has sufficient energy to reach the second detector and if so we can calculate its final energy.

The number of neutrons counted were around 100 for which we needed to generated from $5x10^5$ to $8x10^6$ events. The computing time for these numbers of events was between 1 to 3 hours.

BIBLIOGRAPHY

(Al64) Allison S.K., "Studies in Penetration of Charged Particles in Matter", Nucl. Sci. Series, Rep. No. 39, National Acad. of Sci.-N.R.C. Publ. 1133, 1964.

(An62) Anders E., Rev. Modern Phys. 34 (1962) 287.

(An64) Anders E., Space Sci. Rev. 3 (1964) 583.

(Ar73) Armstrong T.W., K.C. Chandler, and J. Barish, J. Geophys. Res. 78 (1973) 2715.

(Au67) Audouze J., M. Epherre, and H. Reeves, High-Energy Nuclear Reactions in Astrophysics Ed. B.S.P. Shen Univ. of Pens., 1967.

(Be69) Bevington R.F., Data Reduction and Error Analysis for the Physical Sciences, McGraw-Hill Co., 1969.

(Bo74) Broughton P.L., Rocks Miner. 11 (1974) 651.

(Br84) Brown R.M., H.R. Andrews, G.C. Ball, N. Burn, Y. Imahori, J.C.D. Milton, and E.L. Fireman, Earth and Planet. Sci. Lett. 67 (1984) 1-8.

(Bu76) Bullard F.M., "Volcanoes of the World", Ed. University of Texas Press, 1976.

(Bw76) Brown E., J.M. Dairiki, R.E. Doebler, A.A. Snihab-Eldin, L.D. Jardine, J.K. Tuli, and A.B. Buyrn, Table of Isotopes 7th Edition, Ed. C.M. Lederer and V.S. Sherley, 1976.

(Ca87) Castaneda C., Private communication 1987.

(Cu63) Cumming J.B., Ann. Rev. Nucl. Sci. 13 (1963).

(Da55) Davis R., and O.A. Schaeffer, Annals N.Y. Acad. Sci. (1955) 107.

(Dd81) Decker R. and B. Decker, "Volcanoes", Ed. W.H. Freeman and Company, 1981.

(De83) Des Marais D.J., Geochem. Cosmochem. Acta 47 (1983) 1769.

(Dm86) Damon P.E., and T.W. Linick, Radiocarbon Vol. 28, 2A (1986) 266.

(Dm88) Damon P.E., "Secular Solar and Geomagnetic Variations in the last 10,000 years", E.R. Stephenson and A.W. Wolfendale (Editors), (1988) 267.

(En66) Enge H.A., Introduction to Nuclear Physics, Addison-Wesley Ltd., 1966.

(Fi78) Fireman E.L., Proc. Lunar Planet. Sci. Conf. 9th (1978) 1647.

(Ga76) Garber D.I. and .R. Kinsey, "Neutron Cross Sections", Brookhaven National Laboratory 325, 1976.

(Gi86) Guirchard F., Centres des Faibles Radioactivites, Gif, France, Private comunication 1986.

(Go62) Goel P.S., "Cosmogenic ^{14}C and ^{36}Cl in Meteorites", Ph.D. Thesis, Carnegie Institute of Technology (SAEC Report NYO-8922) (1962).

(Gr75) Grosswendt B., and E. Waibel, Nucl. Instr. and Meth. 131 (1975)143.

(Gr84) Greenwood N.N. and A. Earnshaw, "Chemistry of the Elements", Pergamon Press Inc., 1984.

(Gs85) Godfrey-Smith D.,"X-Ray Fluorescence Characterization of the Obsidian Flows from the Mount Edziza Volcanic Complex of British Columbia, Canada", Ms.A. Thesis, Dept. of Archeol., Simon Fraser Univ., Canada, 1985.

(Gu70) Gupta J.G.S., Anal. Chem. Acta 51 (1970) 437.

(Ha75) Hampel W., J. Takagi, K. Sakamoto, and Tanaka, J. Geophys. Res. 80 (1975) 3757.

(He61) Hess W.N., E.H. Canfield, and R.E. Lingenfelter, J. Geophys. Res. 66 (1961) 665.

(Hf79) Heflin E., Gems Miner. 503 (1979) 72.

(Hg78) Hogan J.J., and E. Gadioli, Nuevo Cimento 45A N3 (1978).

(Hn61) Hanna G.C., Can. J. of Phys., 39 (1961) 1784.

(Jg71) Jungerman J.A., F.P. Brady, W.J. Knox, T. Montgomery, M. McGie, J.L. Romero, and Y. Ishizaki, Nucl. Inst. Meth. 94 (1971) 421.

(Ju88a) Jull A.J.T., and D.J. Donahue, Geochem. Cosmochem. Acta 52 (1988) 1309.

(Ju88b) Jull A.J.T., D.J. Donahue, T.W. Linick, and G.C. Wilson, 13th Int. Radiocarbon Conf. 1988.

(Ko63) Kohman T.P., and P.S. Goel, Radioactive dating I.A.E.A. (1963) 395.

(Kt66) Kotlyakov V.M., "The snow cover of the antartic", Ed. by G.A.Avsyk, 1966.

(La67) Lal D., and B. Peters, Handbuch der Physik, Vol XLVI/2, 1967, 551.

(La87) Lal D., Nucl. Instrum. Methods B29 (1987) 238.

(Le87) Leavy B.D., F.M. Phillips, D. Elmore, P.. Kubik, and E. Gladney, Nucl. Instrum. Methods B29 (1987) 246.

(Lg73) Light E.S., M. Merker, H.J. Verschell, R.B. Mendell, and S.A. Korft, J. Geophys. Res. 76 (1973) 2741.

(Li80) Littmark U., and J.F. Ziegler, Handbook of Range Distribution for Energetic Ions in all Elements, Ed. J.F. Ziegler, Pergamon Press 1980.

(Li87) Litherland A.E., Phys. Dept., Univ. of Toronto, Private Communication, 1987.

(Lt68) Littlefield T.A., and N. Thorley, "Atomic and Nuclear Physics", Ed. Van ostrand Reirhold Co. London, 1968.

(Mc85) Michel R., F. Peiffer and R. Stuck, Nucl. Phys. A441 (1985) 617.

(Me73) Merker M., E.S. Light, H.J. Verschell, R.B. Mendell and S.A. Korft, J. Geophys. Res. 76 (1973) 2727.

(Mg83) Meighan C.W., "Obsidian Dating in California: Theory and Practice", American Antiquity 48(3) (1983) 600.

(Mg88) Meighan C.W., and J.L. Sealise (Editors), "Obsidian Dates IV: A Compendium of Obsidian Hydratation Determinations Made at the UCLA Obdidian Hydratation Laboratory", Institute of Archeology, UCLA Los Angeles, 1988.

(Mi74) Middleton R., Nucl. Instr. Meth. 122 (1974) 35.

(Mi88) Middleton R., D. Fink, J. Klein, and P. Sharma, "^{41}Ca Concentrations in modern bone and their implication for dating", Private comumnication, 1988.

(Na76) Nazaret M.A., Ph.. Thesis, Phys. Dept., Case Western Reserve Univ., 1976.

(Ne85) Nelson D.E., Archeol. Dept., Simon Fraser Univ., Private Communication 1985.

(Ne89) Nelson D.E., Private Communication 1989.

(Ni86) Nishiizumi K., D. Lal, J. Klein, R. Middleton, and J.R. Arnold, Nature 319 (1986) 134.

(Pa60) Pandow M., C. MacKay and R. Wolfgan, J. Inorg. Nucl. Chem. 14 (1960) 153.

(Ph86) Phillips F.M., B.D. Leavy, N.O. Jamik, D. Elmore and P.W. Kubic, Science 231 (1986) 41.

(Pr88) Proctor I.D., Private Communication, Data from Evaluated Nuclear Data Cross section Library, LLNL, 1988.

(Ra61) Rama and M. Honda, J. Geophys. Res. 66 (1961) 3533.

(Re72) Reedy R.C. and J.R. Arnold, J. Geophy. Res. 77 (1972) 537.

(Re80) Reedy R.C., Proc. Conf. Ancient Sun, Ed. by R.O. Pepin J.A. Eddy and R.B. Merril, (1980) 365.

(Re83) Reedy R.C., J.R. Arnold, D. Lal, Ann. Rev. Nucl. Sci. 33 (1983) 505.

(Re87) Reedy R.C., Nucl. Instrum. Methods B29 (1987) 251.

(Ro53) Rowland F.S., and W.F. Libby, J. Chem. Phys. 21 (1953) 1493.

(Sc87) Schneider R.J., J.M. Sisterson, A.M. Koehler, J. Klein and R. Middleton, Nucl. Instr. and Meth. B29 (1987) 271.

(Se77) Segre E., "Nucli and Particles", 2nd Ed, The Benjamins/Cummings Publishing Co. 1977.

(Sg83) Segle M., I. Levin, H. Schoch-Fischer, M. Munnich, B. Kromer, J. Tschiersch and K.O. Munnich, Radiocarbon Vol. 25 2 (1983) 583.

(Sh66) Schreider Y.A., "The Monte Carlo Method", Pergamon Press 1966.

(Si51) Simpson J.A., Phys. Rev. 83 (1951) 1175.

(Si83) Simpson J.A., Ann. Rev. Nucl. Part. Sci. 33 (1983) 323.

(Sp69) Spanier J. and E.M. Gelbard, "Monte Carlo Principles and Neutron Transport Problems", Ed. by Addison-Wesley Pub. Co. 1969.

(Sw83) Swart P.K., M.M. Grady and C.T. Pillinger, Meteoritics 8 (1983) 137.

(Ta61) Tamers M.A. and G. Delibras, Comptes Rendus Acad. Sci. (Paris), 253 (1961) 1202.

(Tn68) Tanaka S., K. Sakamoto, J. Takagi, and M. Tsuchimoto, J. Geophys. Res. 73 (1968) 3303.

(Vi86) Virk H.S., Mineral. J., 13 (1986) 34.

(Vo84) Vogel J.S., J.R. Southon, D.E. Nelson, and T.A. Brown, Nucl. Instr. Meth. VB5 (1984) 1175.

(Vo87) Vogel J.S., D.E. Nelson, and J.R. Southon, Radiocarbon V29 3 (1987).

(Wa89) Waddington J.C., Phys. Dept. McMaster Univ., Private Communication, 1989.

(Wl87) Walthan A.C., Geology Today 5 (1987) 172.

(Yo77) Yokoyama Y., J.L. Reyss and F. Guirchard, Earth Planet. Sci. Lett. 36 (1977) 44.

(Zu82) Zumbrunn R., A. Neftel, and H. Oeschger, Earth and Planet. Sci. Lett. 60 (1982) 318.